UNIVERSITY OF CALIFORNIA

Los Angeles

Transmission Power Management for Wireless Health Applications

A dissertation submitted in partial satisfaction of the

requirements for the degree Doctor of Philosophy

in Computer Science

by

Navid Amini

2012

ABSTRACT OF THE DISSERTATION

Transmission Power Management for Wireless Health Applications

by

Navid Amini

Doctor of Philosophy in Computer Science

University of California, Los Angeles, 2012

Professor Majid Sarrafzadeh, Chair

The proliferation of ubiquitous sensing devices along with advances in low power wireless communication technology have resulted in the extensive use of wireless body area networks (WBANs) as the building blocks of the emerging field of wireless health. In these battery-operated WBANs, the sensor devices are strategically placed in/on the human body and the short/mid/long wireless communications are conducted on/off the surface of the body. As the battery energy does not follow Moore's law, energy-efficiency is always one of the design challenges of wireless health-monitoring systems, impacting usability, security, and cost. The idea of transmission power control (TPC) is to automatically reduce the radio amplifier's output power when the transmission power is more than required. Reduced transmission power translates into more energy savings and reduced interference problems. TPC techniques have been used in abundance in cellular networks and wireless LANs. TPC schemes for WBANs, however, are still in their infancy. For example, current IEEE 802.15.4 specifications do not

differentiate between mobile and static settings, thus leaving WBAN transmitters in the dark as to what transmission power level they should utilize.

In this dissertation, we have investigated the potential benefits and limitations of TPC as a means to extend the battery lifetime in WBANs at the first three abstraction levels. Physical and MAC layers' approach to TPC perform a local optimization, whereas network layer TPC is capable of a global optimization. At the network layer, we analytically solve an optimization problem whose solution determines an important parameter, i.e., energy-efficient cluster size, for a class of routing/MAC protocols in WBANs. Assuming that the routes are established in an energy-efficient manner, we then experimentally profile the 2.4 GHz on/off-body radio channel under several scenarios regarding mobility states and environments, and we showed that fixed transmission power either wastes energy or hinders reliability. Finally, we devote our attention to an ambulatory medical monitoring WBAN system, which is tied up with different characteristics in terms of mobility, periodicity, and 'unforgivingness' of the wireless channel as a result of proximity to the ground as well as to human's body. The target ambulatory WBAN system encompasses a pair of wireless instrumented insoles (known as smart insoles) for gait data collection, plantar pressure monitoring, and gait analysis. We design a sensor-assisted TPC scheme that augments in-network information with information from built-in sensors. To this end, multiple mobility states are defined for the smart insoles and the mobility states are incorporated into transmission power control policies. Available sensor information is leveraged to detect the mobility states, based on which the TPC scheme switches strategies.

We validate this new idea of switching transmission power control strategies by implementing and evaluating the sensor-assisted scheme and comparing it against a frame-based TPC scheme, which adjusts the transmit power solely based on recent information about

packet transmission successes and failures. Our testbed experiments involving mixed mobility scenarios show that our TPC scheme obtains up to 50% increase in the battery lifetime, enabling the smart insoles to be used in uncontrolled environments. Such an improvement in battery longevity (from 4.0 hours to 7.8 hours) is made by reducing the average energy consumed for communication of a single packet from 4.51 mJ/pkt to 2.27 mJ/pkt.

Although designed for the smart insoles as a severely energy-constrained device, the sensor-assisted TPC technique is readily deployable on a variety of today's commodity devices to make a connection between the sensing subsystem and the communication subsystem of such devices. In addition, as the underlying mobility state detection methods place relaxed requirements on how the device should be worn in terms of orientation and position, they can be used for a variety of purposes, such as improving the patient's compliance with medical treatments and therapies.

The dissertation of Navid Amini is approved.

Mario Gerla

Jens Palsberg

Dejan Markovic

Majid Sarrafzadeh, Committee Chair

University of California, Los Angeles

2012

To my grandmothers, parents, and brother …

TABLE OF CONTENTS

LIST OF FIGURES

LIST OF TABLES

ACKNOWLEDGEMENTS

First and foremost, I would like to say thank you to my grandmothers for all they have been to me and for their unprecedented role in my life. I was given two pretty and spectacularly devoted grandmothers, Parvin (my mom's mother) and Mahgol (my dad's mother). I wholeheartedly want to dedicate this dissertation to you, as I continuously feel your presence and support while moving along the trajectory of life from childhood and kindergarten days all the way to my Ph.D. studies and onwards. Thank you for picking me up every day after school, for caring about my grades, and for always being on my side. I miss you in abundance and may both of you rest in peace.

I would like to thank my parents, whose support and guidance have helped me go through difficult chapters of my life. My father (Heidar) and mother (Nasrin) have been genuinely caring and ultra-supportive; hence, this dissertation is dedicated to their sacrifices. They always bring hope to my table. Thank you for thinking about me and calling me every day (including just now!). Also, thank you for having me with you on every trip that you took across the world. All I can say is that if my kids find me to be half as supportive a parent as you have been to me, I will consider myself a success.

I very much like to express my appreciation to Nima, my brother with whom I have lived my whole life. You have been unbelievably big-hearted and warm-hearted to me. You inject energy and spirit into my veins. Thank you for the memories, for being on the same page with me all the time, and for the food that you bring into my plate every day.

I would like to acknowledge the efforts, guidance, and support of my advisor, Professor Majid Sarrafzadeh, for helping me with framing my research and searching for jobs. His vision

and great advices on selecting the right topic and taking the correct approach substantially helped me throughout all these years. Moreover, I am grateful to Professor Mario Gerla for his vision and for assisting me with developing new ideas during my coursework at UCLA and later on when I was focusing on my research. Professor Jens Palsberg and Professor Dejan Markovic's insightful comments were of significant help in completing the final phases of this dissertation.

I am grateful to all my UCLA and non-UCLA friends, as well as to my former and current labmates including those that I have never physically met. I have been lucky to have great people around me, who have had a direct impact on my personal and professional life. Thank you Mojtaba Torkjazi, Farzin Naseri, Ali Rahpeyma, Shahrokh Parvaresh, Neshat Jalali, Hessam Kooti, Saman Barghi, Alireza Ghane, Nima Razavi, Sajed Miremadi, Pouria Pirzadeh, AmirHossein Gholamipour, Mohammad Khorramzadeh, Hossein Tajik, Francesco Fraternali, Wenyao Xu, Hyduke Noshadi, Bobak Mortazavi, Hojat Parta, Alireza Vahdatpour, Ani Nahapetian, Foad Dabiri, Zohreh Karimi, Hassan Ghasemzadeh, Soheil Ghiasi, Kouros Nouri-Mahdavi, Hooman Mohseni, Ali Aminlari, Nick Terrafranca, Massoud Agahi, Soheila Mirhashemi, Ankur Srivastava, Behrooz Yadegar, and many others; without your support, it would have been extremely harder to finish my Ph.D. and almost impossible to live life in a smooth and enjoyable way.

VITA

2002-2007	B.Sc. (Computer Engineering), Sharif University of Technology. Department of Psychology University of California, Los Angeles
2005-2007	Research Assistant, Dependable Systems Laboratory, Sharif University of Technology
2009-2011	System Engineer, MediSens Wireless, Inc., California NanoSystems Institute University of California, Los Angeles
2007-2012	Teaching Fellow/Instructor, Computer Science Department University of California, Los Angeles. Taught several sections of CS152A (Introductory Digital Design Laboratory) and CS152B (Digital Design Project Laboratory)
2007-2012	Graduate Research Assistant, Embedded and Reconfigurable Systems Laboratory, Computer Science Department University of California, Los Angeles
2012-	Postdoctoral Fellow, Jules Stein Eye Institute, Los Angeles, CA

PUBLICATIONS

N. Amini, A. Vahdatpour, W. Xu, M. Sarrafzadeh, "Cluster Size Optimization in Sensor Networks with Decentralized Cluster-Based Protocols," Computer Communications Journal – Elsevier, Volume 35, Issue 2, Jan. 2012, pp. 207-220.

H. Ghassemzadeh, N. Amini, M. Sarrafzadeh, "Energy-Efficient Signal Processing in Wearable Embedded Systems: An Optimal Feature Selection Approach," 2012 International Symposium on Low Power Electronics and Design, Redondo Beach, California, USA, pp. 357-362.

N. Amini, M. Sarrafzadeh, A. Vahdatpour, W. Xu, "Accelerometer-based on-body sensor localization for health and medical monitoring applications," Pervasive and Mobile Computing Journal – Elsevier, Vol. 7, Issue 6, December 2011, pp. 746-760.

N. Amini, A. Vahdatpour, F. Dabiri, H. Noshadi, M. Sarrafzadeh, "Joint Consideration of Energy-Efficiency and Coverage-Preservation in Microsensor Networks," Wireless Communications and Mobile Computing Journal, Vol. 11, Issue 6, June 2011, pp. 707-722.

H. Noshadi, S. Ahmadian, H. Hagopian, J. Woodbridge, F. Dabiri, N. Amini, M. Sarrafzadeh, N. Terrafranca,"HERMES: Mobile System for Instability Analysis and Balance Assessment," ACM Transactions in Embedded Computing Systems (TECS), Vol. 12, 2012.

N. Amini, W. Xu, M. Sarrafzadeh, "Experimental Analysis of RF Transmission Characteristics for On/Off body communications," Proc. of the IEEE International Symposium on Personal, Indoor and Mobile Radio Communications (PIMRC), Sept 2011, Toronto, Canada.

A. Vahdatpour, N. Amini, M. Sarrafzadeh, "On-body Device Localization for Health and Medical Monitoring Applications," in Proc. of the IEEE Pervasive Computing and Communication conference (PerCom 2011), Seattle, Washington, pp. 33-39.

A. Vahdatpour, N. Amini, M. Sarrafzadeh, "Toward Unsupervised Activity Discovery Using Multi-Dimensional Motif Detection in Time Series," Proc. of the Twenty-first International Joint Conference on Artificial Intelligence (IJCAI) 2009, Pasadena, California, pp. 1261-1266.

N. Amini, M-C. Hsiao, M. Sarrafzadeh, "A Wireless Home Automation System for Childhood Obesity Prevention," Proc. of the International Conference on Biomedical Electronics and Devices (BIODEVICES 2010), Valencia, Spain, Jan. 2010, pp. 75-81.

N. Amini, J. E. Matthews, A. Vahdatpour, M. Sarrafzadeh, "The Design of a Wireless Portable Device for Personalized Ultraviolet Monitoring," Proc. of 2009 SPIE Nanoscience and Engineering Conference, San Diego, CA, USA, pp. 73970O-73970O-12.

N. Amini, J. Matthews, F. Dabiri, A. Vahdatpour, H. Noshadi, M. Sarrafzadeh, "A Wireless Embedded Device for Personalized Ultraviolet Monitoring," Proc. of the International Conference on Biomedical Electronics and Devices (BIODEVICES 2009), Porto, Portugal, Jan. 2009, pp. 200-205.

W. Xu, Z. Li, M. C. Huang, N. Amini, M. Sarrafzadeh, "eCushion: An eTextile Device for Sitting Posture Monitoring," 8th International Conference on Body Sensor Networks (BSN 2011), Dallas, Tx, May 2011.

H. Noshadi, N. Amini, J. Woodbridge, W. Xu, M. Lan, H. Hagopian, N. Terrafranca and M. Sarrafzadeh, "Lightweight Context-Aware Smart Insole for Gait Analysis, Research and Rehabilitation," Parkinsonism & Related Disorders, Vol. 16, Supp. 1, Feb. 2010, pp. S29.

H. Noshadi, S. Ahmadian, H. Hagopian, J. Woodbridge, F. Dabiri, N. Amini, M. Sarrafzadeh, N. Terrafranca, "HERMES - Mobile Balance and Instability Assessment System," Proc. of the International Conference on Bio-inspired Systems and Signal Processing, Valencia, Spain, Jan. 2010, pp. 264-270.

F. Dabiri, N. Amini, M. Rofouei and M. Sarrafzadeh, "Reliability-Aware Optimization for DVS-Enabled Real-Time Embedded Systems," Proc. of 9th International Symposium on Quality Electronic Design, (ISQED), San Jose, CA, USA, March 2008, pp. 780-783.

N. Amini, M. Rofouei, W. J. Kaiser, M. Sarrafzadeh, "Energy-Aware Heart Rate Monitoring During Stair Climbing," Proc. of 2008 UC Bioengineering Symposium, Riverside, CA, USA, June 2008, pp. 125.

Majid Sarrafzadeh, Nicholas A. Terrafranca JR., Hyduke Noshadi, Shaun Ahmadian, Hagop Hagopian, Jonathan Woodbridge, Navid Amini, Wenyao Xu, Mars Lan, "Method of Assessing Human Fall Risk Using Mobile Systems", Issued Patent, UCLA Case No. 2009-383-2, Serial Number 61/222,900, International Patent Application Serial Number, PCT/US2010/40431.

Navid Amini, Majid Sarrafzadeh, "Exercise Based Entertainment Controller", Provisional Patent, UCLA Case No. 2009-496, Serial Number 61/467,744.

CHAPTER 1

Introduction

1.1 Wireless Health and WBANs

5% of the patient population in the US account for 49% of healthcare costs. The life expectancy in the US is shorter than that in most other developed nations and many developing countries. By 2050, ozone depletion may result in 830,000 and 500,000 additional cases of cataract and skin cancer in the US.

At first glance, this looks like a mixture of out-of-context facts/statistics. People are continually bombarded with such statistics. In the opinion of many healthcare visionaries, these issues can all be remarkably alleviated and fruitfully studied within the framework of genomics and wireless technology. Health experts list the downsides of the ongoing healthcare paradigm as follows:

1) Today's healthcare is inherently centralized, reactive and focused on interacting with patients once they suffer from a debilitating disease. 2) The medical data is collected in artificial settings (hospital, lab, or physician's office) based on a typical 15-minute exam in almost complete isolation. The quality of the data and the resulting diagnosis are therefore vulnerable and dependent on the diligence, accuracy and competence of the health professional and patient. 3) Due to genetic variations, medical treatments have various effects on different people. Nevertheless, current treatment models are population-based, which means that only one care plan is developed for all cases and generalized for the population. 4) In the current healthcare model, patient's compliance with the prescribed treatment is driven by the related brochures or websites and, hence, compliance is completely hope-based and questionable. 5) The current centralized healthcare paradigm is not pervasive. As a result, the research community has sporadic

interaction with the patients to which the treatment is being applied and this trend continues until relatively late stages of the treatment cycle. Therefore, unforeseen negative effects of a treatment are addressed in a very slow manner, if addressed at all.

The above issues underscore the need for more preventive and pervasive healthcare services to overcome the imminent crisis in the healthcare system. It is widely believed that if a remarkable percentage of care shifts from institutions to home, the resulting proactive healthcare paradigm will allow for pervasive data collection. Given that there are more wireless devices (322.9 million) than Americans (312.8 million), it makes perfect sense to make a connection between health and wireless technology. When realized properly, such unparalleled connection will enable new applications currently considered inconceivable. Therefore, more attention should be paid to Wireless Body Area Networks (WBANs). The wide array of information available from genomic sequencing, determines individual's genetic susceptibility to diseases at a molecular level. On the other hand, the contribution of environmental exposure and lifestyle history is determined by pervasive data collection in, on and around a patient's body in his/her own environment. The joint effect of genomic sequencing and continuous health monitoring realizes the dream of preventive and personalized medicine.

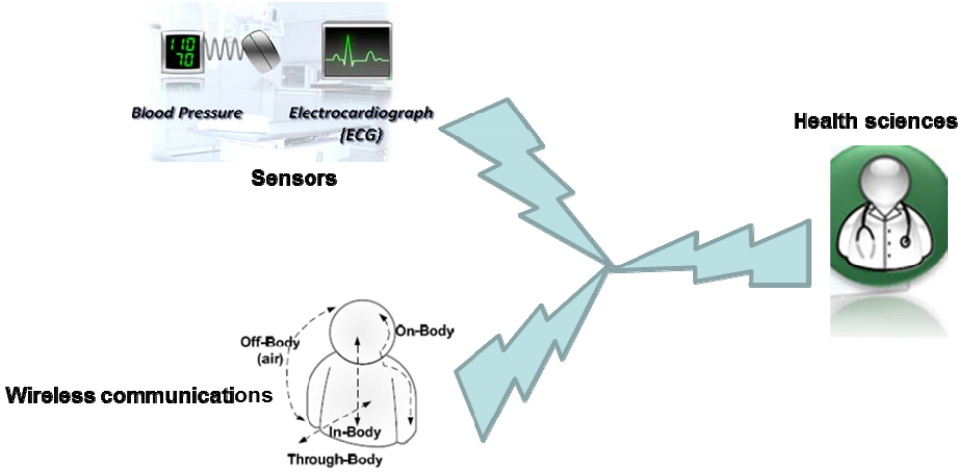

Figure 1. Wireless health: the convergence of sensors, communications, and health sciences.

WBANs enable us to establish a more accessible and affordable healthcare solution, consisting of

smart home environments, new bio-sensors, tiny wireless nodes as wearable point of care systems, energy-efficient communication protocols, and precise classification algorithms. WBANs allow the integration of miniaturized and low-power sensor nodes in, on, or around a human body (Figure 1) to monitor body functions and the surrounding environment [Ullah].

As monitoring, diagnostic and therapeutic systems, WBANs consist of in-body and on-body area networks. An in-body area network allows communication between invasive/implanted devices and a base station (BS). On the other hand, an on-body area network, allows communication between noninvasive/wearable devices and a base station. This latter group of WBANs is also known as body-wearable sensor networks [Amini1].

1.2 Wireless Communications and Transmission Power Control

Unlike typical wireless sensor networks, WBANs have fewer nodes which are normally not similar in the task they perform; nevertheless, they should be small in size and consume the least possible amount of energy. In other words, the lack of node redundancy increases the importance of preserving the reliability of data transmissions, as do safety critical considerations of most medical monitoring applications. Moreover, diminutive packaging bounds battery size and therefore, capacity [Hanson]. This is because it is not comfortable for the user of WBANs to change the power source of the sensors frequently. In addition, changing the power source of the implanted sensors is invasive and should be avoided.

Wireless communications are the most energy-consuming operation that a sensor node performs; the ratio of energy consumption for communicating one bit over processing it is in the range of 1000-10000 [Dardari]. Thereby, the dominant source of energy loss in WBANs is the radio subsystem [Amini2], [Zhao]. As a result, designing an energy-efficient communication protocol is a must. The energy consumption due to wireless communications can be reduced by taking action at multiple layers of the communication stack.

Transmission power control (TPC), broadly speaking, is the intelligent selection of transmission power

in a communication system to achieve good performance within the system [Wiki1]. The notion of "good performance" depends on context and in the WBANs domain may include optimizing metrics such as battery lifetime of the system, link data rate, network capacity, and coverage/range. Energy-reliability tradeoffs are central to many battery-constrained systems, but they are essential in WBANs due to energy and resource constraints, and the critical nature of many medical monitoring applications [Hanson]. TPC enables transmitters in WBANs to control the communication power according to the anticipated channel quality, imposing strict tradeoffs between the energy consumed by communication resources and the reliability, throughput, and latency required by different applications. TPC techniques are very effective in reducing energy consumption while meeting reliability and quality of service (QoS) requirements.

There are at least five reasons to implement TPC techniques, either in dynamic or static fashion, in WBANs: 1- Wireless radio channels are typically affected by external and uncertain factors that have an adverse impact on the system performance. Path loss, shadowing, and fading effects can severely deteriorate the QoS and when mobility is introduced, the problem becomes inevitably harder to solve. 2- The human body includes liquid, bone and flesh, which, in a selective manner, absorb, reflect or scatter wireless signals. Hence, the nodes used in WBANs need to cope with lossy radio transmissions in/around the human body. 3- The nodes produce heat; the rise in temperature of the nodes due to communication should not be very high. A high temperature of the in-body nodes for a prolonged period will damage the surrounding tissues [Bag]. 4- Recent findings indicate that in the range 2-6 GHz, no energy can pass through the body. Rather, radio waves transmitted from an antenna diffract around the body and can reflect from arms and shoulders [Kleisouris]. 5- Generally, attenuation rate and multipath effects increase at higher frequencies; therefore, a 2.4 GHz signal weakens faster than a sub-GHz signal, e.g., 433, 868, and 915 MHz carrier frequencies.

TPC techniques have been extensively used on infrastructured networks [Oh], [Rashid-Farrokhi]. Recent standards, such as WiMax and IEEE 802.11h, mandate that equipments used on wireless broadband solutions should dynamically adjust the transmission power [Qiao]. TPC techniques for

WBANs, however, are still in their infancy. The implementation of TPC is much more complex in WBANs than structured networks. First, there are multiple MAC-level TPC protocols for WBANs [Kubisch]; however, only a few of those were evaluated in real hardware. Second, while the wireless part of structured networks is normally composed of one hop, in WBANs the communication may traverse several hops over wireless links, requiring TPC-aware routing protocols [Shankar].

1.3 TPC-Aware Routing

Since many researchers including those involved in the IEEE 802.15.6 are focusing on PHY/MAC standardization, the network layer has received limited attention. For WBANs, TPC-aware routing is of particular interest as power consumption and its balanced usage across the WBAN nodes while maintaining the overall system performance are major challenges to their practical deployment. Both in-body area networks and body-wearable networks can benefit from TPC-aware routing schemes; examples of such networks are the implanted artificial retina [Shankar], continuous physiological monitoring of first responders [Li], and real-time athlete monitoring [Sivraman]. In these energy and/or heat sensitive systems, the number of monitoring nodes is in the order of dozens. Data transmissions among the sensors should be dispersed around nodes and not rely on only one route. This can be achieved by balancing the communication over the nodes by means of clustered WBANs and corresponding cluster-based protocols. Moreover, one may also consider the temperature to select appropriate routing paths. Cluster-based communication protocols organize the sensor nodes into clusters, where most of the communication takes place within the clusters, and long range transmissions to the base station are performed by the cluster heads to reduce the energy/temperature consumption/rise [Tang]. We analyze the importance of cluster-based routing protocols for WBANs and our analysis specifies how differently design parameters should be selected in order to improve the longevity of WBANs.

1.4 TPC in Lower Network Layers

TPC techniques for MAC and PHY layers are applicable to cases, where the routes are known before data transmissions, or the communications are meant to take place between only a few nodes; examples of the latter are personalized ultraviolet monitoring [Amini3] and the smart shoe system [Noshadi]. Routing protocols depend on the PHY and MAC layers to obtain the information required to calculate the minimum transmission power [Correia]. Further, MAC protocols could adjust the transmission power of each frame, which can be a control, data, or acknowledgement (ACK) frame, while the routing layer is limited to adjusting the transmission power on a coarser granularity. Therefore, we started using a simple energy model, incrementing it with various parameters one at a time and measuring their impact individually. This strategy allows us to identify which parameters (antenna type, environment, antenna height, data rate, packet size, and different mobility states, such as standing, walking, and running) contribute to the performance of TPC techniques and the extent of their contribution. For on/off-body communications, IEEE 802.15.4 standard technology [IEEE] yields the best compromise between data rate, network capacity, battery lifetime and autonomy [Monton]. The nodes in body-wearable sensor networks generally use IEEE 802.15.4 radios which offer low-power consumption and are relatively immune to interference. In light of human body causing large signal attenuation and hence, exacerbating wireless link reliability, we conducted measurements from the IEEE 802.15.4 compliant XBee and XBee Pro [Xbee] wireless modules so as to find spatial impacts on the correlation between the transmission power and link equality estimators such Receive Signal Strength Indicator (RSSI) and Packet Reception Ratio (PRR). Also, the correlation between RSSI and PRR metrics is investigated.

When a WBAN node moves wireless channel quality metrics and packet losses demonstrate a higher degree of statistical correlation with the past behavior as compared to the stationary scenarios. For mobile cases, the packet following a lost packet is significantly more likely to be lost than in the static cases.

There are only a few studies that evaluate the energy and capacity benefits of transmission power control in the context of general sensor networks, such studies are based on mathematical analyses or

simulations; i.e., there is no implementation. Existing TPC schemes and wireless communication protocols in general, adapt their behavior based on in-network information such as loss rate, bit errors, or Signal to Noise Ratio (SNR). To our knowledge, local sensors have not been previously used to augment TPC methods. Our sensor-assisted scheme switches from static-optimized setup to mobility-optimized setup (or vice-versa) as soon as it is informed that the mobility state of the WBAN has changed; furthermore, an empirical study has been performed on the effect of transmission power control for a specific WBAN system.

1.5 Wireless Insoles/Shoes

In a group of WBANS, wireless communications are initiated from inside a shoe (or an insole), i.e., under the feet. Examples of the systems taking advantage of such wireless communications include but are not limited to the PACE wireless insoles [MediSens], developed by us at UCLA, as well as other fitness monitoring, therapeutic, and diagnostic systems in the form of a shoe or an insole, such as Nike+ iPod system [Nike+], Addias Speed_Cell, VitaliShoe [Jagosa][VShoe], and iShoe insole [Aiden].

We designed a unified circuit board to be the successor of our smart shoes (also known as Hermes); this new platform measures foot pressure distribution during ambulation in gait analysis and spatial/temporal gait parameters to evaluate motor impairments. Prototyped in the form of wireless insoles, this platform is the building block of PACE.

Despite the emergence of an increasing number of commercial products and research prototypes/platforms that make use of aforementioned wireless communications, the characterization of these specific wireless communications is still unresearched. Such characterization is needed not only to apply TPC techniques and save energy, but also to be capable of reliably transmitting packets of data with different sizes and data rates to the data acquisition side. The mentioned products and prototypes place their transmitter in the base of the shoe, while the receiver side (i.e., the data acquisition unit) is attached to the user's body or is fixed, e.g., mounted to the wall.

Our characterization results provide guidelines to identify TPC algorithms' parameter settings that meet wireless insoles requirements and operating conditions. For instance, the current foot posture based on acceleration and pressure data provided by the insoles can be utilized to select the best transmit power level.

1.6 Dissertation Contributions

In this dissertation, we present a comprehensive study of TPC techniques for WBANs at Physical (PHY), Medium Access Control (MAC), and Network layers. Different schemes are proposed and studied at different layers, and useful solutions are discussed.

The contributions of this dissertation include:

1- Our first contribution regards the network and MAC layers; we analytically provide the optimal cluster size that minimizes the total energy expenditure in clustered WBANs, where all sensors communicate data through their elected cluster heads to the base station in a decentralized fashion. The analytical outcomes are given in the form of closed-form expressions for various widely-used network configurations. Examples of TPC-aware communication protocols that can benefit from our analytical results include but are limited to LEACH [Heinzelman], LEACH-Coverage [Tsai], DBS [Amini2], and AnyBody [Watteyne], as well as the approaches presented in [Alippi] and [Shankar]. Apart from analyzing the optimal cluster size, which leads to minimum total energy expenditure of the network, we verified the analytical results through comprehensive simulations. More specifically, we show that I) under certain situations the optimal cluster size can be independent of the network dimensions, II) the energy consumption of the transmitter's circuitry has no impact on the optimal cluster size, and III) the energy consumption of the receiver's circuitry can substantially change the optimal number of clusters and more importantly, it can make a decision on whether or not it is worth to cluster the network.

2- With regard to the PHY layer and to address applications that exhibit one-to-one communication needs, I) we have investigated the feasibility of XBee Pro wireless modules for mid/long range off-body

communications intended, for example, for athletic performance monitoring in an open sports field. The analysis of our experiments, which takes into account the concept of Fresnel [Fresnel_Wiki] zone clearance, demonstrates that RSSI values more than -90 dBm signify high quality links with more than 90% of the packets being delivered to the receiver. II) We study the issues confronting IEEE 802.14.5 wireless communications around the human's body, i.e., on-body communications. We attached transmitting sensor nodes of type XBee to six different body positions. On the basis of our experimental results, RSSI values higher than -80 dBm are indicative of reliable communications. Furthermore we found that a number of body locations offer enough room to reduce the transmission power level without compromising the reliability of communications. For instance, transmission power reduction for data communications between the thigh and the waist will bring about up to 50% energy savings. The shins and generally the lower part of legs turned out to be very favorable locations for on-body wireless communications. Examples of the systems benefiting from our findings to implement TPC schemes are the personalized ultraviolet monitoring and the smart insoles.

3- Our final contribution is centered around a specific WBAN system; we characterized the wireless communications of the smart insoles considering the energy-reliability tradeoffs and under several scenarios regarding mobility states and environments. Based on the characterization results, we designed a sensor-assisted TPC scheme that augments in-network information with information from built-in sensors. This idea can be used not only for controlling the transmission power, but also at all layers of the network stack to improve performance. By utilizing the sensor-assisted TPC scheme in mixed stationary/mobile settings, we were able to significantly extend the battery life of wireless insoles while meeting all its constraints as far as the packet loss, packet size, data rate, antenna type/orientation are concerned.

1.7 Dissertation Organization

The organization of the rest of this dissertation is as follows. Chapter 2 provides background information

on TPC and presents our utilized energy model. Chapter 3 introduces preliminary notions regarding TPC-aware communication protocols and covers the first contribution together with simulation results. The second contribution is presented in Chapter 4. Special attention is devoted to the smart insoles in Chapter 5, where their architecture along with the description and evaluation of the proposed sensor-assisted TPC scheme are presented. Chapter 6 concludes this dissertation.

CHAPTER 2

Overview of TPC

TPC schemes can be divided at least into three categories: 1- Link quality-based schemes, which use link quality feedbacks in the form of e.g., RSSI, LQI, or PRR; 2- Frame-based schemes, which react to consecutive acknowledged or unacknowledged packets; and 3- Sensor-assisted schemes, which utilize the current state and/or context of the system, e.g., based on acceleration and pressure data in the smart shoe. Obviously, TPC schemes can cross between the categories explained.

TPC is an example of a cross-layer design problem. The transmission power level affects the transmission range, signal quality, and the interference for other receivers and, hence, it impacts the physical layer. The power levels determine the performance of MAC mechanisms, since the contention for wireless channel access depends on the number of nodes within range. Further, TPC determines the neighboring nodes that can hear the packet, which is crucial for the network layer. TPC is also the key to several performance measures such as throughput, delay, and energy consumption. The challenge is to determine which layer in the communication stack the power control problem belongs to. Afterwards, one needs to determine the appropriate power level by thoroughly investigating its impact on several performance metrics, to provide a solution which deals properly with the multidimensional effects of TPC, and finally, to provide a software architecture for realizing the TPC scheme.

Transmission power control can be executed simultaneously with node sleep scheduling (duty cycling) as a complementary energy-saving strategy. This will significantly extend the battery life of the sensor node in/on human body by keeping the transceivers in their minimum activity status, which is the sleep

mode almost all the time [Quwaider]. There are several benefits on the use of TPC techniques in WBANs. Besides reducing energy consumption, TPC techniques reduce the number of collisions and the rate of packet loss due to interference. Further, they increase spatial reuse, allowing more nodes to transmit at the same time. As a consequence, the capacity and the throughput of the network can be enhanced [Correia] [Gomez].

While altering the transmission power in a wireless system and particularly in WBANs, two considerations must be accounted for. First, the battery life of nodes can be affected by the transmission power level. Nodes with lower batteries should try to maintain lower transmission power levels, while still sustaining the quality of the signal. Second, the wireless transmission power regulations must be considered. There are set limits to how high the power of a transmitted signal can be.

2.1 Benefits of TPC

TPC influences several characteristics of low power wireless communications, such as node connectivity, medium contention, delay, energy consumption, and data rate [Kawadia]. In the following we briefly discuss each characteristic [Correia]:

Connectivity: Network connectivity is determined by the establishment of links among nodes, and depends on the correct reception and decoding of frames. TPC schemes affect this process, since the transmission power determines if the frame will overcome the interference, attenuation, and signal distortions imposed by the medium. TPC techniques can be used to maintain a certain degree of connectivity, increasing the transmission power if link reliability falls below a certain threshold. Wireless links are usually asymmetric, that is, the characteristics of the transmission vary according to the sense of the communication. Link asymmetry may deteriorate the operation of several protocols that rely on messages coming on both ways. One example is frame acknowledgment on CSMA/CA MAC protocols. A node A might be able to send a frame to node B; however, A may not receive the acknowledgment frame, causing unnecessary retransmissions, collisions, and frame losses, hence leading to a reduced

throughput [Correia]. TPC techniques can be used to mitigate asymmetric links by adjusting the transmission power at both sides of the communication.

Security: Performing TPC enhances the security, as data packets with lower power are more difficult to intercept.

Medium contention: The transmission range is determined by signal strength. Thereby, higher transmission powers will increase the potential number of nodes sharing the medium, and as a consequence, the probability of collisions will be heightened. A more pronounced contention on the shared medium might also increase the latency and reduce the delivery rate. The amount of contention can be controlled using TPC techniques. By transmitting data at the exact power required to ensure a successful communication, only nodes that really must share the same "space" will contend to access the channel. Finally, a smaller transmission range will reduce the amount of hidden and exposed terminals [Monks], since fewer nodes overhear transmissions from others [Correia].

Throughput: The throughput of the links is directly impacted by the number of nodes within the transmission range, as a result of their participation in the contention. The adjustment of the transmission power reduces the number of competing nodes, thus less retransmissions will be required to convey the data [Gupta]. TPC may be used to increase medium reuse, since a reduced range allows more simultaneous transmissions to take place [Gomez]. Further, TPC can be utilized to transmit frames using stronger coding and modulation, thus providing higher data rates. In several wireless standards, such as Wi-Fi and WiMax, the data rate of the link is dynamic, changing according to the conditions of the environment. For example, on an IEEE 802.11g network, one might accomplish 54 Mbps in favorable conditions (e.g., a client near the AP with no walls obstructing); however, the data rate may drop for distant clients or for stations experiencing heavy interference. This mechanism compensates for the interference by using more powerful coding techniques; however, this comes at the cost of a reduced data rate. Using TPC, nodes can increase the transmission power on links with higher interference in order to accomplish a high data rate.

Latency: Latency is a function of the number of hops traversed in the communication. TPC schemes may increase or decrease latency by changing the number of hops on each route. Higher transmission powers allow shorter routes, which will have a smaller latency. On the other hand, lower transmission powers will require longer routes.

Energy: The energy consumed by the radio depends on the transmission power employed and the rate of collisions. Therefore, the higher the transmission power, the higher the energy consumption. However, as explained before, a very low transmission power may reduce the data rate of the link and its quality. Thus, TPC solutions must aim at achieving the best compromise between energy consumption and reliability.

2.2 Requirements for Implementing TPC

To implement TPC techniques, the hardware must provide support for the measurement of the incoming signal strength, as well as mechanisms to dynamically change the strength of outgoing packets (frames):

Fast transmission power switching: The transceiver must be able to switch the transmission power online, without restarting the hardware. The modification of the transmission power should also be fast, allowing the use of different transmission powers from one packet to another. While in structured wireless networks packets are always forwarded to the same node (the access point), in WBANSs flows may be forwarded to different nodes. As such, the transmission power may need to be adjusted for each outgoing packet.

Incoming signal strength readings: The radio must provide interfaces to measure the instantaneous values of link quality estimators, for instance strength of the signal received by the radio. Those measurements are used to calculate the average noise floor, as described later in this section, and also as input to the equations used to calculate the minimum transmission power.

Once the radio supports the measurement of link characteristics, we must quantify the condition of the link when idle, as well as the average signal loss incurred when the signal travels from source to

destination, in order to implement efficient TPC algorithms. It should be noted that although in some platforms the hardware completely meets the above requirements, the wireless protocol associated with these platforms still does not allow for online transmission power switching. For instance, SimpliciTI [TI1], a low-power network protocol from Texas Instruments utilized in EZ430- RF2500 [TI2] platforms, does not allow for online power level adjustment, while the associated radio chip CC2500 [TI3] does.

2.3 Radio Energy Dissipation Model

We have adapted the energy model described in [Heinzelman]. This model assumes that the power loss is proportional to squared distance, d^2, between sender and receiver. Here, we transform the model into a more general one ([Braem] and [reusens]) by changing d^2 to d^n, where n represents the path loss exponent. In this energy model, E_{elec}^{Tx} and E_{elec}^{Rx} are defined as the energy being dissipated to run the transmitter's or receiver's circuitry, respectively, to send or receive one bit of the data packet. ε_{amp} represents the energy dissipation of the transmission amplifier to convey one bit of the data packet to the receiver node with a distance of d = 1 m away. The specific values of these parameters are hardware dependent. Transmit (E_{Tx}) and receive (E_{Rx}) energies are calculated as follows:

$$\begin{aligned} E_{Tx}(l,d) &= lE_{elec}^{Tx} + l\varepsilon_{amp}d^n \\ E_{Rx}(l,d) &= lE_{elec}^{Rx}, \end{aligned} \tag{1}$$

where l is the length of the transmitted/received message in bits, d represents the distance over which the data is communicated and n is the path loss exponent, which is specified by radio propagation model. As it can be seen, the transmitter expends energy to run the radio electronics and power amplifier, while the receiver only expends energy to run the radio electronics. The transmitters are presumed to have power control capability (TPC-enabled) and hence, they consume the minimal energy needed to reach the receiver. Four different scenarios are considered:

1- In-body communications between an implant node and an on-body gateway [Abouei]. A biosensor embedded in the body communicates with an apparatus attached to the body or with an external monitoring device in the vicinity of the human body. It has been shown that for short range in-body communications, where the implanted nodes are close to the body surface and the receiver is attached to the body at a small distance from the implanted node, our energy model works fairy accurately [Shankar]. It should be noted that propagation through the body is negligible in the gigahertz frequency range and as such, in-body area networks usually use sub-gigahertz technologies. Examples of implantable devices are cardiac pacemakers, insulin dispensers, neurostimulators, bladder controllers [Receveur], and artificial retinas to restore vision [Shankar]. With such a wireless implantable technology, scientists have designed short-range communication systems for monitoring health conditions of patients such as brain waves in paralyzed persons, glucose levels in diabetic patients, patients with gastrointestinal disorders, and to restore vision to the blind [Shankar].

2- On-body communications between a body surface sensor and an off-body gateway (line-of-sight (LOS) channel) [Sayrafian-Pour], [Yazdandoost]. In LOS propagation, electromagnetic waves travel in a straight line, such as a scenario where both the receiver and the transmitter are located on the back of a subject. A recent study [Reusens] has shown that the path loss along the back, unlike legs, arms, and torso, follows a different trend than the other three body locations. This is because the surface of the back is more flat than the surface of the leg and hence, the path loss exponent is significantly lower (2.28 versus 3.45). The disparity in tissue compositions and in tissue thickness is another explanation for the variation between the path loss models for the different body parts. Due to different tissue compositions and thicknesses, the absorption in the specific body parts will vary, and thus the path loss along the body parts will differ.

3- On-body communications between a body surface sensor and an off-body gateway (non-line-of sight (NLOS)) [Fort]. In on-body NLOS propagation, radio transmission across a path is partially obstructed, for example, a scenario where the communications take place between back and torso. Due to

diffraction around the human body and absorption of a large amount of radiation by the body, a higher path loss and a higher path loss exponent along the NLOS channel than along the LOS channel is observed. It is worth mentioning that at lower frequencies, where we expect signal penetration through the body. NLOS channels do not necessarily incur a higher loss. In this case, the loss depends on the skin depth of body tissues.

4- Short/mid/long range off-body communications. This group of communications are intended e.g., for gait analysis [Noshadi], athletic performance monitoring [Sivaraman] in an open sports field, and physiological monitoring of first responders throughout operations [Li]. In these scenarios, we consider both free space ($n = 2$, $\varepsilon_{amp} = \varepsilon_{fs}$) and two-ray multipath ($n = 4$, $\varepsilon_{amp} = \varepsilon_{mp}$) models to approximate signal attenuation as a function of the distance between transmitters and receivers. The former assumes exactly one path, which must be clear from obstacles, between the transmitter and the receiver. The latter takes into account one dominant reflection from the ground in addition to the clear path. However, the two-ray multipath model is highly optimistic for cases, where the transmitter-receiver separation distance is small. Therefore, in most applications, the two models are combined; the free space model is used at small distances, while the two-ray multipath model is used at larger distances.

Table 1. Path loss exponent for different scenarios.

Different scenarios			**Path loss exponent (n)**
Off-Body	Short Range	LOS	2.0
		NLOS	2.5
	Mid Range	LOS	2.5
		NLOS	3.0
	Long Range	LOS	4.0
		NLOS	5.0
On-Body	LOS	arm	3.35
		leg	3.45
		back	2.28
		torso	3.23
		whole body	3.11
	NLOS	Around torso	5.9
		Along the front	3.0
In-Body	Short range (receiver on body subGHz)	Eye	2.0

Table 1 lists the values of the fitted path loss models for different scenarios. The parameter values for each channel model have been extracted from [Shankar], [Reusens], [Fort], and [Heinzelman] for the first, second, third, and fourth scenarios, respectively.

The few following notes are worthy of attention:

I- By using this extended version of the free space radio energy model, path loss exponents and model parameters of the NLOS scenarios correspond well with the ones of our model for LOS.

II- According to the anticipated channel quality, we change the path loss exponent in different scenarios; we assume that the transmitters are able to control their communication power according to the anticipated channel quality.

III- Propagation also depends on the type of antennas and their position, as well as on the body postures and movements. In addition, the channel characteristics for in-body and on-body area networks are different. In in-body area networks, signals propagate inside the human body and are affected by the body's electrical properties. In on-body area networks, the resulting signal is a combination of surface waves, creeping waves, scattered waves, diffracted waves, and free space propagation [Abouei].

IV- Even though in the studied protocols the trend is to mostly keep the radio off, the receiver's radio must inevitably be kept on in anticipation of an incoming packet. Hence, a more accurate energy model should take the energy spent in idle listening period into account. Typically, the energy dissipated in the idle mode is almost equal to the energy consumption in the receive mode.

CHAPTER 3

Network Layer and Optimal Cluster Size for Clustered WBANs

3.1 Routing Strategies in WBANs

Designing efficient routing protocols in WBANs is a nontrivial task on account of the specific characteristics of the wireless environment. First of all, the available bandwidth is limited, shared and can vary as a result of fading, noise and interference, hence, the protocol's usage of network control information should be limited. Secondly, the nodes that form the network can be very heterogeneous in terms of available energy or computational power. Although a considerable amount of research is being carried out toward energy-efficient routing in Wireless Sensor Networks (WSNs), the proposed solutions are not qualified for WBANs. For example, in WSNs maximal throughput and minimal communication overhead are considered to be more important than energy consumption. Energy efficient ad-hoc network protocols solely aim at finding routes in the network that minimize energy consumption in terminals with small energy resources, thereby neglecting factors such as the amount of operations (measurements, data processing, access to memory) and energy required to transmit and receive a useful bit over the wireless link [Latre]. Most protocols for WSNs only take into account networks with homogeneous nodes and many-to-one communication scenarios. In many cases the network is considered as a static one. In contrast, a WBAN has heterogeneous mobile devices with stringent quality of service (QoS) requirements. In short, specialized communication protocols for WBANs are needed.

In the following, an overview of existing routing protocols for WBANs is provided. They can be

categorized as follows: routing based on temperature, cluster based protocols, and cross-layer based routing. Figure 2 gives an overview of the existing routing strategies for WBANs sorted according to their year of emergence.

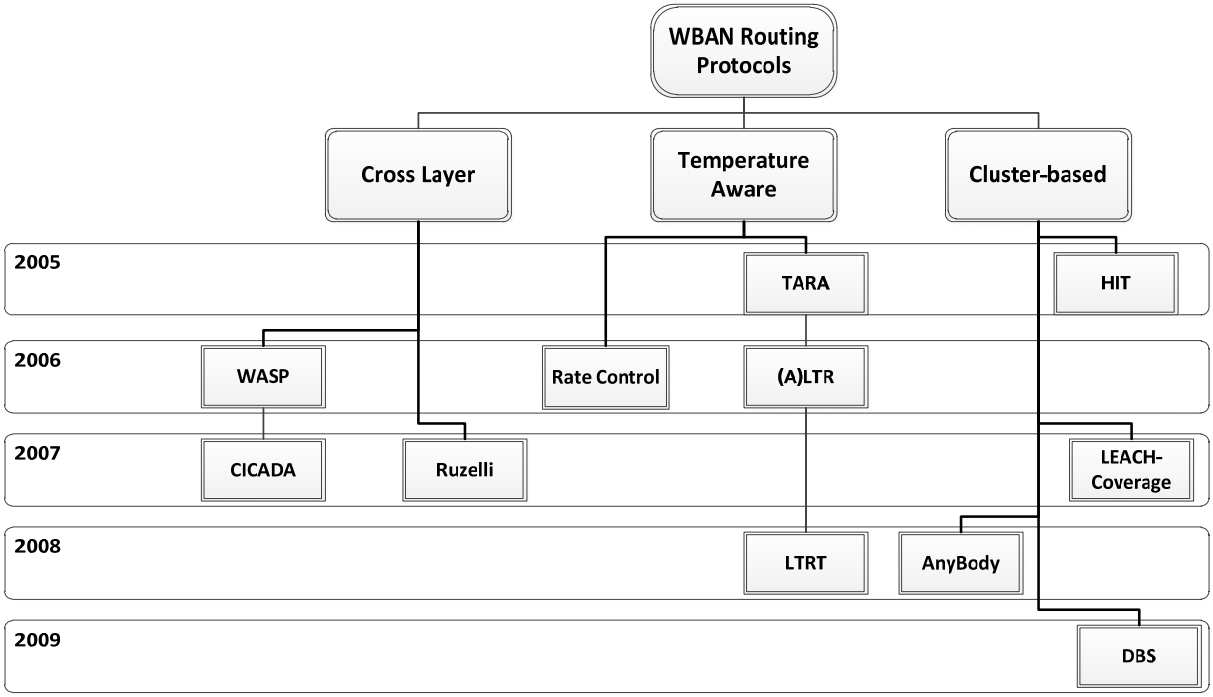

Figure 2. Overview of routing schemes in WBANs.

3.1.1 Cross-Layer Protocols

Cross-layer design is a way to improve the efficiency of and interaction between the protocols in a wireless network by combining two or more layers from the communication stack. This research has been in the interest of many researchers in the WSN area [Madan], [Melodia]. However, to date, only a little attention has been drawn to the WBANs domain.

Ruzzelli et al. [Ruzzelli] propose a cross-layer energy efficient multi-hop protocol built on IEEE 802.15.4 [Zasowski]. They divide the WBAN into time zones, where each time zone takes turn in the transmission. The nodes in the farthest time zone start the transmission. In the next slot, the one next to the farthest sends its data and so on until the BS is reached. The protocol almost doubles the lifetime

compared to regular IEEE 802.15.4. CICADA [Takahashi] exploits a data gathering tree and controls the data transmissions using distributed slot assignment. It results in low packet loss and high sleep ratios, while the network flexibility is maintained. Employing data-aggregation further improved the lifetime of the network further. Another approach for cross-layering completely discards the layered structure and implements the required functionality in different modules which interact and can be changed easily [De Poorter]. Another attempt for using modular approaches in WBANs is presented in [Latre2].

3.1.2 Temperature Routing

Radiation absorption and heating effects are of special importance when wireless communications are taking place in/on/around the body. Thereby, the thermal effects of WBANs should be considered in the routing protocol. To reduce tissue heating the radio's transmission power can be adjusted or traffic control algorithms can be used. In [Ren] rate control is adopted to reduce the heating effects in a single-hop network. Another option is to balance the communications over the sensor nodes. For instance, Thermal Aware Routing Algorithm (TARA) routes data away from high temperature areas (hot spots) [Tang]. Packets are withdrawn from heated zones and rerouted through alternate paths. TARA does not take reliability into consideration and suffers from short network lifetime and high packet loss.

Least Temperature Routing (LTR) and its variation Adaptive Least Temperature Routing (ALTR) [Bag] are improvements of TARA. LTR and ALTR reduce unnecessary hops; ALTR switches to shortest hop routing when a predetermined number of hops is reached in order to decease the energy consumption. A more clever combination of LTR and shortest path routing is Least Total Route Temperature (LTRT) presented in [Takahashi]; the node temperatures are translated into graph weights, whereby routes with minimum temperature are achieved using Dijkstra's algorithm. Enhanced energy efficiency and a lower temperature rise are accomplished, however LTRT has a main drawback, that is, a node requires to know the temperature of all other nodes in the network. Unfortunately, the overhead of obtaining this information was not investigated by the designers.

3.1.3 Cluster-Based Routing

Clustered WBANs yield low and balanced energy consumption due to rotation of energy-intensive tasks as well as performing data aggregation across the WBAN. From another perspective, they can help to achieve temperature-aware routing by rotating energy intensive tasks among the nodes based on their history and their location in the network.

"Anybody" [Watteyne] is a data gathering protocol that employs clustering to reduce the number of direct transmissions to the BS. Anybody is designed on the foundation of LEACH [Heinzelman] protocol. LEACH randomly selects a few sensor nodes as cluster heads and rotates their role to evenly distribute the energy load across the network. The cluster heads aggregate all the incoming data and send it to the BS. LEACH assumes that all nodes can directly communicate with the BS. Anybody solves this problem by applying different policies to the cluster head selection mechanism and building a backbone network of the cluster heads. Another variation of LEACH is Hybrid Indirect Transmissions (HIT) [Moh], which combines clustering the sensor nodes and forming chains of sensor nodes to improve the energy-efficiency of the entire network. LEACH-Coverage and DBS protocols, proposed in [Tsai] and [Amini2], are yet two other extensions to LEACH aiming at improving the sensing coverage and combating the energy imbalance, respectively.

The communications and timing sequence of the aforementioned protocols are nearly the same and the main difference arises from the cluster formation policies. All the aforementioned cluster-based protocols make use of probabilistic approaches to distribute the energy load evenly among the sensor nodes. To this end, they utilize randomization to ensure that the cluster head role is shared equally among all the nodes. These cluster-based protocols divide the schedule of the network into multiple rounds of fixed duration. As Figure 3 suggests, each round consists of a set-up phase and a number of time frames that construct the steady-state phase. During the set-up phase some sensor nodes elect themselves as cluster heads by using a distributed algorithm (which is an exclusive characteristic of each protocol) performed in each node. Afterwards, the elected nodes announce their election as cluster head to the rest of the nodes in the

network, and then other nodes organize themselves into local clusters by choosing the most appropriate cluster head (normally the closest cluster head). During the steady-state phase, within each frame the cluster heads receive sensor data from cluster members (according to TDMA schedule that was created and transmitted to them), and transfer the aggregated data to the BS. The transceiver of each non-cluster head can be turned off until the node's allocated transmission time (see Figure 3). It should be noted that the cluster heads exploit data-aggregation to filter and compress the redundant data before the final transmission to the BS.

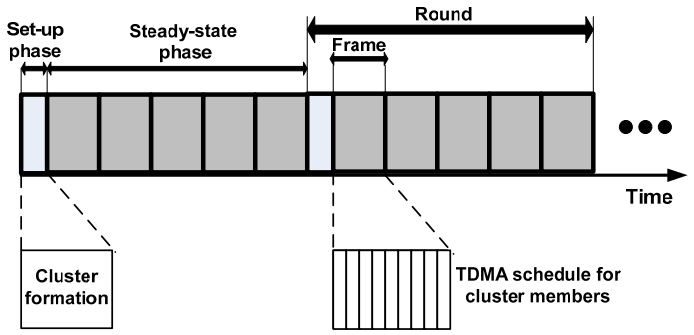

Figure 3. Timing in the studied protocols.

As it is implied, these protocols are all fully-distributed and they terminate in constant number of iterations. In addition, they incur low message overhead. To obtain a thorough understanding of the studied decentralized protocols, Table 2 summarizes the main characteristics of them. One may also incorporate the temperature characteristic in the clustering policies.

All of the aforementioned protocols have a mechanism to remember the nodes that have been elected as cluster head in recent rounds and this means that they consider the "frequency" of being a cluster head as one of their cluster formation metrics. For the sake of brevity, the following paragraphs describe the clustering policy of each protocol. Detailed description of LEACH, LEACH-Coverage, DBS, AnyBody, and HIT protocols can be found in [Heinzelman], [Tsai], [Amini3], [Watteyne], and [Moh], respectively.

Table 2. Comparison of decentralized cluster-based protocols.

Protocol	Cluster head selection metric				Main parameters
	Frequency	Sensing coverage	Connectivity	Distance to BS	
LEACH	Yes	No	No	No	k_{opt}
LEACH-Coverage	Yes	Yes	No	No	k_{opt}, η, α
DBS	Yes	No	No	Yes	k_{opt}, δp
AnyBody	Yes	No	Yes	No	ρ
HIT	Yes	No	Yes	No	ρ

LEACH: Adaptive and dynamic cluster head election was first utilized in LEACH protocol to guarantee the rotation of the energy intensive tasks (i.e., being cluster head) among all the nodes across the network. In LEACH, the optimal percentage of cluster head nodes (p) is equal to the ratio of the optimal number of clusters (k_{opt}) to the total number of sensor nodes in the network (N), i.e., $p = k_{opt}/N$. Correspondingly, the optimal cluster size would be equal to N/k_{opt}. During the cluster formation period, LEACH treats all the eligible sensor nodes without discrimination.

LEACH-Coverage: LEACH-Coverage protocol aims at maintaining the WBAN's sensing coverage. To do so, different probabilities of being cluster head are applied based on effective sensing area of a node that is a function of the node density around a node. Thus, cluster heads will be usually selected in the high density areas, where the death of few nodes does not affect the coverage of the network. LEACH-Coverage defines a parameter called estimated normalized effective sensing area ($0 < \eta(m) \leq 1$) for each node m in the sensor field. A node with a larger value of $\eta(m)$ will be assigned a smaller probability of being cluster head, and vice versa. It is evident that the nodes that die out first are the ones with a smaller normalized effective sensing area and therefore, their death has a minimal impact on the WBAN's sensing coverage, in that several nodes can compensate for their absence. The crucial nodes ($\eta = 1$) will not be elected as cluster heads, as no other node in the network can compensate for them. In other words, they are elected as cluster heads in every ∞ rounds. As it can be inferred, although the cluster head task is circulated among all the nodes, this circulation is weighted towards the nodes in high density areas. The

investigators in [Tsai] argue that the optimal number of clusters that yields the most energy-efficient behavior of the network is equal to that for LEACH protocol (k_{opt}). To adjust the number of clusters, LEACH-Coverage takes advantage of another parameter, denoted by α, which tunes the average number of clusters that are required in the network. It has been shown that for a dense sensor network, LEACH and LEACH-Coverage yield similar outcomes in terms of energy-efficiency [Tsai]. However, LEACH-Coverage outperforms LEACH with regard to the sensing coverage.

DBS: The main idea is that the nodes with more distance from the BS should be cluster head less often than the nodes with closer distance to BS, to ensure that a great difference between energy levels of a near node and a far node would not occur. By applying this idea the WBAN's energy-efficiency and sensing coverage will be enhanced. To this end, DBS divides the entire sensing field into multiple segments with equal areas. It is straightforward to show that in each round of DBS the expected number of clusters (cluster heads) is the same as LEACH by noting that the areas of all segments are the same and the probabilities are distributed fairly around p (i.e., $p \pm \delta p$, $p \pm 2\delta p$, ...). Therefore, DBS does not affect the quality of data, since both protocols deliver the same amount of data per unit time. Hence, as with LEACH-Coverage, the optimal number of clusters for DBS should be equal to that for LEACH. It can be shown that LEACH can be thought of as a special case of DBS if one sets $\delta p = 0$.

AnyBody: Anybody defines the density of a node (ρ) as the ratio between the number of links within the node's 2-hop neighbors and the number of 2-hop neighbors. Nodes with the highest local density, supposedly relatively important nodes, are selected as cluster head. The assumption of 2-hop neighborhood knowledge implies trading several hello packets in the network. The smallest ID will be used to decide between joint winners. Once a cluster head is elected, the cluster head's ID and its density is locally broadcasted by all nodes that have joined this cluster. The cluster can then enlarge itself until it reaches a cluster frontier of another cluster head. The only constraint that affects a cluster is that two neighbors cannot be both cluster head. This ensures that a cluster head is not too off-center in its own cluster, a cluster has at least a diameter of two, and that two cluster heads are separated by at least three

hops.

HIT: HIT uses clustering to reduce the number of direct transmissions to the remote BS, and allows parallel, multi-hop indirect transmissions (chains) even in the presence of multiple adjacent clusters. Nodes are elected randomly as in LEACH, but some nodes may not be eligible to become cluster-head due to lower levels of connectivity (ρ) or energy [Moh]. Although LEACH can evenly distribute the energy consumption among the sensors in the WBAN in long term, in short term (small time scale), it is very probable that some high temperature nodes will be selected as cluster head; this is because, the rotation of cluster heads is made in a completely random fashion.

It should be noticed that none of these protocols takes into account the residual energy of the nodes. Taking the residual energy into consideration, one can avoid the formation of dead-areas [Amini3] within the WBAN, which is known as the energy hole (hot spot) problem. However, the cluster-based protocol will no longer be decentralized (fully-distributed), since solving the energy hole problem requires global knowledge regarding the network in a periodic fashion and therefore, it implies the existence of a powerful node as a centralized controller.

3.1.3.1 Data Aggregation

In cluster-based schemes, the cluster heads are responsible for aggregating their cluster members' data signals to produce a single representative signal, expending lE_{DA} nJ/signal for each l-bit input signal, where E_{DA} indicates the prorated cost of aggregation for a single bit.

Many authors in the literature assume that cluster heads have the ability to perfectly aggregate multiple incoming packets into one outgoing packet. Likewise, we do not deal with a particular data aggregation algorithm, but only with the amount of data generated in the aggregation process. In this paper, it is assumed that all sensors in a cluster sense the same event. This assumption will be met if either of two conditions holds: 1) the distance between nodes within a cluster is small with respect to the distance from which events can be sensed; 2) if the distance between events happening in the environment is large

[Heinzelman]. However, it is worth noting that aside from the data aggregation algorithm, other factors such as application requirements and the type of sensor data impact the aggregated data produced by the cluster head nodes.

3.1.3.2 Lifetime Definition

The lifetime of WBANs/WSNs is the time span from the deployment to the instant when the network is considered nonfunctional. However, when a network should be considered nonfunctional is application-specific. It can be, for example, the instant when the first node dies (e.g., athletic performance monitoring), a certain percentage of sensors die (e.g., the artificial retina), the network partitions, or loss of coverage occurs (physiological monitoring of first responders). In some cases it is necessary that all nodes stay alive as long as possible, since network quality decreases considerably as soon as one node dies. In these scenarios it is important to know when the first node dies. On the other hand, in some cases, sensors can be placed in proximity to each other. Thus, adjacent sensors could record related or identical data. Hence, the loss of a single or few nodes does not automatically diminish the quality of service of the network. For our optimization problem, the latter is considered as the lifetime. Accordingly, the network lifetime is considered as the total available energy (E_{total}) divided by total energy consumption during a round (E_{round}), i.e., E_{total}/E_{round}.

3.2 Optimization of Communication Energy

During the last few years, the optimization of communication energy in WSNs and particularly, in WBANs has been investigated quite extensively. This optimization problem can be in the form of efficient number of hops in multi-hop networks [Shu], efficient cluster size (or number of clusters) in dense many-to-one sensor networks [NKim], and optimal transmission scheme in networks with different channel fading models [Paschalidis], [Madan].

Authors in [NKim] derived an analytical model to achieve the optimal number of clusters for multi-hop WSNs. Their proposed analytical model is based on the assumption that all the sensor nodes employ

multi-hop scheme to convey their data to cluster heads. In order to estimate the energy consumption for communications, they have considered an average hop count between a normal node and its nearest cluster head for the entire network without assuming a specific shape for the sensing field. In a recent work, Wang et al. [Wang] proposed a physical/medium access control/network cross-layer analytical design approach to determine the optimal number of clusters in dense sensor networks. They argue that different layers impose contradicting requirements on the cluster size.

In [Heinzelman], the designers of LEACH communication protocol calculate the efficient number of clusters, whereby the network will save a huge amount of energy. However, their results solely specify an interval to which the optimal number of clusters belongs. It can be shown that in many network configurations, their analytical results produce a long interval and therefore, one has to find the optimal number of clusters through simulations for all the numbers that belong to the aforementioned interval. In the same manner, investigators in [HWang] do not provide the closed-form results.

Recent work by Kumar et al. [Kumar] aims to extract the optimal number of clusters that would lead to minimum energy consumption. Although, their analytical approach is consistent with the results reported in [Heinzelman], they make invalid assumptions about the average distance of the cluster head nodes to the BS. Likewise, the approaches presented in [Chan] and [HKim] attempt to solve the problem of optimal number of clusters, however, they do not take into account the energy consumed by the cluster head nodes when they receive the data from their cluster members.

3.3 Optimal Cluster Size - General Optimization Problem

Unlike approaches in the above-cited papers, a general framework to determine the optimal clustering parameters is presented in this work. This way, several cluster-based protocols that are designed for WBANs can become more energy-efficient through employing the appropriate number of clusters.

Although it has been shown that, in the sense of total energy consumption, the optimal number of clusters for all of the mentioned protocols is the same, none of them properly makes use of the optimal

cluster size. The concepts of cluster size and number of clusters are used interchangeably in this paper. It is because the cluster size is equal to total number of the nodes divided by the number of clusters (i.e., N/k_{opt}).

The optimal construction of clusters (which is equivalent to setting the optimal probability for a node to become a cluster head) is very influential with regard to total energy expenditure and thus, the lifetime of the WBAN. In [Heinzelman], the authors showed that if the clusters are not created in an optimal way, the total energy expenditure of the network is increased exponentially either when the number of clusters constructed is greater than the optimal number of clusters or especially when the number of clusters is less. This implies that there exists an optimal number of nodes that should be cluster heads (k_{opt}). If the number of cluster heads is less than k_{opt}, a remarkable number of nodes have to transmit their data very far to reach the cluster head, causing the global energy expenditure in the system to be large. On the other hand, if there are more than k_{opt} cluster heads, there is less data aggregation being performed locally and an enormous number of transmissions are required to monitor the entire sensing field.

In cluster-based communication protocols, the cluster formation algorithm ensures that the expected number of clusters per round equals k_{opt}, which is a predetermined system parameter. In this section, using the computation and communication energy model presented in Chapter 2, the optimal value for k_{opt} is analytically determined. In order to generalize the results, sensor field is assumed to be an arbitrary shape with area A. In a similar manner, no requirements with respect to the location of the BS and the radio propagation model (free space, two-ray, etc.) are imposed. However, in order to extract a closed-form expression for k_{opt}, subsequently, a number of special cases are considered to obtain an explicit parametric formula. It is shown that the optimization problem leads to an integral whose solution yields the expected nth power of distance between the BS and the sensor field, where n is the path loss exponent. This integral can be evaluated in closed-form under certain network configurations. Moreover, the optimization problem requires us to compute the expected squared distance between cluster members and their cluster head.

In order to extend the network lifetime, one should minimize total energy expenditure of the network and therefore, total energy consumption during a round (see Figure 3), denoted by E_{round}. Assume that the sensing field is of an arbitrary shape of area A over which N nodes are distributed randomly and uniformly. If there are k_{opt} clusters, there will be on average N/k_{opt} nodes per cluster (including one cluster head and (N/k_{opt}) - 1 non-cluster head nodes). Each cluster head dissipates energy receiving signals from the nodes, aggregating the signals, and transmitting the aggregated data to the BS [Heinzelman]. Hence, the energy dissipated in a cluster head node during a single round with the assumption that each round has one frame (see Figure 3) is:

$$E_{CH} = (\frac{N}{k_{opt}} - 1)lE_{elec}^{Rx} + \frac{N}{k_{opt}}lE_{DA} + lE_{elec}^{Tx} + l\varepsilon_{amp}d_{toBS}^{n}, \quad (2)$$

where l is the number of bits in each data message and d_{toBS} is the distance between the cluster head node and the BS. It should be noticed that by adopting perfect data aggregation, each cluster head needs to process N/k_{opt} signals of length l. Please note that the current analysis does not apply to cluster-based communication protocols using multi-hop approaches to convey cluster heads' data to the base station. We defer the multi-hop analysis to the Appendix.

On the other hand, each non-cluster head node transmits its data to the cluster head once per round. Understandably, the distance to the cluster head is small relative to the distance to the BS. Accordingly, the energy dissipation for non-cluster head nodes favorably follows the free-space model [Braem] and can be written as:

$$E_{non-CH} = lE_{elec}^{Tx} + l\varepsilon_{fs}d_{toCH}^{2}, \quad (3)$$

where d_{toCH} is the distance between the non-cluster head node and its cluster head. The area of each cluster is approximately A/k_{opt}. One may argue that each cluster can be approximated by a circle of radius $(A/\pi k_{opt})^{1/2}$, where the cluster head resides at the center.

Since the expected squared distance between a random point in a circle of radius S and its center is

$S^2/2$, the value of d_{toCH}^2 can be determined with respect to A and k_{opt}. This can be obtained straightforwardly by drawing a hypothetical circle around the center (cluster head) and equating the area of this circle to half of the area of the original circle (area of the cluster). Solving the resulting equation for squared radius of the hypothetical circle, which is in fact equal to d_{toCH}^2, yields:

$$E[d_{toCH}^2] = \frac{A}{2\pi k_{opt}}. \tag{4}$$

By substituting (4) into (3), the energy used in each non-cluster head node per round is given by:

$$E_{non-CH} = lE_{elec}^{Tx} + \frac{l\varepsilon_{fs}A}{2\pi k_{opt}}. \tag{5}$$

The energy dissipated in an entire cluster during a single round can be expressed as follows:

$$E_{cluster} = E_{CH} + (\frac{N}{k_{opt}} - 1)E_{non-CH}. \tag{6}$$

Hence, E_{round} can be determined as follows:

$$\begin{aligned} E_{round} &= k_{opt}E_{cluster} \\ &= NlE_{elec}^{Rx} - k_{opt}lE_{elec}^{Rx} + NlE_{DA} + k_{opt}l\varepsilon_{amp}d_{toBS}^n + NlE_{elec}^{Tx} \\ &\quad + \frac{Nl\varepsilon_{fs}A}{2\pi k_{opt}} - \frac{l\varepsilon_{fs}A}{2\pi}. \end{aligned} \tag{7}$$

The first and second derivatives of E_{round} with respect to k_{opt} are:

$$\begin{aligned} \frac{\partial E_{round}}{\partial k_{opt}} &= l\varepsilon_{amp}d_{toBS}^n - lE_{elec}^{Rx} - \frac{Nl\varepsilon_{fs}A}{2\pi k_{opt}^2} \\ \frac{\partial^2 E_{round}}{k_{opt}^2} &= \frac{Nl\varepsilon_{fs}A}{\pi k_{opt}^3} > 0. \end{aligned} \tag{8}$$

As (8) suggests, the non-negativity of the second derivative is evident and hence, by setting the first derivative to zero, the optimal number of clusters can be found:

$$k_{opt} = \sqrt{\frac{N\varepsilon_{fs}A}{2\pi(\varepsilon_{amp}d_{toBS}^n - E_{elec}^{Rx})}}. \tag{9}$$

The above equation for the optimal number of clusters points out that k_{opt} is principally determined by

N, A, and d_{toBS}. Further, path loss exponent (n) and the energy consumption of the receiver's circuitry (E_{elec}^{Rx}) are also of importance as factors that can substantially change the optimal number of clusters and more fundamentally, they can make a decision on whether or not it is worth to perform clustering. To find the optimal value of k_{opt}, one has to substitute the minimum and maximum values of d_{toBS} in (9) and afterwards, the upper and lower bounds of k_{opt} can be achieved. Finally, k_{opt} will be selected from this interval according to simulations regarding the total energy expenditure of the network.

As such, it is desirable to replace d_{toBS} in (9) with a term containing other parameters such as N and A. However, unless the network configuration is symmetric in the sense of the shape of sensing field and the position of the BS, it is not feasible to obtain such a convenient term.

3.4 Optimal Cluster Size - Closed-Form Solutions

A number of widely-used network configurations are considered for which a closed-form expression for the optimal number of clusters can be achieved. The optimal cluster size can then be simply derived, given that it equals N/k_{opt}. In such networks, the shape of the sensing field and/or the position of the BS with respect to the sensing field are, to some extent, symmetric. By symmetry considerations, the expected value of different powers of distance between the nodes across the sensing field and the BS (i.e., d_{toBS}, d_{toBS}^2, d_{toBS}^4) has been derived. Please find the derivations (A through P) at the end of this section.

Plugging the proper expected values into (9) yields the optimal number of clusters and thus, energy-efficient cluster size that the network should possess. Table 3 lists closed-form expressions to achieve the optimal number of clusters for different criteria.

Although the sensing field can be of any shape, circular (radius = R) and square-shaped (side length = M) sensing fields are of special interest in most of the research projects due to their central and axial symmetry. Therefore, these two symmetric shapes are assumed for the sensing field to evaluate the optimal cluster size. Moreover, two radio propagation models (free space and two-ray) are followed for communications during the steady-state phase (see Section 3.1.3). As for location of the BS, to cover all

possible configurations, the BS is put inside, outside and on the boundary of the sensing field. It should be noted that, in network configurations where the BS is outside the sensing field, the distance of the BS to the center of the sensing field is symbolized by L. Furthermore, two main categories are considered and reported; networks containing sensor nodes with negligible receive energy (E_{Rx}) comparing to the transmit energy (E_{Tx}) (see, e.g., [Wu] and [Dardari]) and networks in which the receive energy is comparable to the transmit energy (see, e.g., [Braem] and [Chang]).

Generally, the optimal number of clusters (k_{opt}) is determined by parameters such as total number of nodes (N), dimensions of the sensing field (M or R), distance of the nodes to the BS (d_{toBS}), energy consumption of the receiver's circuitry (E_{elec}^{Rx}), and the energy dissipation of the transmitter amplifier (ε_{amp}), i.e.,

$$k_{opt} = f(N, M \text{ or } R,\ d_{toBS}, E_{elec}^{Rx}, \varepsilon_{amp}). \tag{38}$$

It can be inferred from (9) and Table 3 that the optimal number of clusters and hence, the optimal cluster size are always independent of energy consumption of the transmitter's circuitry (E_{elec}^{Tx}). This can be justified through the fact that E_{elec}^{Tx} does not appear in the first derivative of E_{round} (refer to Section 3.3).

Yet another interesting property pointed out by Table 3 is that under certain conditions, the optimal cluster size is independent of the size of the sensing field. Such conditions imply that E_{elec}^{Rx} should be small comparing to E_{elec}^{Tx}, the wireless transmissions are governed by free space radio propagation model, and the BS is not located outside of the sensing field. As Table 3 suggests, if the above requirements are met, the optimal number of clusters and thus, the optimal cluster size will solely depend on the number of sensor nodes across the network, that is $k_{opt} = f(N)$. More specifically, if the sensing area is square-shaped or circular, the optimal number of clusters can be expressed as $B\sqrt{N}$, where B is a constant with

maximum value of 1. Simulation results in Section 3.5 will verify these claims.

Table 3. Closed-form expressions for the optimal number of clusters.

Sensing field	Radio model	Location of BS	Optimal number of clusters	Optimal number of clusters (small E_{Rx})
Square ($M \times M$)	Free space	Center	$k_{opt} = \sqrt{\frac{N\varepsilon_{fs}M^2}{2\pi(\varepsilon_{fs}M^2/6 - E_{elec}^{Rx})}}$ (10)	$k_{opt} = \sqrt{\frac{3N}{\pi}} = 0.977\sqrt{N}$ (11)
		Corner	$k_{opt} = \sqrt{\frac{N\varepsilon_{fs}M^2}{2\pi(\varepsilon_{fs}2M^2/3 - E_{elec}^{Rx})}}$ (12)	$k_{opt} = \sqrt{\frac{3N}{4\pi}} = 0.489\sqrt{N}$ (13)
		Side's midpoint	$k_{opt} = \sqrt{\frac{N\varepsilon_{fs}M^2}{2\pi(\varepsilon_{fs}5M^2/12 - E_{elec}^{Rx})}}$ (14)	$k_{opt} = \sqrt{\frac{6N}{5\pi}} = 0.618\sqrt{N}$ (15)
		Outside (on the axis of symmetry)	$k_{opt} = \sqrt{\frac{N\varepsilon_{fs}M^2}{2\pi(\varepsilon_{fs}(M^2/6 + L^2) - E_{elec}^{Rx})}}$ (16)	$k_{opt} = \sqrt{\frac{NM^2}{2\pi(M^2/6 + L^2)}}$ (17)
	Two-ray	Center	$k_{opt} = \sqrt{\frac{N\varepsilon_{fs}M^2}{2\pi(\varepsilon_{mp}7M^4/180 - E_{elec}^{Rx})}}$ (18)	$k_{opt} = \sqrt{\frac{90N\varepsilon_{fs}}{7\pi\varepsilon_{mp}M^2}}$ (19)
		Corner	$k_{opt} = \sqrt{\frac{N\varepsilon_{fs}M^2}{2\pi(\varepsilon_{mp}28M^4/45 - E_{elec}^{Rx})}}$ (20)	$k_{opt} = \sqrt{\frac{45N\varepsilon_{fs}}{56\pi\varepsilon_{mp}M^2}}$ (21)
		Side's midpoint	$k_{opt} = \sqrt{\frac{N\varepsilon_{fs}M^2}{2\pi(\varepsilon_{mp}193M^4/720 - E_{elec}^{Rx})}}$ (22)	$k_{opt} = \sqrt{\frac{360N\varepsilon_{fs}}{193\pi\varepsilon_{mp}M^2}}$ (23)
		Outside (on the axis of symmetry)	$k_{opt} = \sqrt{\frac{N\varepsilon_{fs}M^2}{2\pi(\varepsilon_{mp}(\frac{7M^4}{180} + \frac{2}{3}M^2L^2 + L^4) - E_{elec}^{Rx})}}$ (24)	$k_{opt} = \sqrt{\frac{N\varepsilon_{fs}M^2}{2\pi\varepsilon_{mp}(\frac{7M^4}{180} + \frac{2}{3}M^2L^2 + L^4)}}$ (25)
Circle (Radius = R)	Free space	Center	$k_{opt} = \sqrt{\frac{N\varepsilon_{fs}R^2}{R^2\varepsilon_{fs} - 2E_{elec}^{Rx}}}$ (26)	$k_{opt} = \sqrt{N}$ (27)
		Circumference	$k_{opt} = \sqrt{\frac{N\varepsilon_{fs}R^2}{\varepsilon_{fs}3R^2 - 2E_{elec}^{Rx}}}$ (28)	$k_{opt} = \sqrt{N/3} = 0.577\sqrt{N}$ (29)
		Outside	$k_{opt} = \sqrt{\frac{N\varepsilon_{fs}R^2}{2(\varepsilon_{fs}(R^2/2 + L^2) - E_{elec}^{Rx})}}$ (30)	$k_{opt} = \sqrt{\frac{NR^2}{2(R^2/2 + L^2)}}$ (31)
	Two-ray	Center	$k_{opt} = \sqrt{\frac{N\varepsilon_{fs}R^2}{2(\varepsilon_{mp}R^4/3 - E_{elec}^{Rx})}}$ (32)	$k_{opt} = \sqrt{\frac{3N\varepsilon_{fs}}{2\varepsilon_{mp}R^2}}$ (33)
		Circumference	$k_{opt} = \sqrt{\frac{N\varepsilon_{fs}R^2}{2(\varepsilon_{mp}10R^4/3 - E_{elec}^{Rx})}}$ (34)	$k_{opt} = \sqrt{\frac{3N\varepsilon_{fs}}{20\varepsilon_{mp}R^2}}$ (35)
		Outside	$k_{opt} = \sqrt{\frac{N\varepsilon_{fs}R^2}{2(\varepsilon_{mp}(\frac{R^4}{3} + L^4 + 2R^2L^2) - E_{elec}^{Rx})}}$ (36)	$k_{opt} = \sqrt{\frac{N\varepsilon_{fs}R^2}{2\varepsilon_{mp}(\frac{R^4}{3} + L^4 + 2R^2L^2)}}$ (37)

The optimal number of clusters has its largest value when the BS is located at the center of the sensing field (for instance, compare (11) against (13) and (15)). This is as anticipated, since the expected value of the *n*th power of distance between the cluster heads and the BS ($E[d_{toBS}^{n}]$) has its least value in such configuration. Correspondingly, as the BS moves from the center of the sensing area towards the boundary and then to the outside of the sensing field, optimal number of clusters will be reduced.

Eventually, in case the BS is located very far from the sensing field, the network will have one cluster whose size and area are equal to N and A, respectively. In other words, only one long-haul transmission is done within each round to save energy. Likewise, whenever E_{elec}^{Rx} dominates $\varepsilon_{amp} d_{toBS}^{n}$ (transmit amplifier energy), according to (9), k_{opt} becomes very large so that it is no longer worth clustering the sensing field and thus, having N clusters of size 1 is more efficient in terms of total energy expenditure of the network. In general, it should be noticed that whenever the value of each expression reported in Table 3 becomes undefined, one can draw the conclusion that the optimal number of clusters might be equal to N, that is, all the nodes acting as cluster head and there is no intra-cluster communication.

As previously mentioned, the expected value of different powers of distance between the nodes across the sensing field and the BS (i.e., d_{toBS}, d_{toBS}^{2}, d_{toBS}^{4}) has been derived as follows:

A. Calculation of d_{toBS} (BS at the center of the square): Let the sensing field be in the shape of a square of side M and assume that the BS is located at the center of the sensing field. The probability P that the distance between a randomly chosen point and the BS located at the center of the square is less than x should be obtained. Calculation of P for cases in which x is less than or equal to $M/2$ is trivial. However, as indicated in Figure 4, this calculation is more complicated in cases where the hypothetical circle around the center of the square intersects with the perimeter of the square.

The value of angle φ in Figure 4 is used to derive the area of the portion of square that overlaps with the hypothetical circle (see the gray area). According to Figure 4, the angle φ is given by:

$$\varphi = \arctan(\frac{\sqrt{x^2 - M^2/4}}{M/2}). \tag{39}$$

It is evident that the minimum and maximum value of φ are 0 rad and $\pi/4$ rad, respectively. Bases on the above discussions, P can be determined as follows:

$$P(d_{toBS} \le x) = \begin{cases} \dfrac{\pi x^2}{M^2} & if\ 0 \le x \le \dfrac{M}{2} \\ \dfrac{\pi x^2 - 4[x^2\varphi - L(M/2)}{M^2} & if\ \dfrac{M}{2} \le x \le \dfrac{\sqrt{2}M}{2}. \end{cases} \tag{40}$$

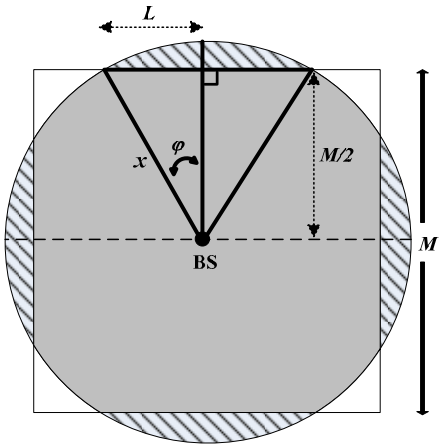

Figure 4. Square-shaped sensing field with BS at the center and $x > M/2$.

Correspondingly, the probability density function is given by:

$$f(x) = \begin{cases} \dfrac{\pi x}{M^2/2} & if\ 0 \le x \le \dfrac{M}{2} \\ \dfrac{\pi x}{M^2/2} - \dfrac{2x}{M^2/4}\varphi & if\ \dfrac{M}{2} \le x \le \dfrac{\sqrt{2}M}{2}. \end{cases} \tag{41}$$

To find the expected value of the distance from the center to the entire area of the square, one must integrate xf(x) in the interval [0, $M\sqrt{2}/2$], which yields:

$$E[d_{toBS}] = \frac{M(\sqrt{2} + \ln(1+\sqrt{2})}{6} \approx 0.383M. \tag{42}$$

B. Calculation of d^2_{toBS} (BS at the center of the square): Let the sensing field be in the shape of a square of side M and assume that the BS is located at the center of the sensing field. Further, assume that

the origin of the coordinate system resides at the center of the field. The expected squared distance from the BS can be obtained as follows:

$$E[d_{toBS}^2] = E[x^2 + y^2] = \frac{1}{M^2}\int_{-M/2}^{M/2}\int_{-M/2}^{M/2}(x^2 + y^2)dxdy$$
$$= \frac{4M^4}{24M^2} = \frac{M^2}{6}. \quad (43)$$

C. Calculation of d_{toBS}^4 (BS at the center of the square): The expected fourth power of distance from the BS is:

$$E[d_{toBS}^4] = E[(x^2 + y^2)^2] = E[x^4] + E[y^4] + 2E[x^2]E[y^2] =$$
$$\frac{1}{M}\int_{-M/2}^{M/2}x^4dx + \frac{1}{M}\int_{-M/2}^{M/2}y^4dy + 2\frac{M^2}{12}\frac{M^2}{12} =$$
$$\frac{M^4}{80} + \frac{M^4}{80} + \frac{M^4}{72} = \frac{7M^4}{180}. \quad (44)$$

D. Calculation of d_{toBS} (BS at the center of the circle): For a circular sensing field, the expected distance from the BS (located at the center) to the entire area of the circle is:

$$E[d_{toBS}] = \frac{1}{A}\int_{r=0}^{r=R} rf(r)dr = \frac{1}{\pi R^2}\int_{r=0}^{r=R} r.2\pi r dr = \frac{2R}{3}. \quad (45)$$

E. Calculation of d_{toBS}^2 (BS at the center of the circle): Similarly, the expected squared distance between the BS to the circular sensing field can be expressed as:

$$E[d_{toBS}^2] = \int_{\theta=0}^{2\pi}\int_{r=0}^{r=R} r^2\rho(r,\theta)\,rdrd\theta =$$
$$\frac{1}{\pi R^2}\int_{\theta=0}^{2\pi}\int_{r=0}^{R} r^3.drd\theta = \frac{R^2}{2}. \quad (46)$$

F. Calculation of d_{toBS}^4 (BS at the center of the circle): In the same manner, the expected fourth power of distance from the BS is given by:

$$E[d_{toBS}^4] = \int_{\theta=0}^{2\pi}\int_{r=0}^{r=R} r^4\rho(r,\theta)\,rdrd\theta =$$
$$= \frac{1}{\pi R^2}\int_{\theta=0}^{2\pi}\int_{r=0}^{R} r^5 drd\theta = \frac{R^4}{3} \quad (47)$$

G. Calculation of d_{toBS} (BS on perimeter of the square): We calculate the expected distance from the points within a square-shaped sensing field to BS that resides in the corner of the field and more generally, a BS whose location is an arbitrary point on perimeter of the sensing field. First consider a network where all of the nodes reside on a segment of a straight line (line segment TS in Figure 5) of length k and the BS is located at distance L from TS. One can verify that the expected distance from the BS to the line segment TS can be determined through the following expression:

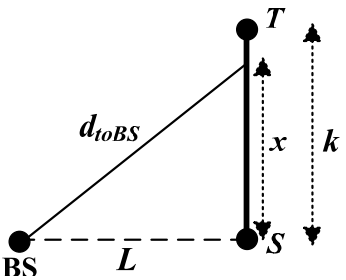

Figure 5. Line segment TS represents the location of the sensor nodes and the BS is an external point.

$$E[d_{toBS}] = \frac{1}{2k}(k\sqrt{L^2 + k^2} + L^2 \operatorname{arcsinh}\frac{k}{L}). \tag{48}$$

As illustrated in Figure 6, suppose that the BS is in the corner of a square-shaped sensing field.

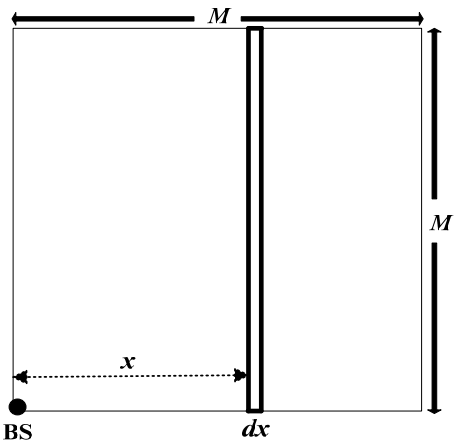

Figure 6. Square-shaped sensing field with BS in the corner.

The contribution of the narrow band shown in Figure 6 to the total distance from the BS is:

$$E[d_{toBS}] = \frac{1}{2}(M\sqrt{x^2 + M^2} + x^2 \operatorname{arcsinh}\frac{M}{x})dx. \tag{49}$$

Therefore, the expected distance $E[d_{toBS}]$ to all the points (sensor nodes) within the square is given by:

$$\begin{aligned}
&E[d_{toBS}] = \frac{1}{2M^2}\int_0^M (M\sqrt{x^2 + M^2} + x^2 \operatorname{arcsinh}(\frac{M}{x}))dx = \\
&\frac{1}{2M^2}(\frac{M}{2}\left[x\sqrt{x^2 + M^2} + M^2 \operatorname{arcsinh}(\frac{x}{M})\right]_0^M + \\
&\left[\frac{x^3}{3}\operatorname{arcsinh}(\frac{M}{x}) + \frac{Mx}{6}\sqrt{x^2 + M^2} - \frac{M^3}{6}\operatorname{arcsinh}(\frac{x}{M})\right]_0^M) = \\
&\frac{1}{6M^2}(M^3 \operatorname{arcsinh}(1) + M^3 \operatorname{arcsinh}(1) + 2\sqrt{2}M^3) = \\
&\frac{M}{3}(\operatorname{Ln}(1 + \sqrt{2}) + \sqrt{2}) \approx 0.765M.
\end{aligned} \tag{50}$$

Hence, the general problem of the expected distance from the nodes in the interior of the square to the BS that is located on an arbitrary point on perimeter of the square (see Figure 7) can be solved.

Let the distance between the midpoint and BS be x. Then the expected distance between the interior nodes and the BS can be evaluated by two consecutive applications of the expression for corner:

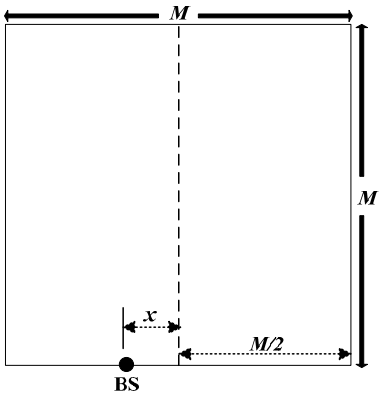

Figure 7. Square-shaped sensing field with BS on perimeter.

$$\begin{aligned}
&E[d_{toBS}] = \frac{1}{6M^2}((\frac{M}{2} + x)^3 \operatorname{arcsinh}(\frac{2M}{M + 2x}) + \\
&M^3 \operatorname{arcsinh}(\frac{M + 2x}{2M}) + M(M + 2x)\sqrt{(\frac{M}{2} + x)^2 + M^2} \\
&+ (\frac{M}{2} - x)^3 \operatorname{arcsinh}(\frac{2M}{M - 2x}) + M^3 \operatorname{arcsinh}(\frac{M - 2x}{2M}) + \\
&M(M - 2x)\sqrt{(\frac{M}{2} - x)^2 + M^2}).
\end{aligned} \tag{51}$$

In the similar manner, consider a network where the BS is put at the center of the side (on midpoint, i.e., $x = 0$ in see Figure 7). Substituting zero in place of x yields:

$$E[d_{toBS}] = \frac{1}{6M^2}((\frac{M}{2})^3 \operatorname{arcsinh}(2) + M^3 \operatorname{arcsinh}(\frac{1}{2}) + M^2\sqrt{\frac{5M^2}{4}} + (\frac{M}{2})^3 \operatorname{arcsinh}(2) + M^3 \operatorname{arcsinh}(\frac{1}{2}) + M^2\sqrt{\frac{5M^2}{4}} = \frac{M}{3}(\frac{\operatorname{arcsinh}(2)}{8} + \operatorname{arcsinh}(\frac{1}{2}) + \frac{\sqrt{5}}{2}) = 0.593M. \quad (52)$$

H. Calculation of d^2_{toBS} (BS on perimeter of the square): Now suppose that the BS is located at the origin of the coordinate system which is considered to be in the bottom left corner of the sensing field. The expected squared distance from the BS can be obtained as follows:

$$E[d^2_{toBS}] = E[x^2 + y^2] = E[x^2] + E[y^2] = \\ = \frac{1}{M}\int_0^M x^2 dx + \frac{1}{M}\int_0^M y^2 dy = \frac{2M^2}{3}. \quad (53)$$

As another configuration, let the BS be located on the midpoint of the bottom side of the sensing field, while the origin is still in the bottom left corner. This time, the expected squared distance from the BS is determined by:

$$E[d^2_{toBS}] = E[(x - \frac{M}{2})^2 + y^2] = E[x^2] - ME[x] + \frac{M^2}{4} + E[y^2] = \\ \frac{1}{M}\int_0^M x^2 dx - \frac{M}{M}\int_0^M x dx + \frac{M^2}{4} + \frac{1}{M}\int_0^M y^2 dy = \frac{5M^2}{12}. \quad (54)$$

I. Calculation of d^4_{toBS} (BS on perimeter of the square): With regards to the expected fourth power of distance from the BS to the sensing field, suppose that the BS and origin of the coordinate are both located in the bottom corner of the square. The expected fourth power of distance can be expressed as follows:

$$E[d^4_{toBS}] = E[(x^2 + y^2)^2] = E[x^4] + E[y^4] + 2E[x^2]E[y^2] = \\ \frac{1}{M}\int_0^M x^4 dx + \frac{1}{M}\int_0^M y^4 dy + 2\frac{M^2}{3}\frac{M^2}{3} \\ \frac{M^4}{5} + \frac{M^4}{5} + \frac{2M^4}{9} = \frac{28M^4}{45}. \quad (55)$$

However, if the BS is put on the midpoint of the bottom side of the sensing field, we obtain:

$$E[d_{toBS}^4] = E[((x - \frac{M}{2})^2 + y^2)^2] = E[x^4] - 2ME[x^3] + \frac{M^2}{2}E[x^2]$$
$$+ 2E[x^2]E[y^2] + M^2E[x^2] - \frac{M^3}{2}E[x] - 2ME[x]E[y^2] + \frac{M^4}{16} +$$
$$\frac{M^2}{2}E[y^2] + E[y^4] = \frac{M^4}{5} - 2M\frac{M^3}{4} + \frac{M^2}{2}\frac{M^2}{3} + 2\frac{M^2}{3}\frac{M^2}{3} +$$
$$M^2\frac{M^2}{3} - \frac{M^3}{2}\frac{M}{2} - 2M\frac{M}{2}\frac{M^2}{3} + \frac{M^4}{16} + \frac{M^2}{2}\frac{M^2}{3} + \frac{M^4}{5} = \quad (56)$$
$$\frac{2M^4}{5} - \frac{11M^4}{16} + \frac{5M^4}{9} = \frac{193M^4}{720}.$$

J. Calculation of d_{toBS} (BS on circumference of the circle): The expected distance from the BS to the entire area of the circular sensing field assuming that the BS resides on circumference of circle is given by:

$$E[d_{toBS}] = \frac{32R}{9\pi}. \quad (57)$$

K. Calculation of d_{toBS}^2 (BS on circumference of the circle): Likewise, the expected squared distance between the BS (residing on circumference) to the circular sensing field can be expressed as:

$$E[d_{toBS}^2] = \int_{x=0}^{x=x_{\max}} \int_{y=0}^{y=y_{\max}} [x^2 + (y+R)^2]\rho(x,\mathrm{y})dxdy =$$
$$\frac{1}{A}\int_{\theta=0}^{2\pi}\int_{r=0}^{r=R}(r^2 + 2rR\cos\theta + R^2)rdrd\theta = \frac{3R^2}{2}. \quad (58)$$

L. Calculation of d_{toBS}^4 (BS on circumference of the circle): In the same manner, the expected fourth power of distance from the sensing area to the BS, which is positioned on the circumference of the sensing area can be written as follows:

$$E[d_{toBS}^4] = \int_{x=0}^{x=x_{\max}} \int_{y=0}^{y=y_{\max}} [x^2 + (y+R)^2]^2 \rho(x,\mathrm{y})dxdy =$$
$$\frac{1}{\pi R^2}\int_{\theta=0}^{2\pi}\int_{r=0}^{\mathrm{R}}(r^2 + 2rR\cos\theta + R^2)^2 rdrd\theta =$$
$$\frac{1}{\pi R^2}\int_{\theta=0}^{2\pi}(\frac{7R^6}{6} + R^6\cos^2\theta) = \frac{10R^4}{3}. \quad (59)$$

M. Calculation of d^2_{toBS} (BS outside of the square): Assume that the BS is located outside the sensing field whose shape is a square of side M. For the sake of symmetry, the BS is positioned above the midpoint of the side in such a way that the distance from the BS to the center of the sensing field is *L*. Clearly, *L* is greater than *M*/2 (i.e., *L* = *M*/2 + *K)*. The origin of the coordinate system is considered to be in the bottom left corner of the sensing field. In this case, the expected squared distance between the sensing field and the BS is:

$$E[d^2_{toBS}] = E[(x-\frac{M}{2})^2 + (y-\frac{M}{2}-L)^2] = E[x^2] - E[Mx] +$$
$$E[\frac{M^2}{4}] + E[y^2] - (\frac{M}{2}+L)E[y] + E[(\frac{M}{2}+L)^2] =$$
$$\frac{M^2}{6} + L^2 = \frac{M^2}{6} + (M/2+K)^2 = \frac{5M^2}{12} + MK + K^2. \quad (60)$$

N. Calculation of d^4_{toBS} (BS outside of the square): As for the expected fourth power of distance from the BS to the sensing field, suppose that the BS is located outside a sensing field of square shape. More specifically, suppose that it L units away from the center of the square. The expected fourth power of distance will be:

$$E[d^4_{toBS}] = E[((x-\frac{M}{2})^2 + (y-\frac{M}{2}-L)^2)^2]$$
$$= \bullet\bullet\bullet = \frac{7M^4}{180} + \frac{2M^2L^2}{3} + L^4. \quad (61)$$

O. Calculation of d^2_{toBS} (BS outside of the circle): The expected squared distance between BS that resides outside of a circle with radius R to the interior sensor nodes can be written as:

$$E[d^2_{toBS}] = \int_{x=0}^{x=x_{\max}} \int_{y=0}^{y=y_{\max}} [x^2 + (y+L)^2]\rho(x,y)dxdy =$$
$$\frac{1}{A}\int_{\theta=0}^{2\pi}\int_{r=0}^{r=R}(r^2 + 2rL\cos\theta + L^2)rdrd\theta = \frac{R^2}{2} + L^2, \quad (62)$$

where, *L* is the distance between the center of the circle and the BS.

P. Calculation of d_{toBS}^4 (BS outside of the circle) : In the same manner, the expected fourth power of distance from the circular sensing area to the BS which is positioned L units away from the center of the sensing area can be calculated as:

$$E[d_{toBS}^4] = \int_{x=0}^{x=x_{\max}} \int_{y=0}^{y=y_{\max}} [x^2 + (y+L)^2]^2 \rho(x,y) dxdy =$$
$$\frac{1}{\pi R^2} \int_{\theta=0}^{2\pi} \int_{r=0}^{R} r^2 + 2rL\cos\theta + L^2)^2 rdrd\theta =$$
$$\frac{1}{\pi R^2} \int_{\theta=0}^{2\pi} (\frac{R^6}{6} + \frac{R^4 L^2}{2} + R^4 L^2 \cos^2\theta + \frac{R^2 L^4}{2}) =$$
$$\frac{R^4}{3} + L^4 + 2R^2 L^2. \quad (63)$$

3.5 Simulation Results

In this section the mathematical results presented in Section 3.4 are further validated through extensive simulations. As for simulation platform, a custom simulator written in MATLAB is used, whereby various parameters such as energy consumption, network lifetime, and sensing coverage can be evaluated for cluster-based communication protocols. Further, this simulator can simulate routing and clustering policies and provide statistical information such as the residual energy of each node, communication paths, wasteful transmissions (if any) during the network operation, and the energy waste due to variability of the number of clusters.

Closed-form expressions presented in Table 3 are evaluated over a set of WBANs. For a single network configuration, one hundred sensing fields are generated over which the above-mentioned protocols are run to accomplish the average result. In each network, the sensor nodes are randomly deployed on a 2D sensing field. Table 4 lists all simulation parameters (including network model, energy model, and protocol-specific parameters) and their corresponding values. It should be noted that although in the simulations, only integer numbers are assigned to k_{opt}, using fractional numbers is also logical.

To investigate the effect of network dimensions on k_{opt}, the sensing field is assumed to be square-shaped with side length ranging from 20 m to 200 m and the BS is put in the corner of the sensing field. Figure 8 shows the average energy dissipation per round as a function of the number of clusters for

sensing fields with different side lengths (M) in the above range.

For each sensing field, we varied the number of clusters between 1 and 15 and ran the studied protocols 100 times. Simulation time is chosen to be 500 rounds so that all three protocols operate stably, in that all of the nodes are alive in this time interval. It should be noted that the pattern at which the nodes die in the network (i.e., energy imbalance issues) is not the objective of the simulations. In this regard, more details can be found on [Amini2].

Table 4. Parameters used in simulations.

Parameter	Value
WBAN Model	
Field span	Square: 20 m × 20 m, 50 m × 50 m, 100 m × 100 m, 200 m × 200 m
Location of BS	Corner: (0,0)
N	100
Sensing radius (R_{sense})	2 m, 7.5 m, 10 m, 15 m
Maximum transmission distance	305 m
Packet size (l)	500 bytes
Number of frames per round	1
Energy Model	
Initial energy of each sensor (E_0)	2 J
E_{elec}^{Tx}	50 nJ/bit
E_{elec}^{Rx}	50 nJ/bit
ε_{fs}	100 pJ/bit/m^2
Path loss exponent (n)	2
E_{DA}	5 nJ/bit/signal
LEACH	
k_{opt}	1 ~ 15
LEACH-Coverage	
k_{opt}	1 ~ 15
$\eta(m)$	0 ~ 1
$\alpha(m)$	$(k_{opt}/N) / \Phi(m)$ ([Tsai])
DBS	
k_{opt}	1 ~ 15
Number of segments	1 ~ 5
δp	0 ~ 0.1

In a more specific manner, in the first set of simulations, M = 20 m, 0 m < dtoBS < 28.28 m. Replacing the energy parameters in (9) with their corresponding values from Table 4, the optimal number of clusters kopt is expected to reside in the interval [23.03,100]. However, according to the associated closed-form expression (12) presented in Table 3, kopt should be equal to 100, that is, if each cluster contains one node (no intra-cluster communication), the total energy consumption will be minimized.

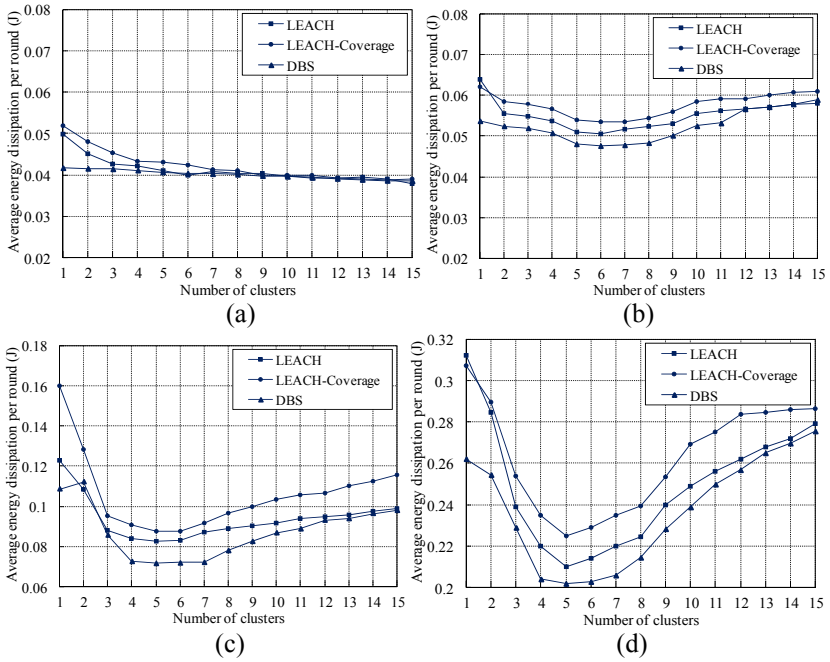

Figure 8. Average energy spent per round when k_{opt} is varied between 1 and 15 in LEACH, LEACH-Coverage, and DBS (a) M = 20. (b) M = 50. (c) M = 100. (d) M = 200. These graphs show that the optimal number of clusters can be independent of the field dimensions under certain conditions, as predicted by Section 3.4.

From Figure 8(a), it is evident that having more number of clusters results in lower average energy dissipation per round and it is why the trend of the function (average energy dissipation per round versus the number of clusters in Figure 8(a)) is decreasing. According to simulations, the most energy-efficient outcomes are experienced when k_{opt} = 100. As it can be seen, the simulation results are in complete agreement with analytical results.

In the second set of simulations, sensing field dimensions are scaled, i.e., M = 50 m, 0 m < d_{toBS} < 70.71 m, while the number of nodes are kept intact, i.e., N = 100. Plugging the proper energy parameter

values into (9), the optimal number of clusters k_{opt} should fall within the interval [5.05,100]. Figure 8(b) illustrates that applying six clusters across the sensing field yields the minimum amount of energy dissipation for all the decentralized protocols targeted in this study. This is in accordance with (12), which suggests that k_{opt} should be set to 5.84. In the same manner, two more sets of simulations have been performed on larger sensing fields, i.e., M = 100, 200 m. By the same analysis, k_{opt} is expected to reside respectively in intervals [2.86,100] and [2.83,100] for these two configurations. Figures 2(c) and (d) depict the average energy dissipated per round against k_{opt} for the two recent configurations. It can be observed that the optimal number for clusters for both cases is around 5 which excellently agrees with mathematical calculations established upon (12) presented in Table 3.

In two recent configurations, owing to the larger field and power control capability of the sensor nodes, the energy consumption of the receiver electronics (E_{elec}^{Rx}) is dominated by power amplifier energy ($\varepsilon_{fs} d_{toBS}^2$). As such, the simplified closed-form expression (13) reported in Table 3 (in this case $k_{opt} = 0.489\sqrt{N}$) can be utilized with a very small error.

As mentioned in Section 3.4, (13) advises that the optimal number of clusters does not depend on the size of the network. Simulation results verify this property by showing that the optimal number of clusters is around 5, regardless of the network dimensions (i.e., M = 50, M = 100 and M = 200). At the first glance, this result seems abnormal; however, intuitively, one can think of a network of size 100 with 100 nodes as a network of size 200 with 100 nodes that has only been scaled by a factor of 2. Therefore, the number of cluster heads should not differ between these two networks. It also should be noted that E_{elec}^{Rx} is presumed to be very small. If E_{elec}^{Rx} is large, it will be in the form of a constant overhead that can fundamentally make the cluster-based schemes questionable.

In another attempt to further confirm the above-mentioned observation, the network size (i.e., the side length of the square-shaped field) is kept unchanged (M = 100) while the number of the nodes is increased to 200 nodes and 400 nodes for the same network. In like manner, protocols LEACH, LEACH-

Coverage, and DBS are simulated. By averaging over one hundred simulation runs, it has been verified that the optimal number of clusters for these two new networks are respectively 7 and 10 which agrees well with (13). This verifies that under certain assumptions (refer to Section 3.4), the simplified closed-form expressions can promisingly provide the best value of k_{opt} in regard of energy-efficiency.

LEACH and LEACH-Coverage do not clearly specify the task of a sensor network in a round whose number of clusters is zero. Fortunately, DBS takes some action to always guarantee the existence of at least one cluster head to overcome this problem. Therefore, as all graphs in Figure 8 indicate, using LEACH and LEACH coverage, once k_{opt} becomes close to one, an abrupt increase in the energy dissipation can be substantiated. This energy waste can be attributed to situations where there is no cluster head across the network and this problem exhibits itself as inutile time and energy consumption in LEACH and LEACH-Coverage.

In all of the studied protocols, k_{opt} solely determines the expected number of clusters that each protocol should possess to be energy-efficient throughout the network operation. In fact, the number of clusters is variable and this number is distributed in a range around k_{opt}. For instance, in a 100-node network, when k_{opt} = 5, the number of cluster heads varies from 0 to 34 and the percentage of rounds that exactly have five cluster heads is less than 20%. Also, we observed that within 100 rounds, there is on average one round whose number of cluster heads is zero. Obviously, as k_{opt} decreases, more occurrences of rounds with zero number of clusters are foreseen.

The energy waste due to variability of the number of clusters could be eliminated by rejecting certain low values for k_{opt} that lead to higher chances of having zero clusters (e.g., $k_{opt} < 5$ for a 100-node network) and choosing the closest value to the one that closed-form analysis recommends. In such situations, the closed-form expressions reported in Table 3 are no longer valid.

As mentioned in Sections 4 and 5, energy consumption of the receiver's circuitry (E_{elec}^{Rx}) is of special importance as a factor that can substantially change the optimal number of clusters and more fundamentally, it can make a decision on whether or not it is worth to cluster the network. Throughout the

simulations, it was assumed that the receive energy (E_{Rx}) is smaller than the transmit amplifier energy ($\varepsilon_{amp} d_{toBS}^{n}$) which can construct (e.g., in wireless LANs) a significant portion [Bhardwaj] of the maximum transmit energy (E_{Tx}). Thereby, as we increased the size of the sensing field, more improvements in terms of energy consumption were achieved. Most of the previous studies make similar assumptions regarding the transmission and receive costs [Dardari], [Heinzelman], [Tsai], [Kumar]. For instance, investigators in [Dardari] argue that the energy spent to receive the packets is negligible with respect to the energy used for the packet transmission. Correspondingly, they mention some cases for which this condition occurs [Zhao]. Among the commercially-available motes, XBee Pro Modules conform to this condition, in that the transmit energy is up to 6 times the receive energy. Likewise, on Crossbow Mica2 motes [Crossbow], the maximum transmit energy is 2.5 times the receive energy.

On the other hand, Chang and Tassiulas [Chang] reason that the receiver's circuitry is in general more complex than its counterpart in the transmitter side. Therefore, it consumes more energy than the transmitter's circuitry within the same order of magnitude. One can verify that the receive energy (E_{Rx}) would be comparable to the transmit energy (E_{Tx}) by considering the energy consumption of the power amplifier (i.e., output transmitter antenna). Among the available motes in the market, on ANT motes from Dynastream Innovations [ANT], the receive energy is greater than the maximum transmit energy by a factor of 1.2. This is because the maximum transmission range is only 20 meters and hence, the amplifier energy cannot grow. Similarly, on mote EZ430-RF2500 from TI [TI2], transmit and receive energies are almost equal. In this context, Bhardwaj and Chandrakasan [Bhardwaj] explain that among various factors that determine how E_{Tx} and E_{Rx} compare, the regulatory limit on output amplifier (i.e., radiated power from the antenna) is the governing one. When a high output power is supported, the transmitter is likely to dominate due to energy dissipated by power amplifier. When regulatory limits are tight, as in ultra-wideband systems, the receiver, owing to its more complex signal conditioning and processing, dominates the transmit energy.

Generally, future amendments to our approach include but are not limited to:

- considering partial data aggregation instead of perfect data aggregation. This way, the reliability of data within each cluster (as a quality of service) should be taken into account as well.
- utilizing a more realistic radio energy model in place of the first-order radio energy model,
- exploring the parameter space to a higher extent, e.g., conducting simulations for different transmit/receive energies and finding the corresponding limits.
- addressing the density of the nodes in the network, i.e., sparse network versus dense network (closely-spaced nodes),
- investigating other node distributions across the network, such as Gaussian distribution,
- integrating packet size optimization considering the errors imposed by the environment,
- and performing optimization for energy balancing (coverage).

CHAPTER 4

TPC in MAC and Physical Layers

In this chapter we investigate the problems associated with TPC in the physical and MAC layers. As mentioned in Chapter 3, TPC-aware routing helps to choose the routes composed of energy-efficient links. In the MAC and PHY layers, the strategy is to adjust the transmit power level of every packet such that the signal-to-interference-and-noise ratio (SINR) at the intended receiver is enough for the packets to be decoded. One point worthy of note is that the intended receiver is determined by the network layer, i.e., by the routing table entry, and not by the MAC layer; nevertheless, in some WBANs only a few nodes constitute the network and thus, the destinations of wireless communications are specified.

We provide insights into the implementation of TPC techniques in MAC and PHY layers, showing that TPC techniques significantly reduce the energy consumption; first, we study the feasibility of XBee Pro wireless modules for mid/long range off-body communications intended e.g., for athletic performance monitoring in an open sports field. Second, we study the issues confronting 2.4 GHz wireless communications around the human's body, i.e., on-body communications. Our experimental results enable transmitters to control the communication power according to the anticipated channel quality.

With most tiny IEEE 802.15.4 platforms having a nominal and practical maximum ranges of respectively 100 meters and 50 meters in line of sight scenarios, one of the shortcomings of current wireless sensors is the communication range; many applications require long-range body-wearable devices, where the transmitter and the receiver nodes are separated by large distances, giving the advantage of being able to monitor a large sports field, as well as enabling the users to move around freely while using ambulatory health monitoring systems. The problem of wireless range limitation has been poorly addressed by the research community, where most solutions propose multi-hop

communications by adopting different routing strategies. However, for health monitoring applications due to a variety of reasons from reliability and transmission delay to privacy issues, such solutions are not practical. In this work, we conducted measurements from the XBee and XBee Pro wireless modules so as to find spatial impacts on the correlation between transmission power and Receive Signal Strength Indicator (RSSI). We also measure the impact of the human body on the wireless propagation channel and, accordingly, one can adjust the transmission power level to reduce the energy consumption of each individual wearable sensor node.

It is envisioned that most of the sensor nodes should be able to adjust their output transmission power on-the-fly in practical applications to increase the battery lifetime, as well as to alleviate problems related to interference to/from other wireless devices.

4.1 Prior work

4.1.1 Mid/Long Range Off-body Communications

Athlete monitoring systems must balance between size, weight and communication range. While commercially available devices such as the SPI Pro from GPSports [GPSports] and VX Log from Visuallex Sport International [VXSport] provide sufficient radio range to directly reach a data acquisition unit, they have sizes in the order of a large cell phone, making them impractical for monitoring athletes in sports fields. In a contrary manner, emerging body-area devices such as the Toumaz Sensium digital plasters have the form factor of a band-aid, thus well-suited for such applications. However the small form factor necessitates tiny batteries, which correspondingly reduces the communication range and makes data acquisition challenging [Kurusingal].

Investigators in [Kurusingal] have conducted experiments to profile the propagation of wireless signals around the body in an open soccer field. To this end, they equip each soccer player in the squad with a MicaZ mote mounted on the player's right arm. The investigators derive a rough map of the received signal strength indicator (RSSI) at various distances and directions from the body-mounted MicaZ, which transmits data every second at the highest available power level of 1 mW. To achieve connectivity, a

multi-hop routing protocol was designed and utilized, which makes a balance between the competing objectives of energy consumption and delay.

4.1.2 On-Body Communications

Investigators in [Srinivasan1] performed empirical measurements of the packet reception rate for MicaZ motes. They observed that RSSI is quite stable over a short period of time, thus being a suitable predictor of short-term link quality, and RSSI values above the sensitivity threshold correspond to a high PRR. They also found that the Link Quality Indicator (LQI) varies over a wider range over time for a given link, but the mean LQI computed over many packets shows a better correlation with PRR. They also observed that while short-term link asymmetries are common, long-term asymmetries are rare. A number of studies have discussed interference caused by the human body and dynamic environments on radio communications. Researchers in [Kara] substantiated the effect of subjects crossing a link between a transmitter and a receiver operating at 2.4 GHz. They use a customized RF transmitter that generates signals with transmission power of 20 dBm. The shadowing effect caused by a human body crossing the line of sight (LOS) links between a transmitter and receiver for transmissions have been discussed in [Obayashi]. The degradation of the radio signal when passing through the human body is researched in [Ruiz]. The indoors and outdoors evaluation of IEEE 802.15.4 radio for static sensing platforms through a characterization of the RSSI for different transmitter-receiver distances has been discussed in [Srinivasan1]. In [Shah] the authors stress the importance of antenna orientation in changing the RSSI values and in the incidence of the asymmetric links.

Jea and Srivastava [Jea] present results on connectivity in a body-wearable sensor network using the Mica2Dot motes. Their results suggested fair connectivity among all nodes on a body beyond a certain transmission power. They used PRR as a metric for wireless communication quality. The factors that they explored in the experiments were the relationships between transmission power values by placing nodes on different parts of the body. They considered two scenarios of standing and walking with different setups for the antennas.

The authors in [Natarajan] examined the performance of IEEE 802.15.4 through and around the human body using network layer metrics such as PRR and latency. They observed that the human body is similar to aluminum, in that it acts like a fine RF shield, such that no packet can get through without creating a multipath. They suggest that a star topology operating at low power levels might suffice in an indoor environment, whereas in an outdoor environment, nodes would have to operate at higher power levels. They also identify design goals and evaluate them against the star and multi-hop network topologies.

Ren et al. [Ren] performed experiments to observe how the quality of sensors is affected by surrounding factors. Varying the postures of the body, they performed experiments varying the power level in different environments. They attached a single sensor on the left arm and varied the distance from the receiver and found the correlations between PRR, distance and transmission power.

Shah et al. [Shah2] conducted experiments on multiple subjects to measure the effect of human body on the performance of Bluetooth and IEEE 802.15.4 radios. They consider different locations on the body such as the ankle, ear, knee, and chest, while the on-body data acquisition unit is always attached to the waist. They allowed mobility of the subjects, while measuring the effect of IEEE 802.15.4 and Bluetooth. [Shah1] evaluates the characteristics of the links in and on-body IEEE 802.15.4 network and the factors that influence link performance. The investigators used Intel Mote 2 nodes and placed them on three locations: the chest, the right side of the waist and the right ankle, while setting the transmission power to 0 dBm. They observed that the wireless links among nodes in an on-body IEEE 802.15.4 network are not as promising as expected. While 802.15.4 radios typically have a range of at least 10 meters in most indoor environments, when placed on a body, the range was observed to be less than a meter.

4.2 Experiments and Results

4.2.1 Experimental Platform

As previously mentioned, we have used Digi's XBee and XBee Pro RF Modules to conduct our experiments. The XBee and XBee Pro modules (shown in Figure 9) have been engineered to meet IEEE 802.15.4 standards and support the unique needs of low data rate, simple connectivity, and low-power

sensor networks. They operate at the ISM 2.4 GHz frequency band, with a maximum nominal data rate of 250 kbps. Furthermore, both XBee and XBee Pro modules provide an RSSI measurement tagged to a specific packet. As for the transmission power, these modules can be configured to operate using five different transmission power levels ranging from 0 to 4. For XBee modules, the levels 0 to 4, respectively correspond to power outputs of -10 dBm, -6 dBm, -4 dBm, -2 dBm and, 0 dBm. For XBee Pro modules, the levels 0 to 4, correspond to power outputs of 10 dBm, 12 dBm, 14 dBm, 16 dBm and, 18 dBm, respectively. Although a chip antenna demonstrates limited reliability and lower transmission range than a whip antenna, on account of its small form factor, we decided to use the modules equipped with chip antennas in both the transmitting and the receiving nodes. As a matter of fact, using a chip antenna has helped us to improve the repeatability and reproducibility of our experiments as well. With respect to radiation patterns, both antennas, albeit not perfectly, exhibit omnidirectional radiation patterns. XBee modules provide up to 30 m ranges for indoor and urban environments and up to 100 m for LOS outdoor conditions (with dipole antennas), both for a 0 dBm output power, whereas XBee PRO modules provide, for a 20 dBm output transmission power, up to 100 m ranges for indoor and urban environments and up to 1200 m for LOS outdoor conditions (with dipole antennas). Furthermore, both modules provide 16 channels, numbered 11 through 26. The channels are 5 MHz apart in the 2.4 GHz band (i.e., 2405 MHz - 2480 MHz), overlapping with both 802.11b (WLAN) and 802.15.1 (Bluetooth). Table 5 lists basic characteristics of XBee and XBee Pro modules.

Figure 9. Dimensions of XBee Pro and XBee wireless modules.

Table 5. Comparison of XBee and XBee Pro modules.

Module/Characteristic	XBee	XBee Pro
Indoor range (m)	30	100
Outdoor line of sight (m)	100	1200
Transmission power	1 mW (0 dBm)	100 mW (20dBm)
Receiver sensitivity	-92 dBm	-100 dBm
Tx Current Max	45 mA (Vcc = 3.3 V)	270 mA (Vcc = 3.3)
Rx Current	50 mA (Vcc = 3.3 V)	55 mA (Vcc = 3.3 V)
Sleep current	10 uA	10 uA
Communication channels	A total of 16	A total of 16
Modulation	OQPSK	OQPSK

PRR is one of the parameters used to determine the link quality. PRR is the ratio of the number of successful packets to the total number of packets transmitted over a certain course of time. Higher PRRs are indicative of a better link quality. In some situations, the probability that a packet will be dropped is independent of the success rate of the packets that are sent before and after the packet. However, there are situations where the errors are more likely to occur in bursts. These groups of errors usually prove to be more detrimental in WBANs as opposed to cases where the errors are independent and uniformly distributed. Receive Signal Strength Indicator (RSSI) measures the strength of an incoming signal by averaging over 8 symbol periods of each incoming packet. The ability of the receiver to pick the weakest of signals is referred to as receiver sensitivity. The higher the receiver sensitivity, the better is the link quality. RSSI value is an integer range roughly from -100 dBm to 0 dBm for IEEE 802.15.4 radios. By means of sequence numbers it is possible to trace lost packets in a sequence of packets, which allows for verification if there are bursts or striking patterns of packet losses.

4.2.2 Open Field Off-Body Experiments

At an early exploratory stage, we conducted our open field experiments on a well-groomed grass field (UCLA's Intramural Field) with both receiver and sender nodes located at the height of 1.5 m above ground. Communication distances in our experiment ranged from 0 m to 250 m with steps of 25 m, i.e., a total of eleven distances. Measurements were performed on one male subject on a partially cloudy day in

March 2011. The transmitter was attached to the chest of a male subject, while the receiver was mounted on an adjustable stand. The XBee Pro module in the transmitting node is connected to an Arduino Pro Mini 8 MHz microcontroller [Arduino]. The XBee Pro chip on the receiving node is connected to a laptop via a USB port and another Arduino Pro Mini. The lack of human activity ensured a human interference-free environment. However, due to the presence of IEEE 802.11 signals, all communication channels were suffering from the 802.11's interference, deteriorating the PRR. It should be noted that, even for athletic performance monitoring applications, it is not realistic to assume the existence of IEEE 802.11-free environments. The sender and the receiver are always kept in line of sight in the experiments. The data baud rate is set to 115200 bps, which is applicable for most of the scenarios. In each experiment, the transmitting node sends 1000 packets at five different power levels and the receiver records the packet's sequence number and the RSSI reading. The receiver did not acknowledge the reception of a successfully received packet. Furthermore, the transmitter sent each packet only once. The transmitter and receiver were alike, meaning that the module-type and antenna-type were identical. More details regarding the experiment setup are summarized in Table 6.

Table 6. Basic configuration/setup for off-body experiments.

Experiment Configuration	**Transmitter**	**Receiver**
Address	1	2
Height (from ground)	1.5 m (chest)	1.5 m (on stand)
PAN ID	70	70
Channel	11	11
Destination Address	2	1
Paylod	30 bytes	n.a.
ACKs	No	No
Receiver's sensitivity	n.a.	-100 dBm
Transmit/Receive current	270 mA at 18 dBm	55 mA

In transmission of radio signals between two nodes, height above the ground becomes a very influential factor, in the sense that solely guaranteeing line of sight communications does not suffice. The strongest signals are on the direct line between transmitter and receiver and always lie in the Fresnel zone [Fresnel_Wiki]. Fresnel zone defines volumes in the radiation patterns surrounding the direct signal path,

which represent a reflection-free zone. It is generally accepted that antenna heights less than 60% of the Fresnel zone radius (FZR $=17.32\sqrt{d(km)/4f(GHz)}$) will lead to significant signal attenuation and fading. In our experiments for communication distance of 200 m, FZR is equal to 2.48 m. For this FZR value, the height of 1.5 m is marginal and hence, we anticipate significant signal attenuations for communication distances beyond 200 m.

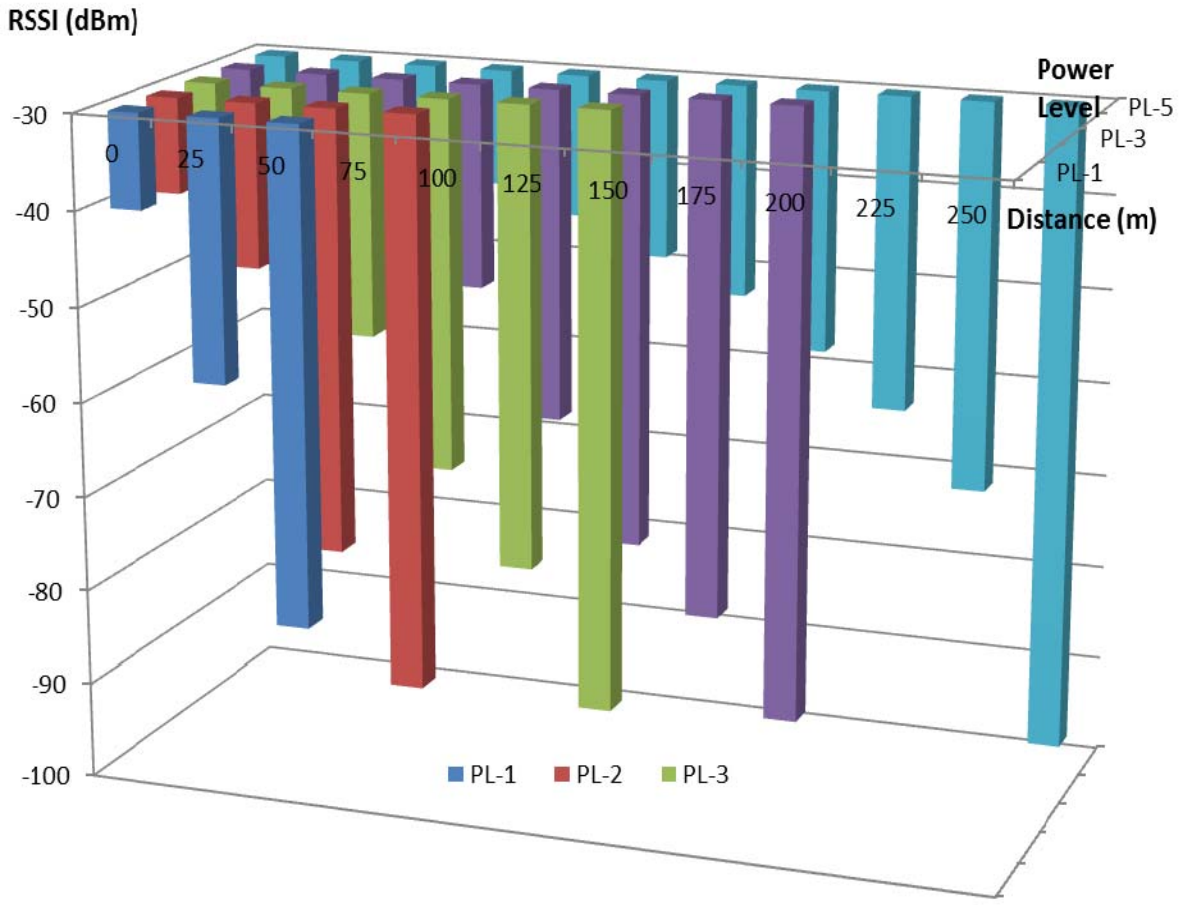

Figure 10. Average RSSI measurements for different distances at different transmission power levels.

Figure 10 shows the average RSSI measurement results for different separation distances at different transmission power levels. Due to the fact that the XBee Pro's receiver sensitivity is -100 dBm and the maximum receiver signal strength is -40 dBm, the measured RSSI range is in the interval [-100 dBm, -40 dBm]. For distances above 200 m only the maximum transmission power, i.e., PL-5, is able to convey data packets to the receiver with about 50% of the packets being lost. As shown in Figure 10, as a result

of antenna height becoming smaller than FZR, significant deterioration of RSSI is observed as we increase the separation distance from 225 m to 250 m. The minimum and maximum transmission powers are 10 dBm (~10 mW) and 18 dBm (~63 mW), respectively, which is indicative of a large optimization room for power control, capable of energy savings of six-fold in energy consumption. Per our experimental results, RSSI values more than -90 dBm signify high quality links with more than 90% of the packets being delivered to the receiver.

4.2.3 Open Field On-Body Experiments

In another set of experiments, we have evaluated the effect of human body on 802.15.4 communications by attaching transmitting sensor nodes to six different body positions namely, the head, upper arm (left and right), the forearm (left and right), the waist, the thigh (left and right), and the shin (left and right). The receiver node was taped to the subject's waist. The experiments were repeated with three different pairs of nodes in the same environmental conditions to achieve statistical confidence. Measurements were performed on two male subjects on an open grass field to prevent radio wave reflections from the environment.

The subjects were asked to fully extend their arms horizontally while performing the experiments pertaining to upper arms and forearms. In each experiment, the transmitting node sends 1000 packets at five different power levels and the recipient logs the packet's sequence number and the RSSI reading. More details regarding the experiment setup are listed in Table 7.

As shown in Figure 11, the average RSSI values gradually increase with the transmission power level. At the transmission power level of -10 dBm, in experiments where we attached the transmitter nodes to the shin, head, and forearm, the resulting packet drop rate was dramatically high (more than 50%). As a result of such a high packet drop rate, we inevitably report the RSSI value as -100 dBm, which is lower than the receiver's sensitivity level. Expectedly, the experiment concerning the waist yields the best RSSI values, since the receiver is in the transmitter's line of sight. Indeed, the physical distance between the transmitter and the receiver in this case is only 10 cm. This is why the data success ratio was always

100% even when the XBee modules operate at the lowest transmission power level.

Table 7. Basic configuration/setup for on-body experiments.

Experiment Configuration	Transmitter	Receiver
Address	1	2
Position	Six on-body location: head, upper arm, forearm, waist, thigh, shin	Waist
PAN ID	70	70
Channel	11	11
Destination Address	2	1
Paylod	30 bytes	n.a.
ACKs	No	No
Receiver's sensitivity	n.a.	-92 dBm
Modulation	OQPSK	OQPSK
Transmit/Receive current	45 mA at 0 dBm	50 mA

On the basis of our experimental results as well as similar studies such as [Hackmann] and [Kleisouris], RSSI values higher than -80 dBm are indicative of reliable communications. In fact, choosing such a conservative threshold of -80 dBm always allowed for communications with packet drop rates less than 5%. Thereby, when we attach the nodes to the thigh, shin, and waist, as Figure 11 suggests, there is enough room to reduce the transmission power level without compromising the reliability of communications. For instance, transmission power reduction for data communications between the thigh and the waist will bring about up to 50% energy savings.

The shins and generally the lower part of legs turned out to be very favorable locations for on-body wireless communications. This is because, the legs are relatively close to the ground, where reflections increase the total received power with major contributions from the multipath components rather than the direct received signal, which in turn leads to less steep changes in the RSSI values.

The human body adversely affects the radio propagation and communication such that nodes on some parts of the body have limited connectivity to nodes on other parts in certain scenarios. Our experiments verify that the human body by itself, not only affects the radio propagation, but also causes attenuations in signal levels received by on-body sensors, as a result of which the nodes experience varied connectivity.

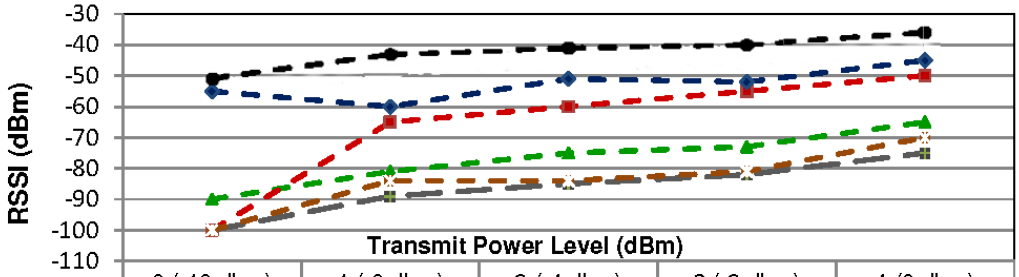

	0 (-10 dbm)	1 (-6 dbm)	2 (-4 dbm)	3 (-2 dbm)	4 (0 dbm)
Upper arm	-90	-81	-75	-73	-65
Shin	-100	-65	-60	-55	-50
Head	-100	-89	-85	-82	-75
Forearm	-100	-84	-84	-81	-70
Thigh	-55	-60	-51	-52	-45
Waist	-51	-43	-41	-40	-36

Figure 11. Average RSSI measurements for different body parts at different transmission power levels.

Two most common applications for body-wearable sensor networks placed on the human body are ambulatory health monitoring and athlete's performance monitoring. In these applications, body-wearable sensor networks are expected to perform long-term monitoring, thus it is sensible for such systems to communicate their data at a lower transmission power. Based on our experiments, the body location to which the node is attached significantly affects the radio propagation channel. RSSI measurements are simple and inexpensive, but they suffer from inaccurate measurements or delays due to the random nature of fading channels. Throughout our experiments regarding both on-body and off-body scenarios, we learned that:

- weak signals in the presence of noise will yield low RSSI values;
- weak signals in the absence of noise will lead to low RSSIs;
- a strong signal without noise being present achieves high RSSI values;
- and finally, strong signal in a noisy environment will achieve high RSSIs.

CHAPTER 5

Sensor-Assisted Transmission Power Control

In this chapter we direct our attention to off-body wireless communications that are initiated from inside a shoe (or an insole), i.e., under the feet.

5.1 Overview of Smart Shoes/Insoles

Our smart shoe project (also known as Hermes) was motivated by the recent findings that consider gait variability to be an effective measure to analyze the risk of falling. Hermes provides a mobile, affordable and long-term instability analysis, which is customizable to individual users, and is context-aware, with the capability of being guided by experts. With these features, the system is able to provide long-term monitoring of patients outside a hospital or clinical setting at a reduced cost with greater user convenience, compliance and inference capabilities that meet the physician's or investigator's needs.

Hermes was prototyped using pressure and inertial sensors integrated into the shoe along with an embedded computing platform to support data acquisition, synchronization and low-power radio communications. A smart phone with Bluetooth capability was used as a central aggregation and processing unit. Data is wirelessly sent from the embedded device to the smart phone, where it is processed. Results are displayed to the user, as well as propagated to a centralized server for further analysis and long-term storage. The Microleap [Au] embedded sensing platform with Bluetooth capabilities was used in the Hermes. Microleap contains an onboard 3-axis accelerometer and 3-axis gyroscope and it connects to seven discrete pressure sensors integrated within the shoe's insole. The accelerometer and gyroscope are used to detect the linear acceleration and angular movement of each foot.

The software architecture of the system consists of two main components: 1- the embedded software running on each processing unit embedded inside the shoe, which is responsible for data acquisition, preliminary signal analysis, time synchronization between the two shoes and energy-efficient data transfers to the personalized device; 2- the software on the personalized device, which is responsible for computational and storage intensive tasks, such as motif detection, visual data display, notification and guidance.

We have conducted several experiments on twelve subjects in both controlled and non-controlled environments to determine the feasibility of the smart shoe system to compute gait parameters and instability measure. Our results verified the effectiveness of the computed instability value. For the first time, a baseline has been established for each test subject to identify when he/she is at a heightened risk of falling.

Our successful experimental results pertaining to plantar pressure, gait, and fall risk assessment motivated us to upgrade the smart shoe platforms into smart insoles. Our goal to integrate all the components in shoe insoles was to make this platform more convenient (so that it can be used in patient's shoe) and more pervasive (so that it can be used in uncontrolled environments as well). Figure 12 shows the Hermes system and its next version in the form of a wireless insole.

In the first prototype, we used similar components to the ones used in the smart shoe solely as a proof of concept. The only difference was changing the Bluetooth communication scheme to SimpiciTI [SimpliciTI]. The system was able to deliver the same performance as far as the gait parameters were concerned. However, it was not able to measure the plantar pressure due to the fact that only seven discrete pressure sensors were placed on spots, from which gathering pressure data provides significant information about pressure distribution and walking pattern.

To design the second prototype, we constructed a sensor matrix consisting of 40 resistive textile pressure sensors with the spatial 2D resolution of 1 cm along with inertial sensors. This sensor matrix, as a multi-layer printed circuit board, measures the foot pressure distribution during ambulation in gait

analysis. This computing platform is also able to measure spatial and temporal gait parameters to evaluate motor impairments.

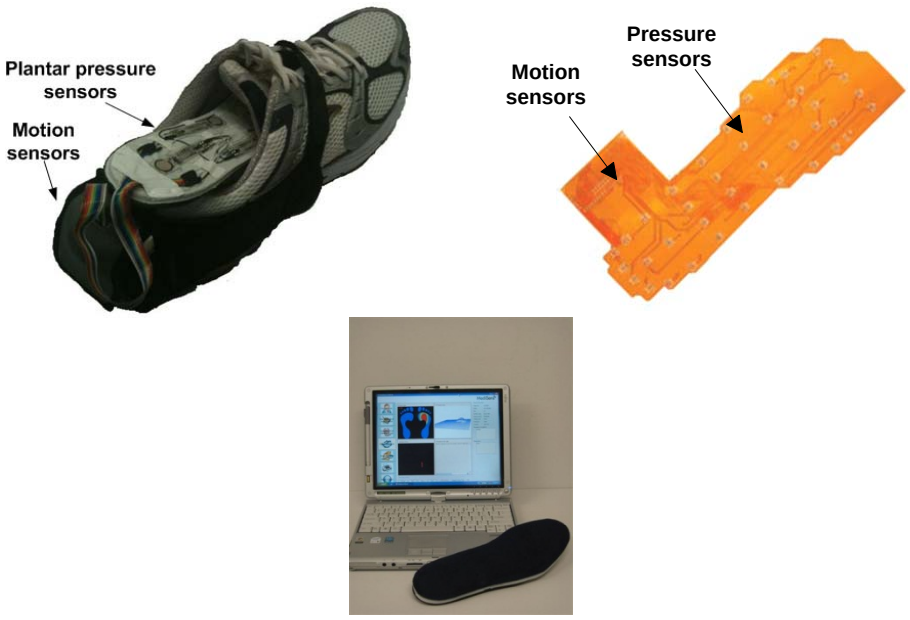

Figure 12. Hermes system (a shoe instrumented with multiple discrete components), its successor unified circuit board and the prototyped wireless insole.

The platform's architecture consists of four closely-interacting subsystems (Refer to Figure 13 and Figure 14). These subsystems are:

I) The sensing subsystem comprising pressure sensors, an accelerometer, gyros, and their conditioning circuit, which includes three analog multiplexers,

II) the processing subsystem, TI's MSP430 microcontroller which includes a 10-bit ADC as well,

III) the communication subsystem, CC2500 on which the SimpliciTI protocol runs. SimpliciTI is a variation of 802.15.4 with more limitations as far as the packet size and reliability of the communications are concerned. It should be noted that with regard to code size, SimpliciTI is remarkably lighter than ZigBee.

IV) And the power-supply subsystem, a lithium-ion 3.7 V battery with the capacity of 1100 mAh along with efficient voltage regulators to produce the exact supply voltage of 3.3 V.

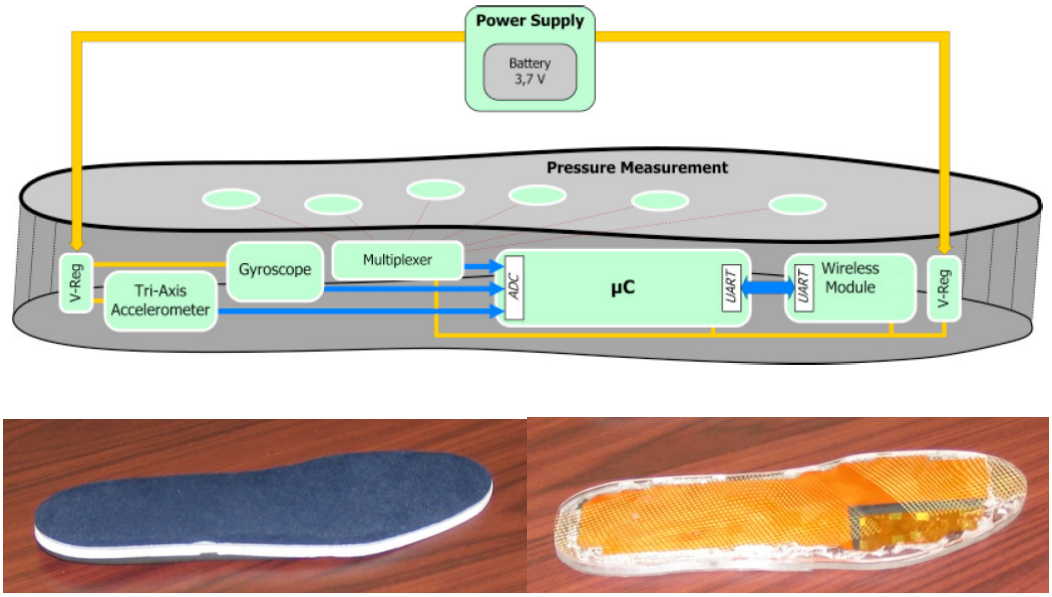

Figure 13. Schematic diagram of wireless insoles.

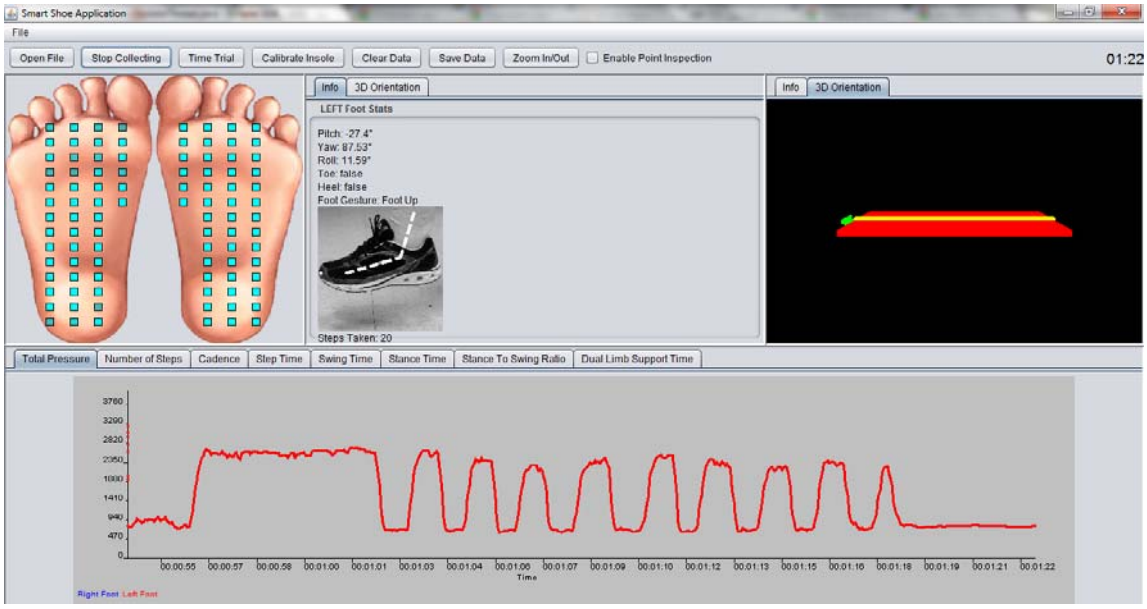

Figure 14. A snapshot of our gait analysis software.

We applied one major upgrade to the second prototype in order to increase the reliability of the wireless communications as well as to increase the range of communications by an order of magnitude. To do so, we replaced the EZ430-RF2500 module by the XBee Pro module, which utilizes a variation of IEEE 802.15.4, called XBee. Arduino Mini [Arduino], based on the ATmega168 microcontroller, serves

as processing unit to send proper commands to the XBee Pro module. We also added eight more pressure sensors to improve the granularity of the plantar pressure measurement.

The XBee Pro is engineered to meet IEEE 802.15.4 standards and support the unique needs of low-cost, low data rate, simple connectivity, and low-power WBANs. It operates at the ISM 2.4 GHz frequency band, with a maximum over-the air data rate of 250 kbps. Due to the overhead of the protocol the actual theoretical maximum data rate is approximately half of the theoretical maximum. IEEE 802.15.4 specifies the use of Direct Sequence Spread Spectrum (DSSS) and uses an Offset Quadrature Phase Shift Keying (O-QPSK) to modulate the RF carrier. This helps to enhance the communication immunity to ambient noises, especially to those with wide frequency bandwidth, such as impulse noises commonly observed in high voltage power line environment. The XBee-Pro also includes ZigBee features, allowing for communication in a point-to-point, point to multipoint, or peer-to-peer configuration, and each device can be configured as a Coordinator, End Device, or Router. These features are very helpful in organizing a WBAN by a cluster tree topology, which is more suitable to networks that cover larger physical areas [Kurusingal], where no single device is able to directly link with every other device (refer to section 4.1.1 for various related applications).

5.2 Characterization of Smart Insoles Wireless Communications

In this section we study the energy savings that could be achieved by applying TPC techniques to smart insoles. As discussed in Chapter 1, it is widely accepted that the communication subsystem consumes a significant amount of energy in WBANs. However, smart insoles encompass more than fifty sensors, which make the share of the sensing subsystem's energy consumption more pronounced. Not to mention the fact that each pressure sensor's resistance decreases with an applied force, resulting in a much higher current draw when the foot hits the ground and the insoles bear the weight of the entire body. Nevertheless, in the third prototype of our wireless insoles, owing to employing a mid/long rage transmitter, on average more than 50% of the total energy is consumed by wireless communications with the output power of +18 dBm (60 mW).

We used a multimeter to calculate the power consumed by the smart insole; that is, we measured the voltage provided by the battery and the current drawn by the node. Since the voltage is roughly constant (and equal to 3.3 V), the power consumed by the node is proportional to the current drawn [Torres], [Anastasi]. An alternative and a more accurate approach (Refer to [Shnayder]) would be utilizing an oscilloscope to measure current with high resolution, so that we keep track of all power transitions and log the data digitally for further analysis. This requires placing a small resistor (~ 1 ohm) in series with the node and using an instrumentation amplifier in order to amplify the voltage across the node. The oscilloscope will measure the amplified voltage and the input offsets induced by the amplifier will be accounted for.

Table 8 lists the itemized current draw for each functional subsystem of the wireless insoles for the three aforementioned prototypes.

Table 8. Current draw for different components of wireless insole.

Experiment Configuration	**Sensor type**	**First prototype**	**Second prototype**	**Third prototype**
Sensing	Gyros (2 axis + 1 axis)	15 mA	15 mA	15 mA
	Accelerometer	1 mA	1 mA	1 mA
	Pressure sensors	5 mA	50 ~ 185 mA Avg = 118 mA	55 ~ 207 mA Avg = 123 mA
	Sensing total	21 mA	134 mA	139 mA
Communication	802.15.4	22 mA	22 mA	270 mA
Processing		4 mA	4 mA	5 mA
Total		47 mA	160 mA	414 mA
Battery lifetime		23 h	6.5 h	2.5 h

XBee Pro modules can be configured to operate using five different transmission power levels ranging from 0 to 4. For XBee modules, the levels 0 to 4, respectively correspond to power outputs of -10 dBm, -6 dBm, -4 dBm, -2 dBm and, 0 dBm. For XBee Pro modules, the levels 0 to 4, correspond to power outputs of 10 dBm, 12 dBm, 14 dBm, 16 dBm and, 18 dBm, respectively. XBee Pro modules, when transmitting at 10 dBm draw 170 mA less electrical current as opposed to when transmitting at 18 dBm. Accordingly, in the best case scenario, applying TPC techniques can lead to 40% saving in energy

consumption, translating into an additional ~2 hours of operations (4.3 hours versus to 2.5 hours for the insoles battery life).

The following are the considerations that need to be taken into account with respect to the wireless insoles:

1- **Data rate:** as a 802.15.4 compliant protocol, XBee provides the RF data rate of 250 Kbps; nevertheless, the bound of 115.2 Kbps on the interface (serial interface between XBee Pro modules and Arduino) data rate will dictate the maximum achievable data rate. Yet, per our experience for baud rates greater than the threshold of 38.4 Kbps the communication between the Arduino and the XBee Pro module becomes unstable in high transmission rates; especially, when the number of received packets per second on XBee Pro is above 150. In the wireless insoles, our preferred sampling rate for all the sensors (a total of 54 sensors each represented by a single byte) is equal to 100 Hz. Therefore, we intend to convey 100 packets of size 54 bytes per second, which can safely be done as far as the baud rate limitation is concerned.

2- **Reliability (packet loss):** From the reliability point of view, wireless insoles can tolerate the loss of up to 20% of the packets. Per our experience with the smart shoes, after filtering and processing the sensor data at the PC side, we need 50 samples (acceleration, angular velocity, and pressure) a second in order to accurately derive the gait parameters; hence, even with 20% of packets lost, we can still run our algorithms. This sampling rate of 50 Hz suffices for the analysis of walking, since typical bandwidth of kinematics of human gait is between 4 and 6 Hz. As a matter of fact, 98% of the gait data's power lies below 10 Hz.

3- **Packet size:** generally, the larger the packet size, the greater the percentage of packet loss. It is highly desirable that all the data belonging to time instant *t* is delivered to the receiver side in a single packet. As mentioned above, the wireless insole contains a total of 54 pressure/inertial sensors; therefore, the payload of each data packet will have 54 bytes. It should be noted that: 1- the maximum packet size on XBee Pro modules is 100 bytes (Refer to Figure 15). 2- the maximum packet length allowed by the IEEE. 802.15.4 is equal to 133 bytes, that is a maximum MAC

protocol data unit (MPDU) of 127 bytes which, after accounting for the PHY-layer preamble (6 bytes), translates to a total packet size of 133 bytes.

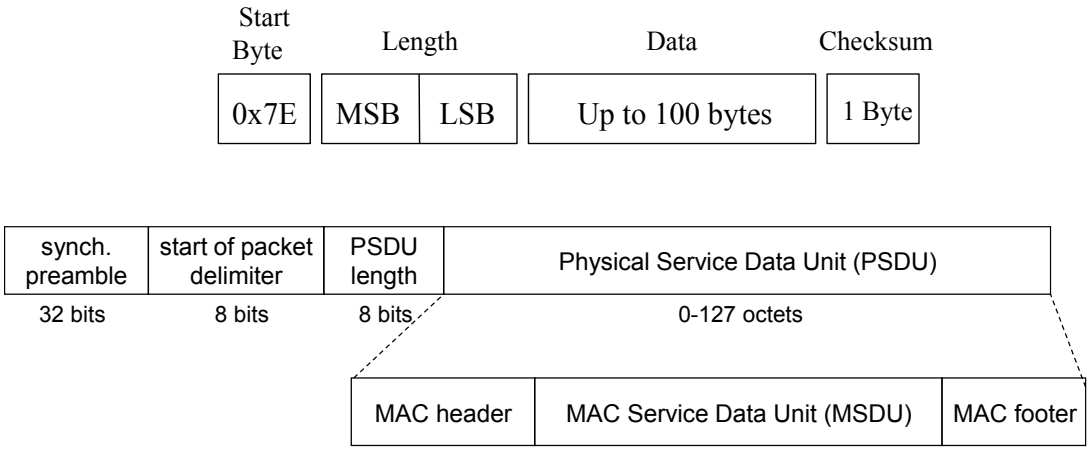

Figure 15. XBee Pro MAC frame structure (top) and 802.15.4 MAC and physical frame structure (bottom).

4- **Antenna type:** XBee Pro modules come with a variety of antennas such as whip and chip antennas. Although a chip antenna demonstrates limited reliability and lower transmission range than a whip antenna, on account of its small form factor, we decided to use the modules equipped with chip antennas in both the transmitting and the receiving nodes. As a matter of fact, using a chip antenna has helped us to improve the repeatability and reproducibility of our experiments as well. With respect to radiation patterns, both antennas, albeit not perfectly, exhibit omnidirectional radiation patterns.

5- **Transmitter/antenna location:** The transmitter and the antenna (i.e., the XBee Pro module) are placed inside the insole under the arch area. Nike+ iPod and Adidas Speed_Cell systems, intended for performance monitoring, both follow the same placement and insert their transmitters under the arch area (Figure 16). The former is capable of communicating with an iPhone/iPod, whereas the latter is able to connect with both iPhone/iPod (i.e., on-body wireless communications) and MAC/PC (i.e., off-body wireless communications), The design with the whip antenna sticking out of the insole will result in a less robust prototype and hence, would reduce the repeatability/reproducibility of our experiments. It is worthy of attention that the situation was

much more desirable in our first prototype, i.e., the smart shoes, since the transmitter was mounted in the back of the shoe.

Figure 16. Nike+ iPod (old and new versions) and Adidas Speed_Cell systems; note that the transmitter is placed in a hollowed out space in the sole of a compatible shoe in both cases. The last two systems detect activities such as shuffling, stepping, lunging and jumping.

Taking the above constraints into account, we are now characterizing the wireless communications of these smart insoles considering the energy-reliability tradeoffs. We have recently asked an enclosure design company to professionally design shoe inserts that will be built around our circuit. This way, we can maximize the repeatability, reproducibility and accuracy of our experiments.

5.2.1 Effect of Packet Size on Battery Lifetime

The size of a transmitted packet in a WBAN affects the power consumption of both the sender and receiver nodes. In error prone environments, e.g., smart insoles, optimal packet size can improve the energy efficiency. The work by [Wang2] presents several factors, such as the number of contending nodes, packet size, contention window, packet transmission collision probability and channel condition that affect the energy efficiency of 802.11 networks. The analysis and experimental results can be generalized for various available wireless technologies. We carried out experiments for packet payload size of 24 B, 54 B, and 84 B. For each packet size, we measured the current drawn at the sender node transmitting five packets per second to a receiver located 1 m away. We intentionally choose the distance to be small in order not to experience packet loss and observe the absolute effect of packet size on energy consumption. Obviously the results in more realistic WBAN scenarios will be different as longer packets are more prone to error and retransmissions are costly. Table 9 summarizes the average current consumption of the transmitting XBee and XBee Pro nodes for this low data rate experiment.

Table 9. Current draw for different packet sizes for XBee and XBee Pro modules.

Transmitter	**XBee**	**XBee**	**XBee**	**XBee Pro**	**XBee Pro**	**XBee Pro**
Receiver	XBee	XBee	XBee	XBee Pro	XBee Pro	XBee Pro
Packet size (Bytes)	24 B	54 B	84 B	24 B	54 B	84 B
Packet rate (Packets/s)	5	5	5	5	5	5
Average current over the entire duty cycle	2.5 mA	2.6 mA	2.7 mA	15.6 mA	15.9 mA	16.5 mA
Expected Battery life (1100 mAh)	440 h	423 h	407 h	71 h	69 h	67 h

The packet length affects the battery life of a WBAN. The battery life is reduced by 4-5% as we increase the packet size from 24 B to 54 B and from 54 B to 84 B. The energy consumption and battery life also depend on the function of the node, that is, if a node is the recipient of the data, it is expected to last few percent longer than the sender side for XBee based WBANs and up to five times longer than the sender side for XBee Pro based WBANs. In the smart insole platform, the receiver side is usually

assumed to be a computer workstation or a laptop. Thus, the power consumption of the receiver side is not a matter of concern. It should be noted that for higher data rate applications, e.g., smart insoles, he battery lifetime will be substantially reduced as a result of an increased duty cycle.

Packet retransmissions lower the average lifetime of the node by approximately 45 percent. The extra current consumption estimation due to retries can be stated as follows:

$$I_1 = \frac{I_t T_t + I_p T_p + I_i T_i + I_r T_r}{T_{ON}}, \tag{64}$$

where, I_r is the average current drawn when the node receives the acknowledgment ACK. T_r represents the time interval that the receiver remains on when receiving an ACK. I_p is average current when the node probes its destination for data. T_p represents average amount of time the receiver remains on when the node probes the destined node. It denotes the average current consumed when the node transmits the data to its parent. T_t is the duration of time the transmitter remains on when it sends 24/54/84 bytes of data. I_i is the average current consumed when the node is idle and T_i is of time the node remains in idle state when is waiting for an ACK.

When an XBee/XBee Pro node transmits a data packet, it will wait for network level ACK from the destination. If the node does not receive the ACK, it will retransmit the data. However, the node must poll the destination to check for available data in order to receive the ACK. Probing is performed every 100 ms. It is noteworthy that it takes approximately 4 ms for the node to switch from the transmitter mode to the receiver mode.

Based on the above, in smart insoles, we use the Broadcast Mode (as opposed to the Unicast Mode [XBee]) in order to prevent the insoles from retransmitting data packets. In the broadcast mode, any XBee/XBee Pro module within reach will accept a packet that contains a broadcast address. When configured to operate in Broadcast Mode, destination nodes do not send ACKs and transmitting modules do not automatically re-send packets as is the case in the Unicast Mode [XBee]. In the Unicast Mode, the number of retries can be controlled by the firmware (less than or equal to 3) and the selection of the number is made depending on the application and environment.

As previous study shows, only a small change in RSSI (and hence, SNR) may cause PRR to drop from 1 to 0 [Lin2], [Zuniga], [Srinivasan2].

5.3 Experimental Study of Off-Body Communications in Wireless Insoles

Although off-body communications and their on-body counterparts have many characteristics in common, e.g., radiation pattern distortion and antenna-body interaction, the primary signal paths forming the communications link show disparity in their propagation mechanism [Cotton].

Previous studies showed that path loss characteristics in LOS (line of sight) scenarios are dominated by interference between the direct path signal and the radiation reflected from the ground. It's noteworthy to notice that at 2.4 GHz no packet can get through the human body without utilizing multipath.

5.3.1 Stationary Scenarios (NLOS and Partial LOS)

We asked a male subject of height 175 cm to wear the smart insoles of size 10 in both outdoor and indoor environments. Throughout 60 seconds of RSSI measurement, the user was asked to stand still facing towards the receiver. The experiment was performed in both outdoor and indoor environments, in the middle of UCLA Intramural grass field and in a typical office environment in Boelter Hall at UCLA, respectively. The receiver is located few meters away from the smart insoles and 0.5 m above the ground in both cases.

Figure 17(a) shows RSSI values captured at the receiver throughout 60 seconds at three different transmit power levels (PL-1 = 10 dBm, PL-3 = 14 dBm, and PL-5 = 18 dBm) when the smart shoes were 2 m away from the receiver.

As expected, higher RSSI values are achieved for greater transmit powers. For example, for transmissions at 18 dBm, average RSSI values are about 17.4 dBm stronger than those when the power output level is set to 10 dBm.

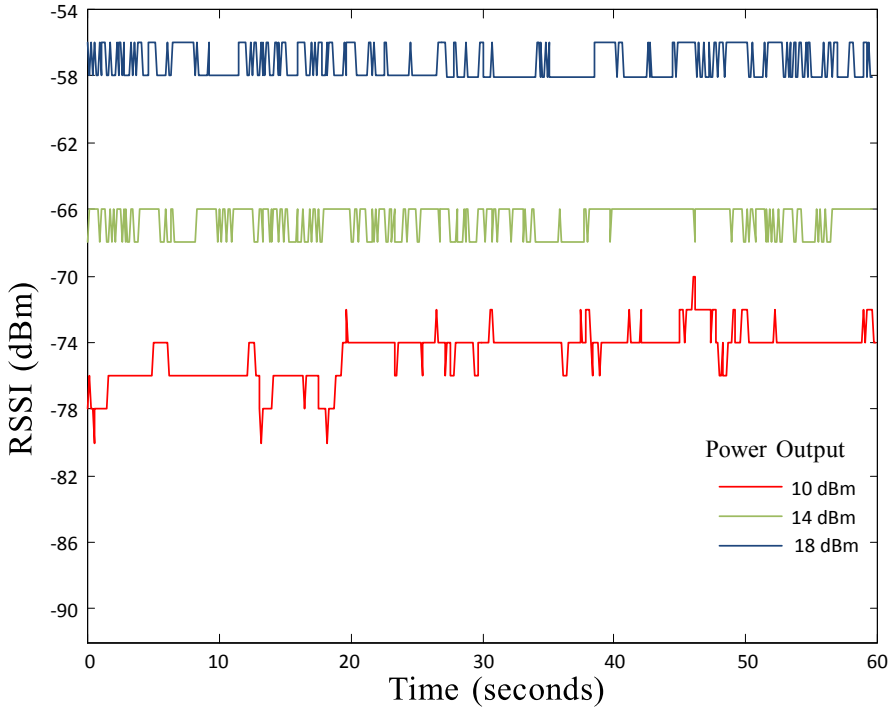

(a) Outdoor

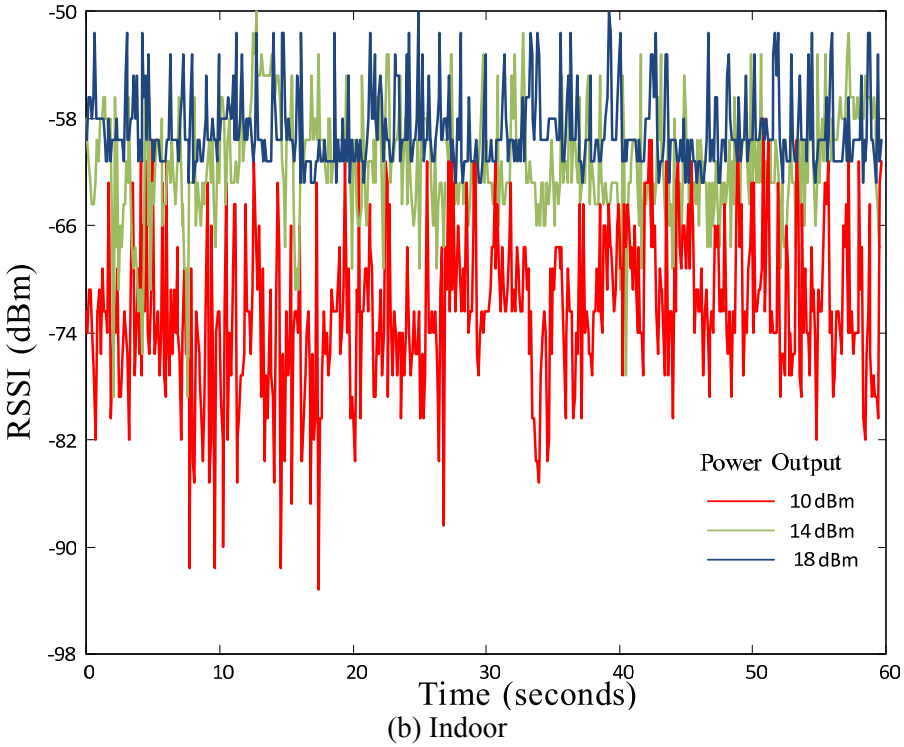

(b) Indoor

Figure 17. RSSI measurements versus time for a subject standing still for different transmission power levels utilized in smart insoles: (a) outdoor (b) indoor.

In indoor scenarios, due to the existence of multiple multi-path components, RSSI values oscillate to a

much greater extent. As illustrated in Figure 17(b), higher transmission power levels lead to much less deviations between the RSSI values observed at the receiver. Compare blue and red curves in Figure 17(b) as an example, where the red curve (power output of 18 dBm) presents an extremely chaotic trend comparing to the blue curve (power output of 10 dBm).

In our open outdoor environment, there is almost no multipath contribution except for multipath generated by the human body itself. On the other hand, in the office the contribution of multipath propagation is more pronounced, where reflections from the ground and surrounding objects can increase the total received power, and hence, RSSI. In this latter case, major contributions from the multipath components rather than the direct received signal (if any) comprise the received signal power. Although the surrounding objects are static, more steep changes can be seen in the RSSI values.

In another experiment, we regularly increased the distance to 5 m with increments of 1 m. Figure 18 displays average RSSI values for different distances for indoor and outdoor environments. The minimum distance in this experiment is when the subject stands right in front of the chair on which the receiving node resides.

As Figure 18(a) suggests, the rule “the higher the distance the weaker the RSSI values” holds for outdoor experiments where the number of multipath components arriving at the receiver is minimal. However, in the office environment, due to the existence of various obstacles and objects multipath effects are dominant and hence, the above rule does not hold at least for any distance between the smart shoes and the receiver. Furthermore, in the experiments performed at the office environment, we encountered situations, where RSSI values for lower transmit power levels were higher at the same distance between the smart shoes and the receiver. See Figure 18(b), where the red curve passes the green curve at distance of 4 m. The location of objects and obstacles, as well as their shape and the material from which they are built affect the intensity of multipath effects.

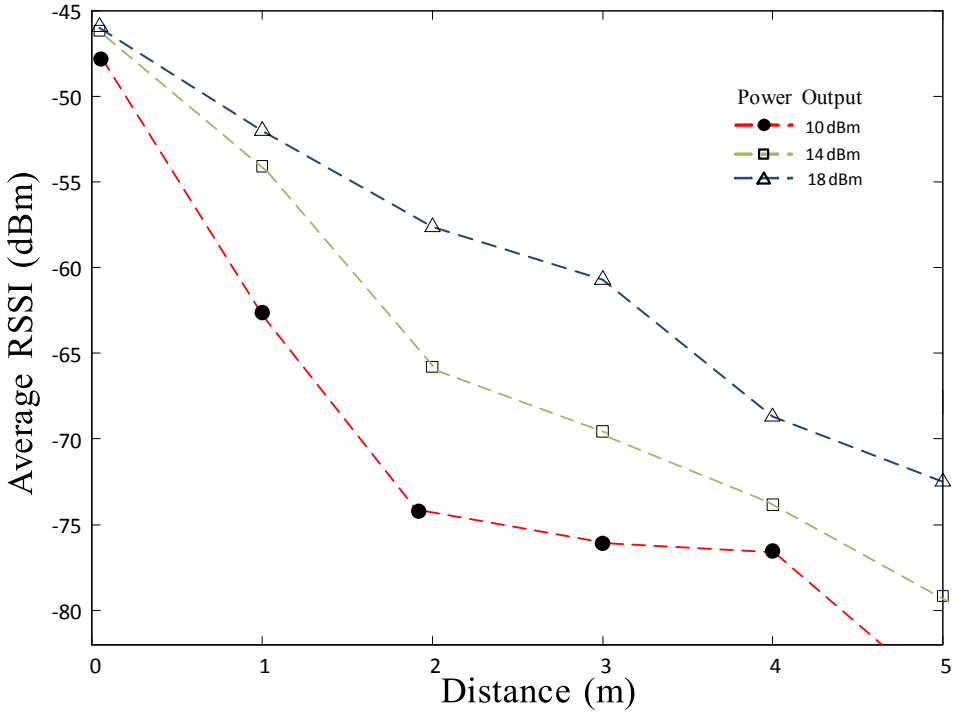

(a) Outdoor

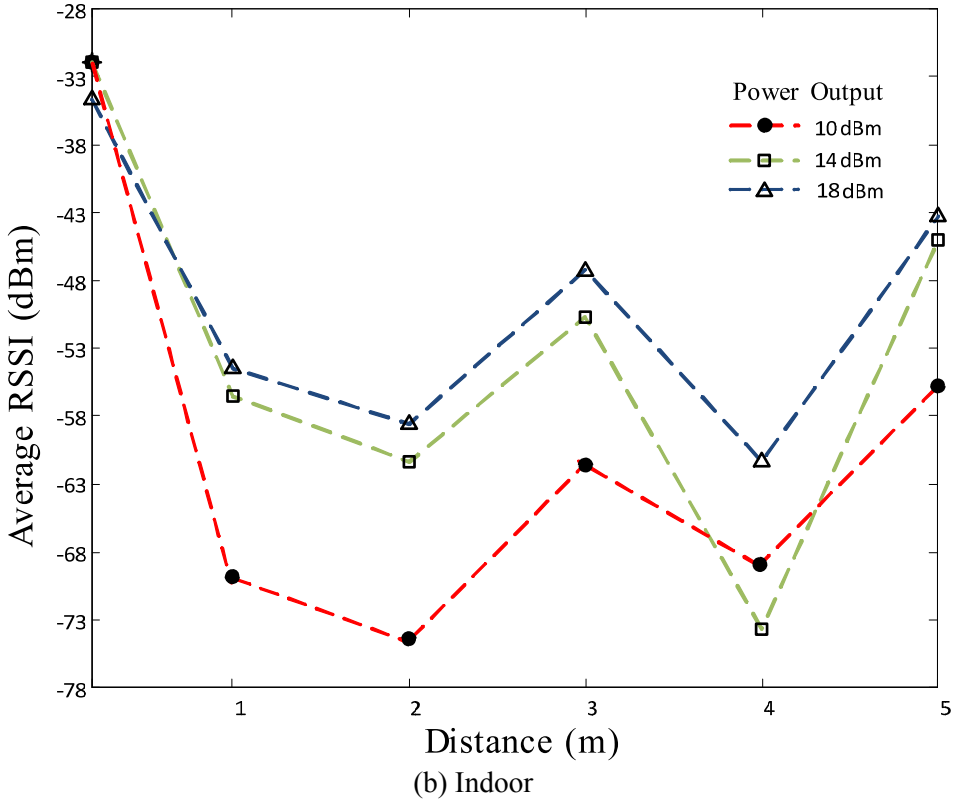

(b) Indoor

Figure 18. Average RSSI measurements versus distance for a subject standing still for different transmission power levels utilized in smart insoles: (a) outdoor (b) indoor.

Figure 19 illustrates the standard deviation of extracted RSSI values for all the experiments carried out in indoor and outdoor environments.

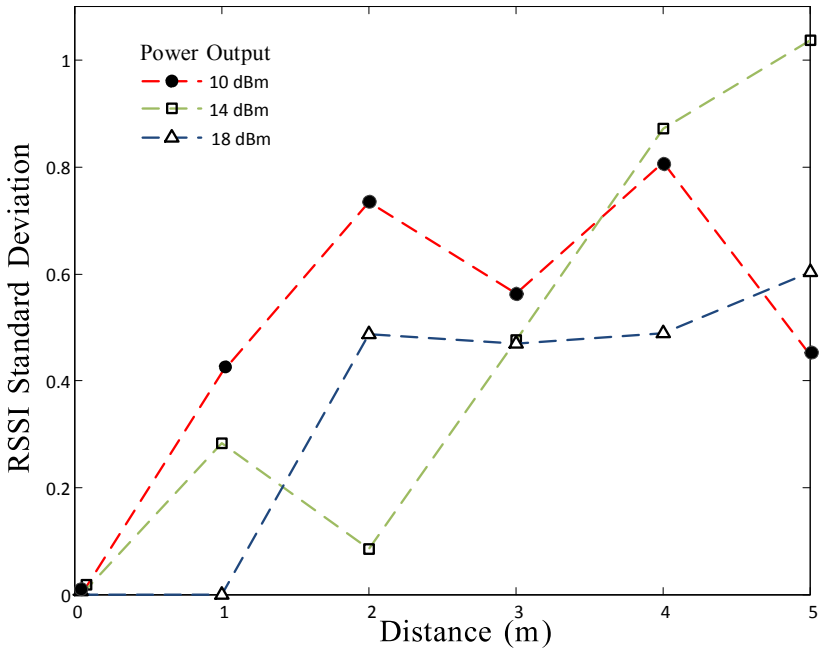

(a) Outdoor

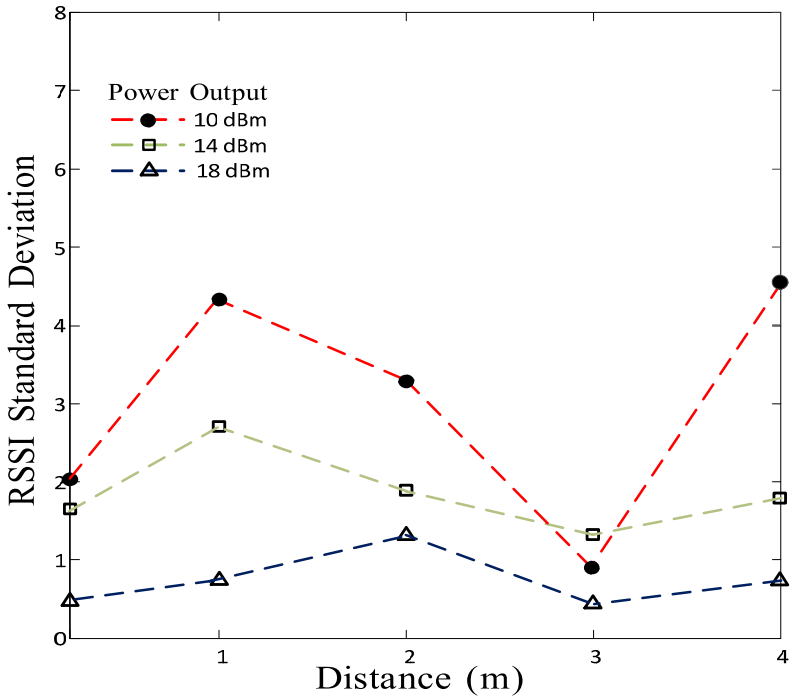

(b) Indoor

Figure 19. Standard deviation of RSSI measurements versus distance for a subject standing still for different transmission power levels utilized in smart insoles: (a) outdoor (b) indoor.

In outdoor experiments, the RSSI values are mostly stable and thus, the standard deviation does not significantly vary. This is clearly illustrated in Figure 19(a), where the maximum standard deviation is 1.04. As more uncertainties are involved in indoor scenarios, our indoor experiences show much more irregular results (see Figure 19(b)). However, both Figure 19(a) and Figure 19(b) confirm that the stronger the transmit power, the lesser the standard deviation of RSSI values.

With regards to the packet receive ratio, for all the experiments utilizing transmit power levels of 18 dBm and 14 dBm, the PRR was above 95%. However, in experiments in which the transmit power level was set to 10 dBm, we experienced packet drop rate of 5%, 12%, 20%, and over 50% for distances 2 m, 3 m, 4 m, and 5 m, respectively. In fact, even choosing a conservative threshold of -80 dBm for RSSI values does not always allow for communications with packet drop rates less than 5%.

Consequently, utilizing the maximum transmit power allowed by the XBee modules (+18 dBm) would be a reasonable option if no packet loss can be tolerated. Of course, for longer distances, even the maximum transmit power cannot guarantee the delivery of all packets.

We performed a range test for smart insoles while a subject was wearing them and we ask him to increase his distance from the receiver with increments of 2 m. The maximum range for which the PRR is above 90% was only 25 m for an open grass field. However, in indoor scenarios the range fundamentally depends on where the experiment is taking place. For instance, in a long corridor with no objects obstructing the path from the transmitter to the receiver, we were able to achieve over 50 m of data range. Nevertheless, in the library environment with many objects on the way of the signal, the data range was no more than 10 m. It is important to note that lower achieved ranges (as opposed to off-body experiments in Section 4.2.2. and Figure 10) in case of smart insoles are as a result of violating the Fresnel-zone clearance, human body shadowing, and negative effects of ground.

Janek and Evans [Janek] have performed field measurements indicating that the effect of antenna placement close to the ground (especially within 10 cm) significantly changes the omnidirectional transmission pattern.

5.3.2 Walking Scenarios

Human locomotion is considered to take two primary forms: walking and running. Walking is a form of locomotion defined by a double support phase when both feet are on the ground at the same time. Running is a form of locomotion that does not have this double support phase. In human running, the feet are never in contact with the ground simultaneously and there is a phase where neither of the feet is in contact with the ground and both feet are temporarily airborne [Wiki_Locomotion].

Humans are able to walk at speeds faster than 2.0 m/s, and capable of running at speeds less than 2.0 m/s. The preferred walking speed is the speed at which humans choose to walk. In the absence of significant external factors, humans tend to walk at about 1.4 m/s (5.0 km/h). Although humans are capable of walking at speeds from nearly 0 m/s to over 2.0 m/s (7.2 km/h), humans typically choose to use only a small range within these speeds. Although walking speeds can vary greatly depending on factors such as height, weight, age, terrain, surface, load, culture, effort, and fitness, the average human walking speed is about 5.0 km/h, or about 1.3 m/s [Raynor].

We profile, at different radio transmit levels, the variations in link quality with time as smart insoles are utilized in routine walking activities. We should ideally take simultaneous RSSI measurements at all power levels, which is infeasible. As such, we make the smart insoles transmit every packet multiple times instantly after each other at three different transmit levels used in the previous experiment, i.e., 18 dBm, 14 dBm, and 10 dBm. The receiver can thus simultaneously record the RSSI values corresponding to each transmission power level. Measurements for three power levels are shown in Figure 20. In this scenario, the subject was asked to walk back and forth on a grass field for four minutes at his normal walking speed, i.e., 1.0~1.3 m/s. The subject was asked to stay between 1 m and 8 m from the receiver.

The RSSI values are plotted in Figure 20 for the three transmission power levels. We observe that for each transmission power, RSSI values greatly fluctuate: at the transmission power of 18 dBm, the signal strength at the receiver spans between −64 dBm (at the 33th second) to −95 dBm (at the 87th second), i.e.,

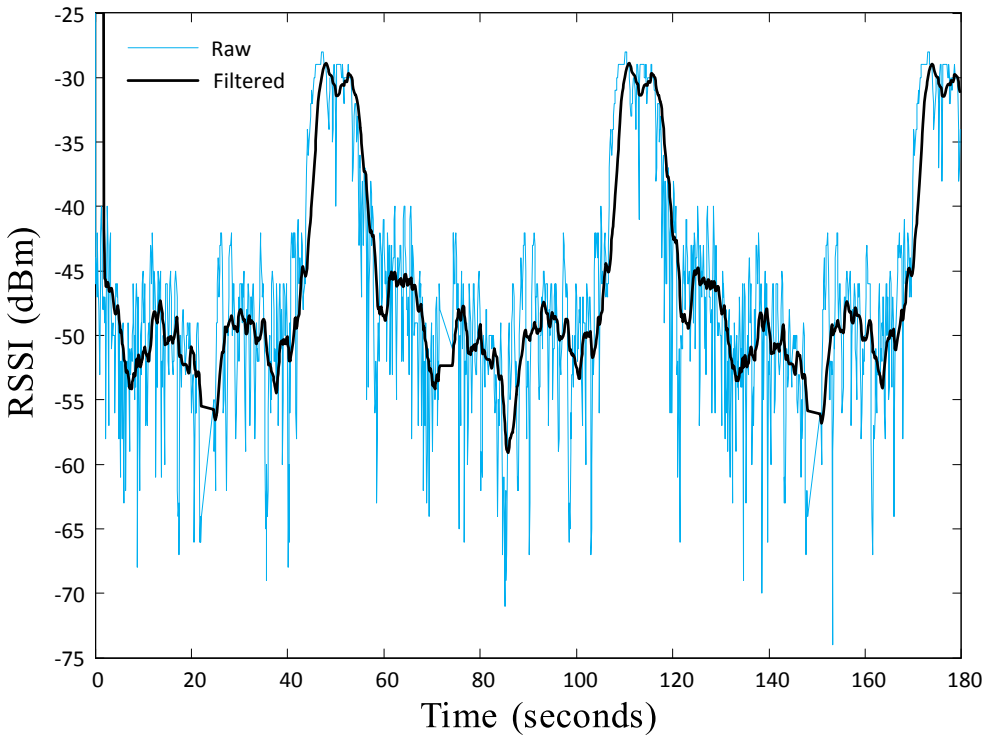

(a)

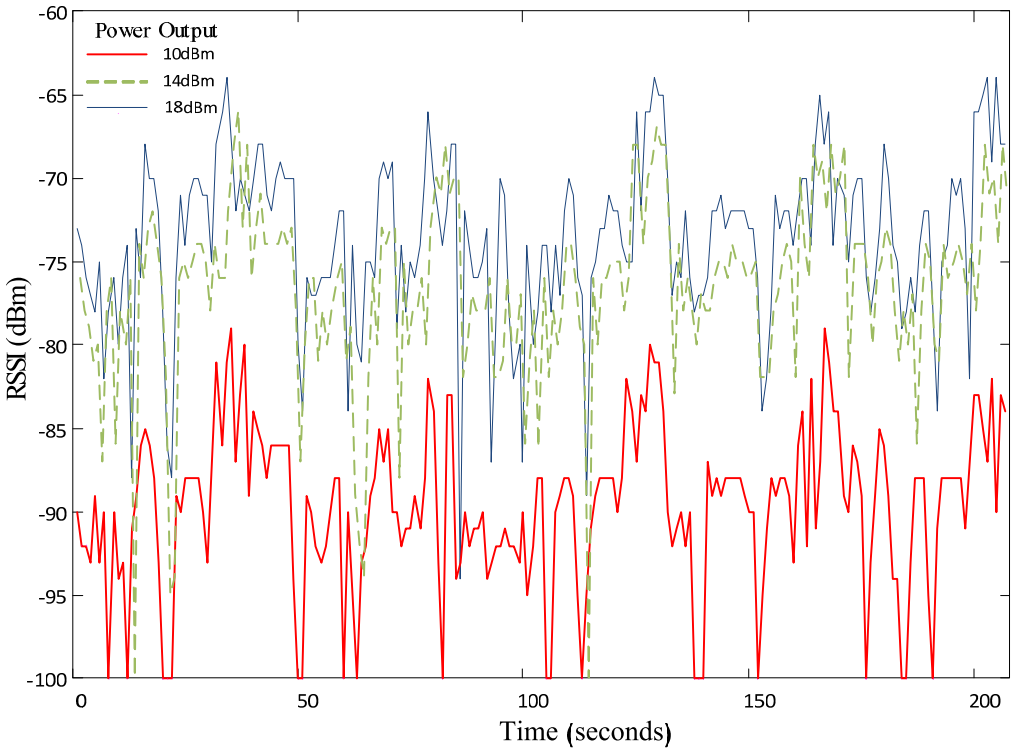

(b)

Figure 20. (a) Raw RSSI data versus filtered RSSI data for walking scenarios (b) RSSI measurements versus time for a subject walking back and forth with respect to the receiver. Data transmissions are conducted at three power levels, 10, 14, 18 dBm.

a variation of 31 dBm in less than a minute. Nevertheless, there are a number of distinguishable trends: for example, in the interval 30~33 s, the RSSI values are consistently above −73 dBm due to more clearance in the Fresnel zone as opposed to complete obstruction for farther distances. It is noteworthy that the subject walks towards the receiver in this time interval. Fine-grained patterns can be attributed to the instantaneous position/elevation of the shoes with respect to the ground, whereas, coarse-grained patterns are mostly as a result of the distance and moving direction of the subject. The coarse-grained trend in the plot is obvious: the RSSI values are fairly low for the first half of each back and forth period, since the subject's body completely blocks the line-of-sight; then the RSSI values rise up to higher values due to the intermittent appearance of line-of-sight.

Figure 21 illustrates the correlation between RSSI values and the PRR in stationary and walking experiments for transmission power level of 10 dBm. The solid curve represents the analytically determined RSSI values corresponding to each PRR value. The derivation of the analytical RSSI values is presented in Appendix C. The error bars show the range of the measured RSSI values for PRRs associated with non-overlapping windows of 250 samples (or equivalently 5 seconds of data). From the experimental results, we made the following observations:

- Packets cannot be consistently received when the RSSI values are below a certain target, otherwise the PRR is close to 100%;
- the RSSI target is strongly correlated with the noise floor when there is no interference effect;
- the analytical RSSI target is derived assuming the noise floor of the receiver is known and there is no mobility. Moreover, it is assumed that the 2.4 GHz interference is minimal and there is an LOS path between the smart insoles and the receiver. The effect of distance and packet length can also be included in the analytical model;
- variations of RSSI values increase significantly in the walking scenarios. Moreover, in walking scenarios due to the effects of fast fading, the mean RSSI needs to be higher in order to yield almost the same PRR as stationary cases.

- packet losses become extremely bursty in the walking scenarios and assessments of channel quality are quickly outdated.

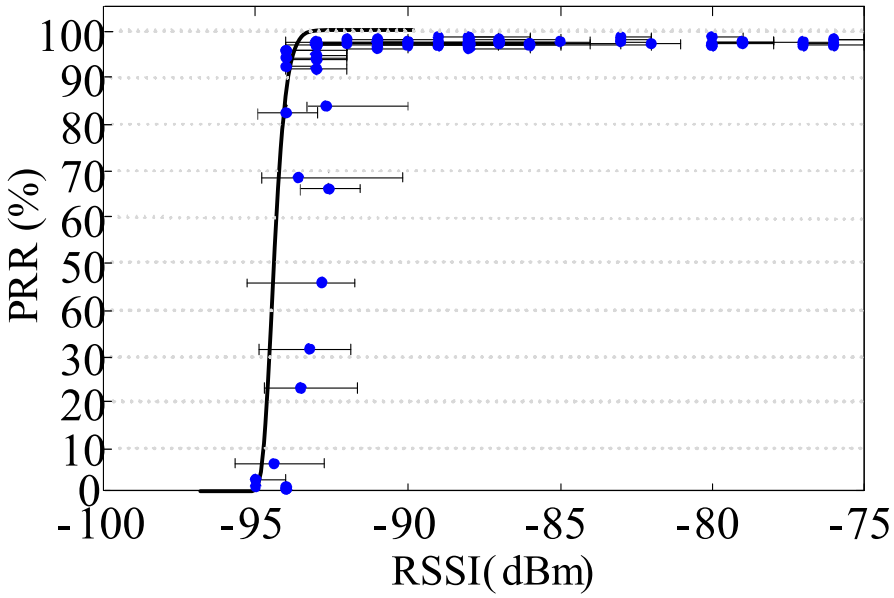

(a)

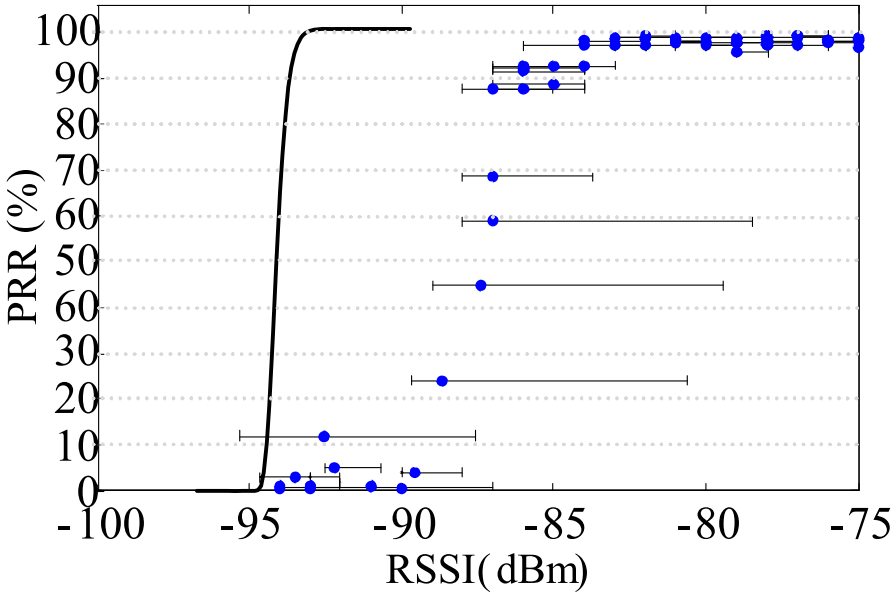

(b)

Figure 21. Correlation between RSSI and PRR for stationary and walking scenarios. The solid line denotes the analytically determined PRR as a function of RSSI (See Appendix B).

Wireless communications experience shadowing conditions, since the transmitter is obstructed by

user's feet. Moreover, additional path loss is experienced as a consequence of fresnel-zone clearance violation. Additional path loss would be as a consequence of the user's orientation. Whenever the user faces towards the receiver, the flexible patch antenna inside the insole will possess its maximum gain.

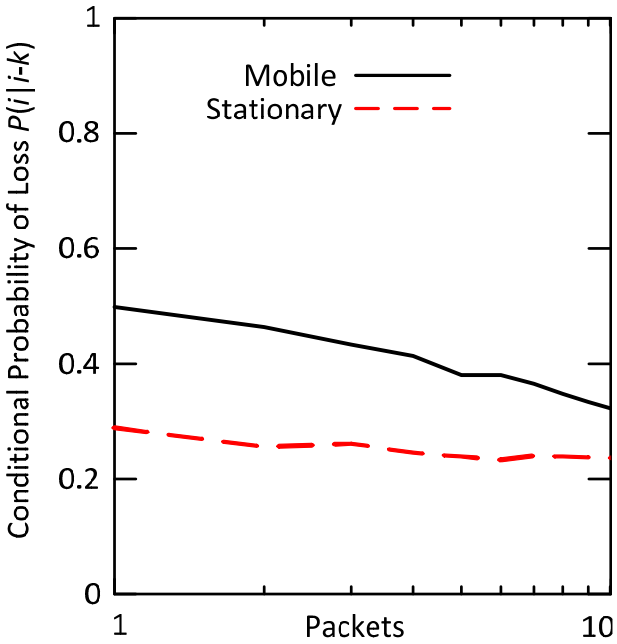

Figure 22. Probability that packet i is lost if packet $i - k$ is lost as a function of k. The transmission power is 10 dBm.

In order to further analyze the packet loss pattern and its burstiness in the walking scenarios, we asked a subject to walk, while wearing the smart shoes, in a circle around the receiver on UCLA's intramural grass field. The receiver was placed on a box with height of 0.5 m. The radius of the circle was set to 10 m, which on average yields PRRs of 25%-30% and 20%-25% for mobile (walking) and stationary scenarios, respectively.

Figure 22 depicts the conditional probability of losing packet i, at transmission power level of 10 dBm, given that the packet $i - k$ was lost. Although the PRR (which represents unconditional loss probability) for both mobile and stationary cases was around 25%, a much higher conditional loss probability, especially for small values of k, is demonstrated for the mobile case. While the subject walks, packets demonstrate a higher degree of dependence with the recent few packets, resulting in a higher loss

probability for small values of k in the mobile case. On the other hand, for stationary cases the fate history of prior packets does not change the fate of the current packet.

It should be remembered that the data rate and transmission power level at which the transmissions are conducted affect the conditional probability as well. For lower data rates the conditional packet loss probability plots progressively converge and they merge for packet rates of only one packet per second. Thus, packet losses become more independent of each other over time. As for the transmission power, employing a higher power level in the above experiment resulted in less discrepancy between the conditional probability plots for mobile and stationary cases. This is as expected; since, employing higher transmissions power levels in this experiment leads to PRRs of 70% and 90% for transmission power levels of 14 dBm and 18 dBm, respectively. Accordingly, there will be less room for discrepancy between mobile and stationary scenarios. Nevertheless, if we increase the separation distance in addition to utilizing a higher transmission power level, we observe the same phenomena in the conditional packet loss probability curves.

In the next subsection we investigate the variations in the RSSI signal while the subject turns (rotates). The question of whether these patterns provide opportunities for energy savings by adapting the transmission power will be dealt with in Section 5.4. We will develop intelligent TPC algorithms that can use the notion of "walking" to improve the control of transmission power and hence, reduce the energy consumption of smart insoles and similar systems.

5.3.3 Turning Scenarios

Turning around is a task frequently performed by us during various activities of daily living. The ability to turn during walking is an essential part of goal-directed locomotion. A normal turn requires a pivot. One foot is kept on the ground and rotation occurs on the ball of that foot. Accordingly, the body's center of mass experience minimal displacement. Changes in turning are one of the early motor deficiencies, which increases the risk of falls and fall injuries in diseases such as Parkinson's Disease (PD) [Wang_3]. 180° turns are also one the main components of the Timed Up and Go (TUG) test, a widely-used clinical

test to evaluate balance and mobility.

We performed a further set of experiments to find the impact of body shadowing as a subject turns 360° and to help identify a pattern for shadowing in off-body channels.

Figure 23 depicts RSSI values as the user turns 360° at the distance of 3 m from the receiver laptop. The subject had an angular velocity of approximately $60°s^{-1}$. We observe that the RSSI values deteriorate until the point where the subject has turned for approximately 120°. At this point, we enter the maximum body shadowing region, where the rate at which RSSI values change (using a moving window of 1 s) is notably decreased. In this region, while the average RSSI value does not considerably change, the instantaneous RSSI values are subject to significant fluctuations greater than 10 dB around the average RSSI values.

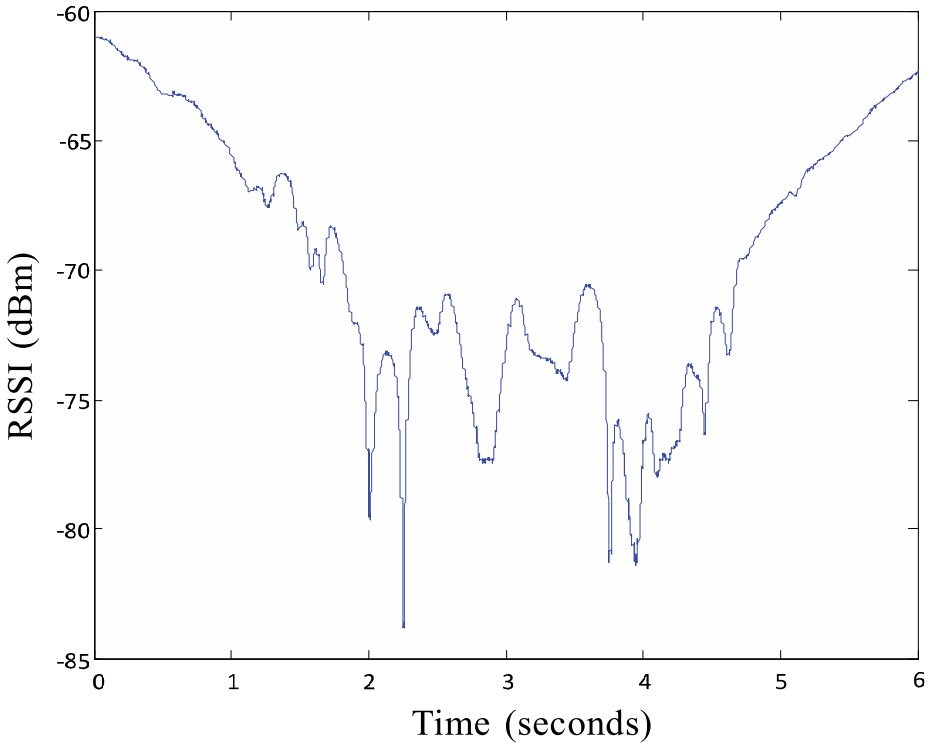

Figure 23. RSSI measurements versus time for a subject performing a 360° turn in 6 seconds while wearing the smart insoles. The user is 3 m away from the receiver and the transmissions are conducted at 18 dBm.

Body shadowing has a major effect on radio propagations from the smart insoles; however, when

combined with small changes in body posture, it may cause even higher fluctuations in RSSI values. It should be noted that we experience less signal variation in this experiment as compared to the ambulation results reported in the previous section; this is because: a) the rotation speed is relatively low, i.e., 60 per second, and b) there is no step taken and hence, the intensity of the impact between the foot and the floor is much less than ambulation scenarios. In the ambulation scenarios, we experience a great deal of RSSI variations exactly at the moment that each foot hits the ground. Body shadowing has a major effect on radio propagations from the smart insoles, however, when combined with small changes in body posture, it may cause even higher fluctuations in RSSI values. It should be noted that we experience less signal variation in this experiment as compared to the ambulation results reported in the previous section; this is because: a) the rotation speed is relatively low, i.e., 60 per second, and b) there is no step taken and hence, the intensity of the impact between the foot and the floor is much less than ambulation scenarios.

It also should be noted that even if we exclude the body shadowing effects, the XBee's chip antenna still will not be able to radiate to all directions in an isotropic manner.

Walking in a straight line is difficult for patients with Parkinson's disease and turning is even more challenging. Freezing of gait and falls commonly occur while turning.

5.3.4 Radiation Pattern

Since electromagnetic radiation is dipole radiation, it is not possible to build an antenna that radiates equally in all directions, although such a hypothetical isotropic antenna is served as a reference to calculate antenna gain [Wiki2].

As Figure 24(b) indicates, the radiation pattern for a whip antenna is similar to that of a dipole antenna, in that it is shaped like a donut. Thus, the performance of the XBee Pro module using a whip antenna is relatively independent of its orientation in the plane perpendicular to the whip antenna. On the other hand, the radiation pattern of the chip antenna is not as uniform and long-range as that of the whip antenna, based on Figure 24(c) and Table 10. Therefore, certain orientations yield better performance than others. Nevertheless, in the smart insoles both the body-worn antenna, i.e., the one in the insole, and

receiver antenna are of type chip antenna, which meets the tight spacing requirements inside the smart insoles in light of to its smaller form factor.

Similar to experiments described in Chapter 4, the transmitter was programmed to transmit packets containing a sequence number that was incremented from one packet to the next. The receiver (and associated lap-top PC) was configured to keep track of PRR. The transmitter and receiver were alike, i.e., the module-type and antenna-type were identical. 99% successful packet delivery was chosen as a benchmark for comparison purposes in Table 10. The receiver did not acknowledge the reception a packet. Furthermore, the transmitter transmits each packet only once.

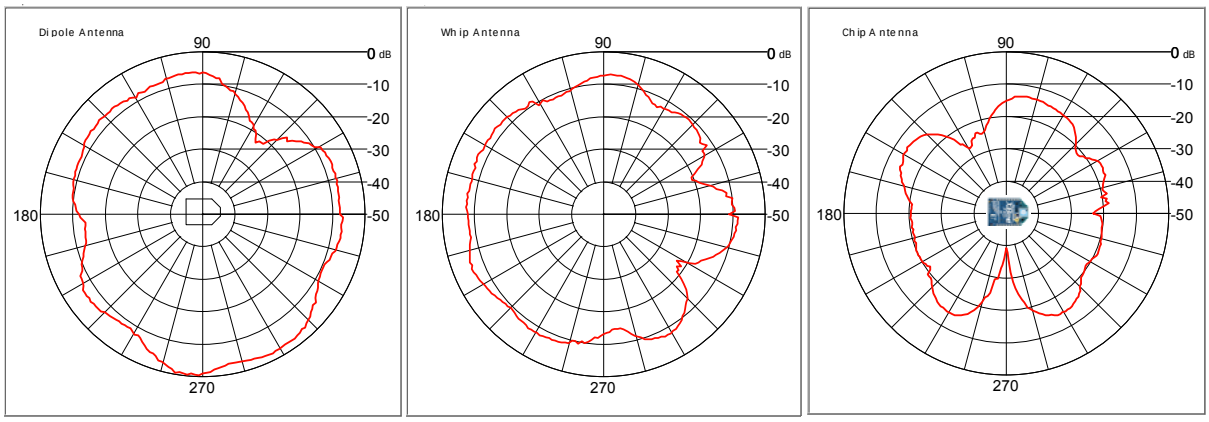

(a) (b) (c)

Figure 24. Radiation patterns of a (a) dipole antenna, (b) a whip antenna, and (c) a chip antenna connected to an XBee-PRO module. The patterns for the last two cases are normalized to the peak of the dipole antenna.

The following important observations should be remembered after reviewing Figure 24 and Table 10: I- Both the XBee-Pro and XBee achieve more range in outdoor settings than their indoors counterparts. II- XBee-Pro modules provide more range than XBee modules. III- Only for outdoor environments, the whip antenna has a range advantage over the chip antenna. IV- A number of outdoor receiver locations were not within RF line-of-sight of the transmitter; however, they were within visual line-of-sight of the transmitter. V- If more range is required, and space is a constraint, then the XBee-Pro module with a chip antenna is more effective.

Table 10. Current draw for different packet sizes for XBee and XBee Pro modules.

Module	Antenna Type	Outdoor LOS Range	Indoor Range
XBee	Chip antenna	143 m	24 m
	Whip antenna	258 m	24 m
XBee-Pro	Chip antenna	515 m	43 m
	Whip antenna	1335 m	43 m

5.4 TPC and Off-Body Communications in Wireless Insoles

In this section we explain different types of transmission power control methods. Then we present a number of TPC schemes that have been utilized in sensor networks and WBANs; and lastly we present a novel method to dynamically adjust the transmission power for smart shoes based on the type of activity that the user performs for different granularities, i.e., coarse-grained activities and fine-grained activities.

5.4.1 Observations from Characterization Process

The relationship between dynamics of link quality and packet receive ratio was investigated in Section 5.3 for different transmission power levels. We performed experiments at different environments (indoors and outdoors) since the smart insoles are intended for both controlled and uncontrolled settings. In light of insoles always being on the ground and in the user's shoes, we can never achieve the Fresnel clearance; thus, the ground effect limits the transmission range and more importantly it makes the characterization process more sophisticated. Furthermore, the bottom of the foot is very close to the transmitter and the resulting body shadowing effect will add up to the complexity of the characterization process. It should be remembered that 2.4 GHz signals are not able to pass through the human body. Last but not least, wireless insoles are mobile and movement affects the wireless signals. We observed that the following factors affect the quality of the wireless channel and thus, the reliability of wireless communications:

I) Direction of movement with respect to the receiver, II) Speed of walking, e.g., fast walk versus slow walk, III) the time interval when the user turns around or changes his/her direction, and IV) the portion of each gait cycle, where the feet are off the ground. This recent case may lead to a partial line of sight (LOS).

For on-body wireless communications we were able to identify critical thresholds representing the best compromise between false positives (i.e., the links meeting the RSSI threshold but below the PRR threshold) and false negatives (i.e., the links meeting the PRR threshold but below the RSSI threshold). Figure 25 displays the relationship between PRR and RSSI values for the on-body wireless communications on an open grass field presented in Section 4.2.3.

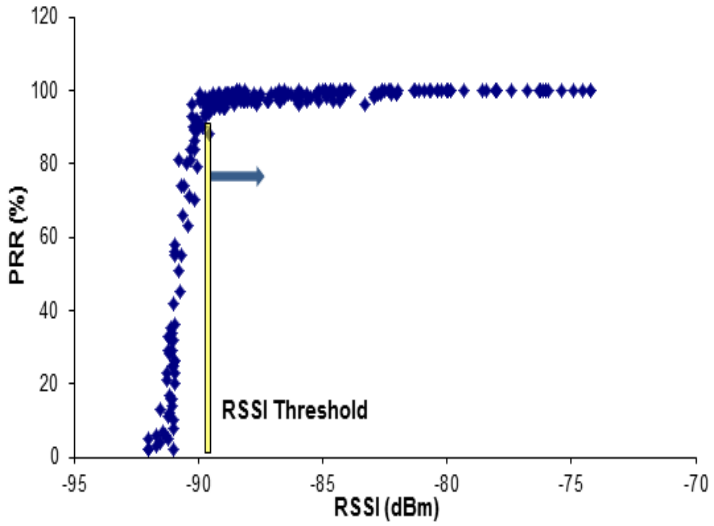

Figure 25. Packet receive ratio versus RSSI for on-body wireless communications on a grass field for XBee motes.

As it can be seen in Figure 25, RSSI values can be effectively used as binary link quality estimators for on-body wireless communications. This is the case for all of the scenarios, where the LOS and/or NLOS links do not alternate. Such assumption makes sense, since the sensors (and hence, the transmitters) do not substantially move on the human body, and neither does the receiver (e.g., a cell phone).

For off-body communications from the smart shoes, unless we choose a very conservative threshold, there is no specific threshold separating "good links" from "bad links". This can be attributed to the following reasons:

a) Unlike on-body communications, the transmitter-receiver distance greatly varies as the receiver is stationary and the user is supposed to walk in order for the system to derive gait parameters.

b) For on-body communications, LOS or partial LOS type scenarios for the most part maintain their

type; however, in the smart shoes the communications mostly take place through NLOS signals and partial LOS scenarios quickly turn into NLOS scenarios.

c) Unlike on-body communications, the contribution of diffracted signals around the body is not of significant help.

5.4.2 Open-Loop and Closed-Loop Transmission Power Control

Many different schemes exist to determine the transmission power for mobile devices in Mobile Ad-Hoc Networks (MANETs) and cellular networks ([Chen], [Correia]).

In closed-loop TPC, the appropriate transmission power control is obtained by using control packets and/or acknowledgement packets (see Figure 26). In the open-loop TPC, each node estimates the link quality using its own estimation of the link quality. The estimated quality degradation is then compensated by adjustment of transmission. Open loop TPC operates transmitting nodes adjust their transmit power level independent of the base station.

Closed-loop schemes mainly take advantage of link quality related metrics (e.g., received signal strength indicator (RSSI), signal to noise ratio (SNR), Link Quality Indication (LQI), signal to interference ratio (SIR)) computed for incoming packets at the receiving node and compare the resulting values to dynamic or static thresholds to determine the transmission power at the transmitting node. There exist a number of TPC methods that utilize packet delivery rates (e.g., PRR) instead of variable signal strength measurements; such methods are expected to be more stable.

The TPC methods utilizing link quality metrics incur minimal delay, as metrics such as RSSI and LQI are reported without delay. Such methods consider fixed thresholds for all the scenarios, which only works for few scenarios. On the other side, The PRR-based TPC schemes are expected to perform better; since, they directly make use of the PRR to power level correlation, however, they suffer from an inherent delay because PRR is not an instantaneous parameter and a certain number of packets must be received before we can calculate the PRR in a fairly accurate fashion.

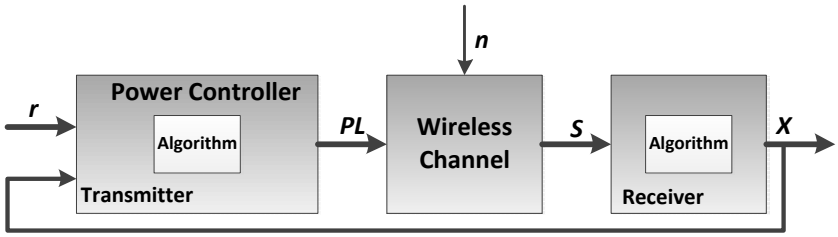

Figure 26. Closed-loop and open-loop transmission power control.

In both link quality based and PRR-based TPC methods, the base station measures PRR or the intended link quality metric and compares it to the target threshold. If it is less than the target, the base station will command the transmitter to increase its transmission power. Likewise, if the link quality metric is greater than the target, the base station will have the transmitter decrease its transmission power. The transmitter itself can also make decisions and run TPC algorithms; for instance, if acknowledgements are on and the recent packet is not acknowledged, the transmitter can increase its transmit power for the future packets. Likewise, it can always estimate the current PRR, and react appropriately.

Regardless of in which side TPC decisions are made, the goal of those schemes is to maintain a constant link quality or PRR measurements at the receiver by informing the transmitter of the latest measurements which then adjusts its transmission power, accordingly.

5.5 TCP/IP-Inspired TPC

One class of control algorithms is inspired by the TCP congestion control mechanism, in which the receiver side maintains a running average of the link quality metrics, generally denoted by $\overline{X}$, where X can be RSSI, LQI, a combination of them, or PRR. Using the weighted average stabilizes the scheme against unreliable samples. Exponential smoothing is used to update the running average; thus for every new X, the running average will be updated [Xiao].

Exponential smoothing is similar to moving average; however, it places more weight on the most recent samples. The weight on early samples drops exponentially; hence, the older the sample, the less its

influence. The weights assigned to older samples are in general proportional to the terms of the geometric sequence, $\{1, (1-\alpha), (1-\alpha)^2, (1-\alpha)^3, \ldots\}$. A geometric sequence is the discrete version of an exponential function, where α is called the smoothing factor. Exponential smoothing and moving average also differ in that exponential smoothing takes into account all past samples, whereas moving average only takes into account k past samples. From the point of view of memory demands, they are different in that moving average requires the past k samples to be kept, whereas exponential smoothing only needs the most recent sample to be kept. Exponential smoothing and moving average are similar in that they both assume a stationary, not trending, time series, therefore lagging behind the trend if one exists. They also both have roughly the same forecast error distribution when $\alpha = 2/(k+1)$ [Wiki3].

Figure 27 outlines a general case of TCP/IP-Inspired TPC (left) and a customized form for XBee Pro motes (right). It should be noted that the current version of XBee protocol does not provide LQI measurements and thus, RSSI will be the most suitable choice for X.

	General	XBee Pro
1:	$\overline{X} \leftarrow (1-\alpha)\overline{X} + \alpha X$	$\overline{X} \leftarrow (1-\alpha)\overline{X} + \alpha X$
2:	if $\overline{X} < T_L$ double the transmiss ion power	if $\overline{X} < T_L$ increase the transmiss ion power by two levels (capped at 4)
3:	if $T_L < \overline{X} < T_H$ keep the previous transmit power	if $T_L < \overline{X} < T_H$ keep the previous transmit power
4:	if $\overline{X} > T_H$ reduce the transmiss ion power by a constant	if $\overline{X} > T_H$ reduce the transmiss ion power by one level (capped at 0)

Figure 27. TCP/IP-inspired transmission power control.

This scheme increases or reduces transmission power level by comparing the running average of X against lower and upper thresholds, namely T_L and T_H. If it falls below T_L, the transmit power is doubled immediately to avoid impending packet loss in the allegedly deteriorating channel. On the other hand, if the transmitting node finds the running average of X to be greater than T_H, the transmission power is reduced by a fixed amount.

The above approach was inspired by the congestion avoidance mechanism used in the Transmission Control Protocol (TCP), in which the policy of additive increase enlarges the size of the congestion window by a fixed amount every round trip time. When congestion is detected, the sender decreases the transmission rate by a multiplicative factor; for instance, it cuts the congestion window in half after loss.

The TCP congestion avoidance mechanism is the primary basis for congestion control in the Internet.

In this TCP inspired transmission power control technique, the increase in transmit power is multiplicative, while the decrease is additive, and hence, it is biased towards reacting faster to a decaying channel than an improving one. Here α is a weighting factor which decides how heavy the current X (e.g., RSSI) should be weighted.

Our on-body experiments for stationary scenarios in Chapter 4 indicate that $T_L = -80$ dBm is appropriate for the XBee platforms and $T_L = -90$ dBm is suitable for XBee Pro modules. Lower values for T_H make the target RSSI range $[T_L, T_H]$ too narrow while greater values lead to higher transmission power (and hence, more energy consumption) than required [Xiao]. In one setup for XBee Pro modules, one may set $\alpha = 0.8$, $T_L = -90$ dBm and $T_H = -85$ dBm.

If the current packet becomes lost, the sender side assumes that the current X is equal to the minimum value of the link quality metric; for instance, if we use RSSI as our quality metric for XBee Pro modules, the receiver's sensitivity (-100 dBm) will be used as the current X.

In general, applications where energy savings are given the highest premium and data loss is not as critical may adopt an aggressive strategy with such a high $\alpha = 0.8$ that rapidly reacts to improvements in channel conditions; on the other side, assigning a low value to α (e.g., $\alpha = 0.2$) works for applications whose intention is to ignore a transient bad channel. In the latter case, the transmission power is reduced cautiously when good channel conditions are established.

This class of TPC schemes is very flexible and easy to implement in platforms with very limited CPU and memory resources such as MicaZ and XBee platforms. The parameters α, T_H, and T_L can be adjusted to achieve the most appropriate energy-reliability trade off.

In TCP/IP inspired power control schemes, the base station measures the link quality metric (such as RSSI) for each received packet and sends the measures value back to the transmitting node via the acknowledgment packet. It is assumed that the acknowledgment packets are communicated at the maximum transmit power level and are never lost.

5.6 Sensor-Assisted TPC

TCP/IP inspired power control schemes can either adapt the transmission power aggressively or conservatively. Therefore, they treat mobile and stationary WBANS equally. However, a variety of WBANs, and smart shoes in particular, are used in mixed mobile and stationary scenarios in various environments.

As shown in Section 5.3.2, packet losses during walking activities become more bursty and thus, assessments of channel quality are quickly outdated. Investigators in [Srinivasan2] have shown that for a 802.15.4 wireless link with PRR of 50%, the probability of having two consecutive packet losses is only slightly lower than having a single packet loss (0.4 as opposed to 0.5). Not surprisingly, instantaneous RSSI variation is high when WBAN nodes are mobile. In particular, the walking activity data is characterized by its highly variable RSSI values at the receiver; while, on the other side, the RSSI values for the standing still scenario vary to a much lesser extent.

This observation motivates a sensor-assisted transmission power control scheme that alternates between the two scenarios, which adapts differently depending on whether or not the WBAN nodes are mobile. In the static case, where the channel remains relatively stable, it is reasonable to save energy by maintaining a longer history of link quality values to avoid dealing with periods of short-term fading. On the other hand, it is reasonable in mobile cases to keep only a short history and react quickly to channel degradation; hence, making more informed decisions in increasing the transmission power.

Figure 28 outlines the idea behind our approach, where the TPC loop takes advantage of a subject's mobility state from available sensors in the smart shoe platform to switch between conservative and aggressive mechanisms. Correspondingly, we propose a sensor-assisted TPC method that changes strategies based on coarse-grained and fine-grained mobility state information. Our method relies on mobility state information achieved locally or received from the base station to switch between the two strategies.

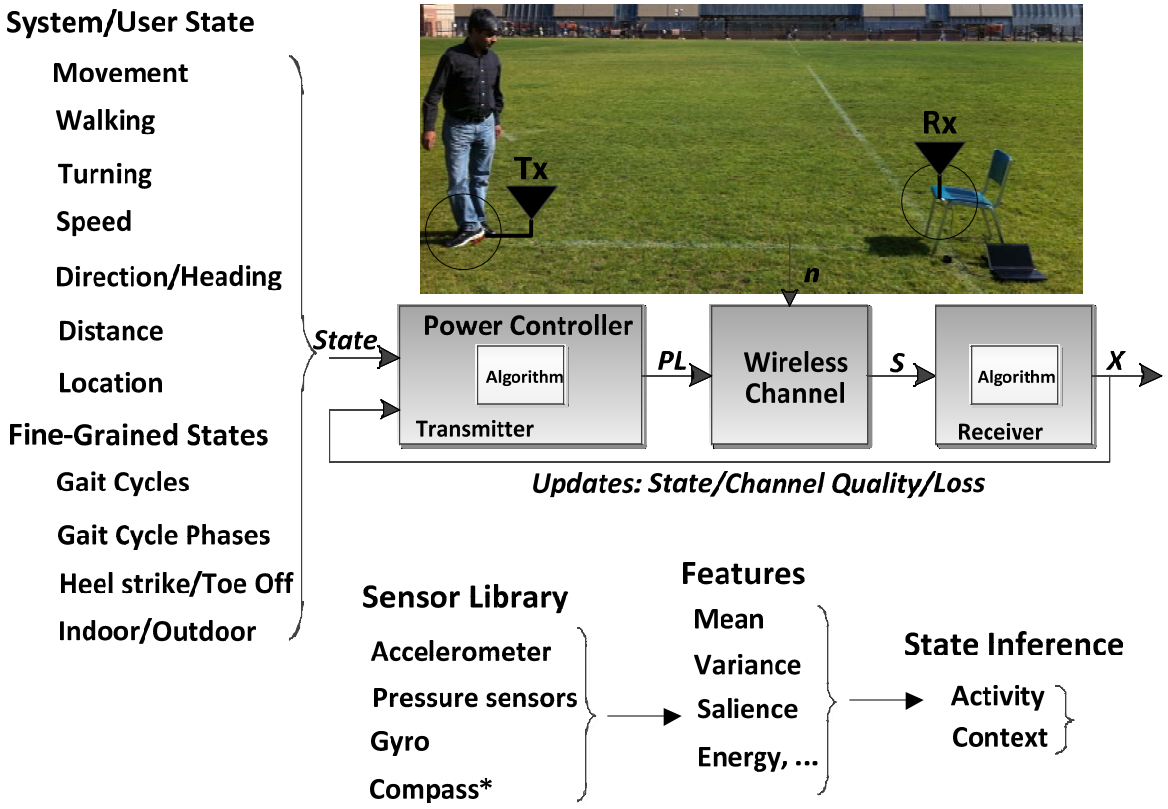

Figure 28. Sensor-assisted transmission power control.

Smart shoes, although reminding us of walking activities, are likely to spend a significant fraction of their time stationary, during which they produce plantar pressure data; or similarly, they are being used in sit-to-stand (STS) tests; or the user is standing still or sitting. Movement and mobility are referred to random movements (such as shaking our feet while seated) as well as to more periodic ones (e.g., running, jogging, walking, stair climbing, and different gait tests such as timed up-and-go (TUG) tests). We use the available sensors in the smart insoles (from the most energy efficient to least energy efficient: accelerometers, compasses, pressure sensors, and gyros) to provide an adaptive transmit power selection algorithm that reacts to the user's mobility state. Ideally, this collection of sensors can provide information about movement, movement type (such as walking), turning, speed, direction/heading, distance, location (including indoor/outdoor), and more fine-grained information, such as gait cycles and gait cycle phases. Featured extracted from sensors data vary from the simplest features, such as mean, to more complicated ones, such as salience, energy, and frequency domain features (See Figure 28).

One way to alternate between the two mobility schemes is to use a conditional exponential smoothing function with the condition determined by the mobility state of the system. Especially, walking is a continuous process that lasts for a relatively long time duration, which makes it a suitable candidate for us to pursue system optimization through activity-specific design for smart shoes and a variety of WBANs.

We augment the smoothing function used in Section 5.5 with more information, in that different weights are placed on energy savings and packet loss goals and hence, reacting differently to a perceived deterioration or improvement in channel quality according the current mobility state of the system. If the system is stationary, α_s (e.g., 0.8) will be used as the smoothing factor:

$$\overline{X} \leftarrow (1-\alpha_s)\overline{X} + \alpha_s X, \tag{65}$$

and if it is made sure that the system is mobile, α_m (e.g., 0.2) will alternatively be used:

$$\overline{X} \leftarrow (1-\alpha_m)\overline{X} + \alpha_m X. \tag{66}$$

Therefore, he recent channel quality values are given more weight, resulting in short update periods. On the other hand, when the shoe is stationed (such as resting, standing, and tests including stationary plantar pressure measurements and sit-to-stand (STS) transfers) a longer history about the channel will be of more value.

The sensor-assisted TPC algorithm is summarized in Figure 29; the routines CalcPTXStationary and CalcPTXMobile are called based on system's mobility state. The algorithm sets the transmission power level to maximum, if more than t_{cancel} (e.g., 2 s) units of time have passed since the last successful packet transmission.

Our scheme switches from static-optimized setup to mobility-optimized setup as it is informed that a movement is detected. When the mobility state detection routine running on the smart insole or at the receiver detects that the subject is walking (i.e., mobile = 0), the algorithm updates the smoothing factor to α_s immediately, and aggressively finds the transmit power capable of reliable transmissions in mobile scenarios. When the user goes from the moving to stationary state (i.e., mobile = 0), the algorithm updates

the smoothing factor to α_m and prepares for avoiding short term channel fluctuations. The mobility state detection algorithm is detailed in the next section.

MobilityAdaptiveTPC(gotACK,*X*,mobile)
Require: X {Link quality metric from the most recent packet}
Require: $\overline{X}$ {Running average of X}
► Modifies transmission power (P_{TX}) considering mobility state

1: **if** (!gotACK) **then**
2: failedTime ← **currTime**()
3: $X \leftarrow X_{lowest}$
4: **if** (**currTime()** – failedTime > t_{cancel}) **then**
5: $P_{TX} \leftarrow P_{TX}^{\max}$
6: **else if** (!mobile) **then**
7: **CalcPTXStationary(*X*)**
8: **else** {mobile, e.g., walking}
9: **CalcPTXMobile(*X*)**
10: return P_{TX}

► Depend on observations from all packets
► Ignore short-term variations
CalcPTXStationary(*X*)
1: $\overline{X} \leftarrow (1-\alpha_s)\overline{X} + \alpha_s X$
2: if $\overline{X} > T_{sH}$ **then**
3: slightly decrease P_{TX}
4: **else if** $\overline{X} < T_{sL}$ **then**
5: increase P_{TX}
6: **else** { $T_{sL} \le \overline{X} \le T_{sH}$ }
7: no action

► Place more weight on recent observations
► Do not ignore short-term variations
CalcPTXMobile(*X*)
1: $\overline{X} \leftarrow (1-\alpha_m)\overline{X} + \alpha_m X$
2: if $\overline{X} > T_{mH}$ **then**
3: slightly decrease P_{TX}
4: **else if** $\overline{X} < T_{mL}$ **then**
5: increase P_{TX}
6: **else** { $T_{mL} \le \overline{X} \le T_{mH}$ }
7: no action

Figure 29. Sensor-assisted TPC adapts differently depending on whether or not the transmitting node is moving.

Figure 30 shows a graph representing the proposed sensor-assisted TPC scheme; we account for the five power levels available on the XBee Pro platform. Using XBee and XBee Pro, at the same time along with each other, will increase the number of available power levels to ten. Please note that the graph can represent both mobile and stationary scenarios; however, the thresholds (T_H and T_L) and smoothing factor (α) vary for the two scenarios.

5.7 Mobility State Detection

In WBANs, mobility unavoidably increases the probability of packet loss due to the complex behavior of wireless radios in a practically mobile environment. Human being's frequent activities (such as sitting,

lying or walking) are continuous processes that last for a relatively long time, which enables us to define mobility states and pursue system optimization through activity-specific design and transmission power control. The processing and computation of sensor data and derivation of mobility states can be performed at the base station or alternatively, at the transmitting node if the processing resources are not occupied, which is the case in smart insoles.

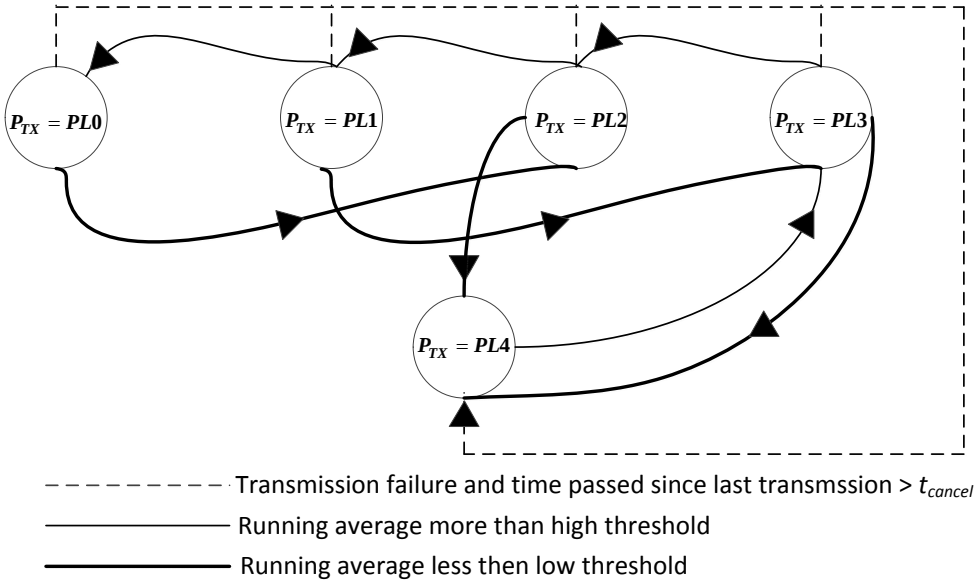

Figure 30. A graph representing the power level selection in the proposed sensor-assisted TPC. Each node denotes one of the available transmit power levels on XBee Pro modules. The transmit power is increased by increments of two levels and it is reduced by one level. Note that there are different threshold values for mobile and stationary scenarios in order to make the scheme reactive to the current channel updates for mobile cases. If the running average remains between T_L and T_H, no action will be taken.

Mobile activities contribute valuable information in many applications as they incur fluctuations in multi-path fading effects as well as obstructing the line of sight path. For instance, as shown in Figure 31, accelerometer data in the smart insoles can help us to beware of fluctuations in RSSI signal (gray area in the figure), which may lead to more packet loss at the receiver. In this example, a subject wears the smart insoles and walks for four steps towards a stationary receiver 20 meters away at an elevation of 0.5 meter above the ground in an open outdoor field. The transmission power was set to 18 dBm.

Our mobility state detection methods do not require any training and perform well across a variety of

conditions. Such techniques are simple and accurate, and they take advantage of the already built-in sensors in smart insoles such as accelerometers, pressure sensors, gyros and compasses.

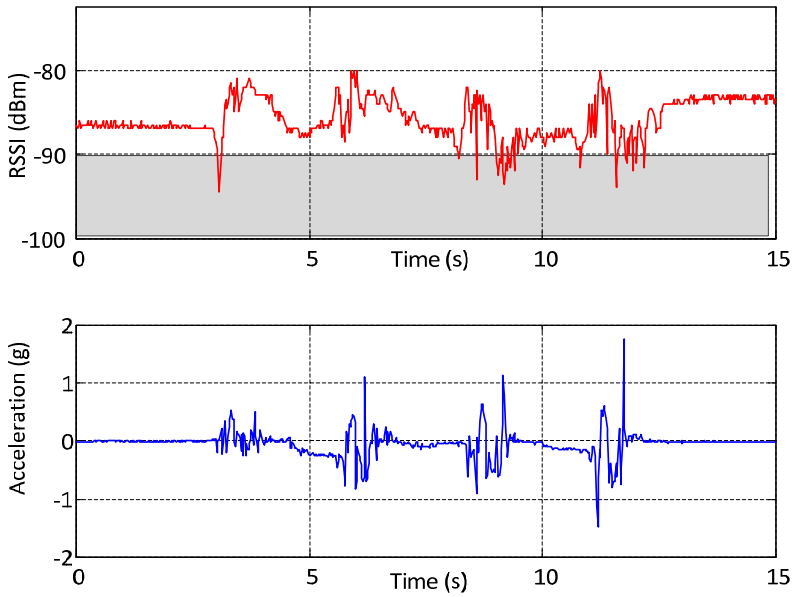

Figure 31. RSSI/acceleration signal measured/received at a static receiver from the right smart insole.

Link quality data is probably the most energy-and cost-efficient means to detect mobility states, as it is already in place regardless of the specific use of WBANs. Thus, we investigated the feasibility of utilizing RSSI values at the receiver to detect movement. We found that, with the exception of few scenarios such as the one indicated in Figure 31, RSSI is not a proper candidate to detect movement, let alone walking. The problems associated with the RSSI approach include: 1- RSSI values show large variations even when a node is static; 2- the magnitude of these variations depends strongly on the environment and the device. It also varies significantly across time and across different RSSI ranges. Low RSSI ranges showed more fluctuations than high RSSI ranges; and 3- the reported RSSI values are extremely sensitive to movement in the environment and trigger many false positives.

In designing the mobility state detection techniques, emphasis is placed on using inexpensive, low power commodity sensor elements, such as accelerometers, as opposed to more expensive and less energy-efficient ones, such as pressure sensors and gyros. In the following subsections, we explain how to

derive the mobility states shown in Figure 28.

5.7.1 Movement Detection

We use a variance-based movement detection technique similar to the one used in [Ravindranath]. The accelerometer exhibits a higher variance while moving than when stationary. We use this fact to detect movement. For every new accelerometer sample, the standard deviation of the combined acceleration signal is computed over a sliding window (w) of samples. The combined acceleration is the Euclidean norm of acceleration signals in all three dimensions:

$$r = \sqrt{A_x^2 + A_y^2 + A_z^2}. \tag{67}$$

The window slides by one sample for each computation. If the standard deviation of a window is beyond a threshold (T_a), movement will be detected. When the standard deviation does not exceed the threshold for n consecutive sliding windows, the smart insoles are reported as stationary. Given the sample rate of 50 Hz in the smart insoles, on average we were able to detect movement within 250 ms and detect stationary states in less than 500 ms. Similar to the approach taken in [Ravindranath], we tested a wide range of values for w, a, and n; we found that $w = 5$, $T_a = 0.03$ g, and $n = 25$ create only a few false positives.

It is noteworthy to remember that movements include every mobility state for which an insole's speed or its acceleration is not zero. In such mobility states, locomotion (moving from one place to another) may or may not take place. Therefore, mobility states such as walking in place and even shaking one foot without locomotion are accounted for.

5.7.2 Walking Detection

Despite the fact that the presented movement detection technique is very simple and useful, it is more beneficial to find out whether a user is walking as opposed to performing other types of movement. These movements consist of jumping, walking in place, climbing up and down the stairs, and many common or

random activities in which the user is stationary while the WBAN nodes (smart insoles in our study) are mobile.

Walking is the most basic, common, consistent, and natural mode of transportation. Furthermore, walking is the most important mobility state for which the smart insoles data is meant to be analyzed. Therefore, it is of immense value to automatically extract the walking episodes, in an online manner, using commodity sensors. This way, the walking activity could be used as an identifier for TPC techniques to increase the battery lifetime of WBANs.

We use an unsupervised activity (mobility state) discovery method to discover time intervals that include walking patterns in long time series data. An important advantage of unsupervised techniques is that these methods derive the activity models during the run-time and, hence, they do not require predefined activity models and patterns in the setup phase.

Our unsupervised technique discovers walking activity occurrences based on their frequency and consistency during long time intervals. Once the time series subsequences representing walking activity are discovered, TPC techniques will be applied, accordingly.

5.7.2.1 Most Frequent Activity Discovery

Discovering most frequent activities has been in the interest of the research community in the recent years [Amini5, Vahdatpour]. Motif detection in time series data is a technique to discover the frequent subsequences in a longer time series. A recent study by us [Amini5] has extended the motif discovery mechanism to multi-dimensional time series data for discovering the most frequent activities in wearable systems. However, as the study by [Chiu] suggests, motif discovery is computationally intensive and is not suitable for embedded computing and applications with a huge amount of data. Hence, for the purpose of WBANs and smart insoles, we use an approach similar to the method presented in [Vahdatpour2] for discovering the most frequent activity (walking and running) in 3-dimensional accelerometer data. Our approach for most frequent activity discovery consists of two steps. In the first step, each dimension of the accelerometer data is analyzed separately to discover frequent patterns. In contrast to [Vahdatpour1],

we use a binning approach to classify similar patterns in single dimensional accelerometer data. In the second step, classified patterns are grouped together with a clustering approach to form the activities. In the next subsection, we describe each step of the frequent activity discovery method.

5.7.2.2 Activity Primitive Discovery in Single-Dimensional Time Series

Numerous approaches have been used to discover similar patterns in a time series data. Although using motif discovery results in accurate classification of patterns, it is computationally intensive and sensitive to noise in the data. Here, we classify patterns in single dimensional accelerometer data based on the total displacement that is resulted from the activity in the corresponding axis. We define an activity primitive to be a subsequence between two consecutive stable regions (or default sensor value) in the accelerometer time series data. Such subsequences are mostly observed as bell shape patterns (with local minimum or maximum points) or linear slopes between two stable values in human actions, which depending on the speed and nature of the activity have different length and frequency. The acceleration data can be converted to displacement information, using the following equation on a subsequence of length m ($a_1 a_2 .. a_m$).

$$displacement = D.\sum_{k=1}^{m}\sum_{i=1}^{k} | a_i - a_1 |, \tag{68}$$

where D is the calibration constant factor, which depends on the placement of the sensor and other parameters such as the frequency of data sampling. The accelerometer sensor has a fixed location in the smart insoles, i.e., under the foot in the heel area. Nevertheless, in order to calculate displacement information in our method, the location of the accelerometer does not have to be known. This is as a result of the fact that the displacement information is used to compare activity primitives in the same axis of the accelerometer and it is constant for all primitives and can be eliminated from the calculations. Figure 32(a) depicts three accelerometer signals and several activity primitives found in them (labeled by capital letters).

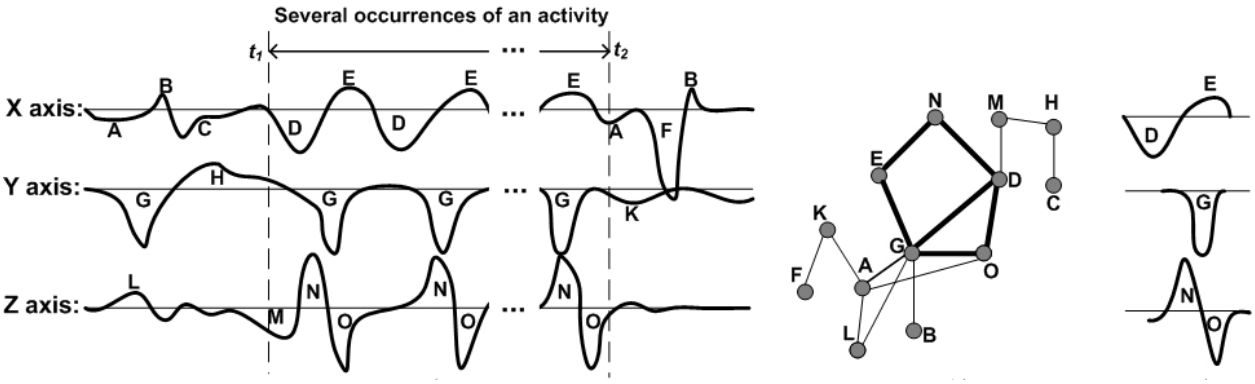

Figure 32. An illustrating example of the clustering algorithm for the recurrent activity discovery. (a) Three dimensions of accelerometer data with several occurrences of an activity between t_1 and t_2. (b) The interval coincidence graph, representing the primitives in the time series data. The thickness of edges shows higher coincidence between the primitives. (c) Primitives with high coincidence are clustered and the recurrent activity is discovered. t_1 and t_2 are sent to output as the start and end time of the most frequent activity.

SingleDimensionalActivityPrimitiveExtraction(*T*)
Require: Time series $T = t_1 \ldots t_n$
Output: List of activity primitives along with their occurrence indices, *p_occurrence*(1…*j*), *start*(1…*j*)

```
1: i ← 1
2: while true do
3:     while t_i = default_value | t_i is in stable region do
4:         increment i
5:     end while
6:     start(j) ← i
7:     while t_i ≠ default_value & t_i is not in stable region do
8:         d ← d + Σ_{i=1}^{start(j)} | t_i − t_start(j) |
9:     end while
10:    length(j) ← i − start(j)
11:    displacement(j) ← D . d
12:    d ← 0
13:    if i = n then
14:        p_occurence(1…j) ← discretize(displacement(1…j),length(1…j))
15:        return p_occurrence(1…j),start(1…j)
16:    end if
16:    j ← j + 1
17: end while
```

Figure 33. Extracting primitives of activity subsequences.

Figure 33 presents our algorithm for extracting primitives of activity subsequences projected on single-dimensional time series accelerometer data. The algorithm extracts the patterns from the time series,

groups them based on the physical attribute of the data and according to the discretization cardinality, and assigns a symbol to them. It also assigns a starting time to each symbol. There are a variety of methods in literature regarding effective discretization, especially in time series. Here, in order to discretize the calculated displacement and assign symbols to it, we consider using the probability distribution of the calculated displacements and assigning symbols to primitives such that primitives are classified fairly considering the variation of displacement in the application runtime. Regardless of the method used to discover recurrent activity patterns in the single-dimensional time series, the output of this phase is passed to the multi-dimensional activity and abnormality detection algorithm, described in the next section.

5.7.2.3 Activity in Multi-Dimensional Time Series

By using 3-dimensional accelerometers, accelerations pertaining to each mobility state are projected on one, two, or three dimensions of the accelerometer depending on the mobility state in which the user is. The orientation of the accelerometer somewhat changes as a user employs smart insoles for mobile states. Besides, in a general WBAN such changes in the sensor orientation are even more steep and unpredictable. Accordingly, all dimensions (x, y, and z) should be jointly considered in order to discover recurrent activities. If only a subset of dimensions is used for counting the occurrence of multi-dimensional activities, activities with similar projection will be classified together and overcounted. As a result, we first use a graph clustering approach to construct activity structures in multi-dimensional data. This step basically groups several activity primitives from different dimensions together according to their temporal characteristics.

In order to construct the multi-dimensional activity structures, we first convert the list of discovered activity primitives into a weighted directed graph, so that a graph clustering mechanism can be applied to construct the model of activities in multi-dimensional data. In the proposed graph, each vertex represents an activity primitive, and the weight on the vertices represents the number of occurrences of the primitive in the corresponding time series accelerometer data. The weight on each directed edge in the graph is calculated by the following equation:

$$e(i,j) = \frac{coincidenc\ e(i,j)}{total\ \_\ occurrence\ s(i)}. \quad (69)$$

The *coincidence*(i, j) denotes the number of times there is a temporal overlap between occurrences of primitives i and j. As a result, $e(i, j)$ will be at most 1, when all the occurrences of primitive j have overlap with occurrences of primitive i; and it is at least 0, when there is no overlap between occurrences of primitives i and j.

Subsequently, a graph clustering approach is used to construct multi-dimensional activities structure from the primitive coincidence graph. Figure 34 presents our method for constructing the activity structures from the coincidence graph. This method is similar to the clustering mechanisms proposed in [Aslam]. Clustering the primitives starts with sorting the list of vertices based on the number of occurrences of the primitives. Then, the most frequent primitive is selected as a candidate core for activity structure, and the graph is searched for primitives with high occurrence correlation with the candidate core primitive. If there are several primitives with equal frequency, the one with the larger number of highly correlated neighbors is selected as the core primitive. The threshold for the correlation is set to $1 - \beta$, where β is the abnormality frequency constant. Upon construction of an activity by clustering correlated primitives, selected primitives are removed from the graph, and the algorithm continues discovering new activity structures by selecting a new core activity primitive.

Figure 32(c) illustrates the results of applying the algorithm to the coincidence graph in Figure 32(b) (the weights in the graph are omitted to make the figure readable). As it is denoted in the figure, the activity structure extracted contains primitives E, D, G, O, and N (G is the activity core primitive, due to its frequent number of occurrences). Note that the effective construction of activity structures highly depends on the frequency of primitives, and in a real world application the frequency and coincidences are significantly higher (β will be set to less than 0.1 in real world applications). The depicted graph is formed from a set of short time series and is selected to be small to better illustrate the logic behind the algorithm.

ActivityStructureConstruction(*G*)
Require: $G(V,E)$ {The primitives coincidence graph: *total_occurrence*(v) for each v and $e(v_1,v_2)$ for all directed edges}
Output: $S = \{S_i\}$ {The set of most recurrent activity structures in the time series (each S_i is an activity)}
► Sort the vertices list in G in descending order of *total_occurence*
{if some primitives have equal frequency, the primitive with the highest number of highly correlated neighbors will have the highest priority}

1: **for** each vertex v_k in the sorted list of vertices **do**
2: add v_k to activity S_i
3: **for** all neighbors of v_k, if $e(j,k) > 1-\beta$ **do**
4: add v_j to activity S_i
5: remove v_j from the graph
6: **end for**
7: $i \leftarrow i + 1$
8: update the sorted list of vertices
9: **end for**
10: **return** $S = \{S_1, S_2, \ldots, S_{i-1}\}$

Figure 34. Extracting primitives of activity subsequences.

For detailed description and evaluation of unsupervised multi-dimensional activity detection algorithm, we refer the reader to [Vahdatpour1]. However, it should be noted here that the execution overhead of this method is linearly correlated to the execution overhead of the activity primitive discovery algorithm (refer to Figure 33). The computational intensity of algorithms for activity primitive discovery can be reduced by introducing assumptions about the input signals such as the minimum and maximum length of subsequences and the frequency of activities.

In order to distinguish running mobility states from the walking ones, we apply a threshold-based approach to the standard deviation of the combined acceleration signal (refer to (67)). This approach is similar to the approach taken in Section 5.7.1 to perform movement detection.

More specifically, in the time domain accelerometer signal, acceleration spikes, representing the impact acceleration stem from the heel strike during ambulation. Such high energy accelerations are induced by the impact between the heel and the ground for walking states and the impact between the ball of the foot and the ground for running states. More details on the impact acceleration will be provided in Section 5.7.3.

Running and walking mobility states both result in projection of consistent and frequent patterns (activity primitives) onto the three axes. Not only does the running mobility state possess higher speeds

than the walking mobility state (speeds higher than 2.0 m/s as opposed to less than 2.0 m/s), but also the running mobility state creates higher magnitude accelerometer signals. Given that at the same speed (e.g., 1.8 m/s), human beings can both run and walk, it is difficult to definitively distinguish the two solely based on the speed of individuals – refer to Section 5.3.2. The problem further intensifies when the speed estimation is not accurate.

The acceleration peaks stemming from the running mobility state are always considerably higher than their counterparts from the walking state. Therefore, the standard deviation or variance of the acceleration signal is a good indicator for telling the two states apart.

As mentioned earlier in this section, our smart insoles and hence, the accelerometer sensor embedded in them, have known location. Furthermore, the accelerometer's orientation does not extremely change as the smart insoles are being used. Nonetheless, our walking detection technique can be utilized to almost all orientations and on-body locations.

5.7.3 Step Detection

Once the walking episodes are recognized, we can detect the steps taken by the user in order to obtain more fine-grained information such as the speed of walking. Every gait related accelerometer signal is made of segments with noisy start and end values, and a periodic middle section, named gait cycles (known as strides as well). The goal of the step detection is to extract the periodic middle section and identify the starting indices of each stride.

Physically, strides are associated with two consecutive steps of an individual. As indicated in Figure 35, during a single walking stride, each foot experiences two main phases. The stance phase is the weight bearing portion of each gait cycle. It is initiated by heel contact and ends with toe off of the same foot. Swing phase is initiated with toe off and ends with heel strike [Gait1]. Step length is defined as the distance between the point of initial contact of one foot and the point of initial contact of the opposite foot. Likewise, stride length is the distance between the point of initial contact of one foot and the point of initial contact of the same foot.

The existing step detection (gait cycle detection) algorithms are not automatic, that is, they require the user to explicitly identify the start and end of the periodic section of the signal (e.g., by looking for the acceleration spikes described below) and the algorithms would then identify the indices corresponding with each period. Furthermore, most of the existing approaches (locating the zeros of a signal, computing the signal energy, etc.) provide overly complicated algorithms with respect to the detection accuracy that they offer. In contrast, we have developed a fully-automatic solution, assuming the accelerometer signal contains a periodic section that comes after, and is followed by a noisy beginning and end. Before we detail the gait cycle detection algorithm, we introduce the notions of acceleration spikes and salience:

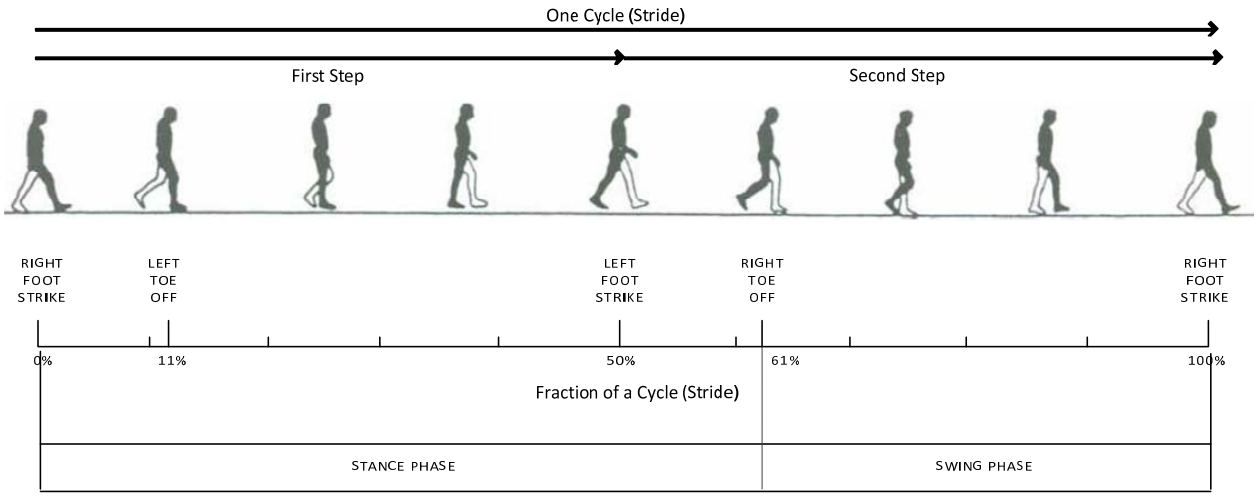

Figure 35. Gait cycle phases.

Acceleration spikes (impact acceleration): In the time domain, the impact acceleration is defined as the maximal amplitude of the acceleration data at foot strike. For walking states, such high energy accelerations are induced by the impact between the heel (shoe heel) and the ground at the end of the swing phase. The energy of a discrete-time signal, $x(t)$, is the sum of the squares of its time-domain values, i.e., $\sum x(t)^2$. According to Parseval's theorem, this quantity is equal to the sum of the squares of the signal's frequency-domain components, i.e., $\sum X(f)^2$, where X is the discrete Fourier transform (DFT) of $x(t)$. Broadly speaking, a signal from a faster-paced activity possesses more energy in higher frequencies than a signal from a slower-paced activity; for instance, running compared to walking or

waking fast in comparison with normal walking. Acceleration spikes, representing the impact acceleration for both walking and running states, usually translate into frequencies less than 10 Hz. Correspondingly, frequencies more than 10 Hz are usually discarded, as the amount of energy embedded in those components is negligible.

Salience: The salience of a given sample is defined as "the length of the longest interval over which the sample is a maximum" [Mertens]. Therefore, the salience of the global maximum is N, if there is no other sample with the same amplitude. However, a sample with a large salience does not necessarily have a large value and vice versa. We can also define right salience $s_r(k)$ and left salience $s_l(k)$ as the number of samples over which sample k is a maximum among the samples to its right and left, respectively. $s_r(k)$, $s_l(k)$, and total salience are related as follows:

$$s(k) = s_l(k) + s_r(k) + 1. \tag{70}$$

As an example, consider the fourth sample in the signal shown in Figure 36; despite the fact that it has a higher magnitude than the seventh sample, it has a smaller salience comparing to the seventh sample ($s(4) = 4$ versus $s(7) = 8$). In this example the salience vector and the left and right components are:

$$\begin{aligned} s(k) &= \{\ 14,1,2,4,1,13,8,1,4,2,1,5,2,1,15\},\ 1 \le k \le 15 \\ s_l(k) &= \{0,0,1,2,0,4,0,0,1,0,0,2,0,0,14\},\ 1 \le k \le 15 \\ s_r(k) &= \{13,0,0,1,0,8,7,0,2,1,0,2,1,0,0\},\ 1 \le k \le 15. \end{aligned} \tag{71}$$

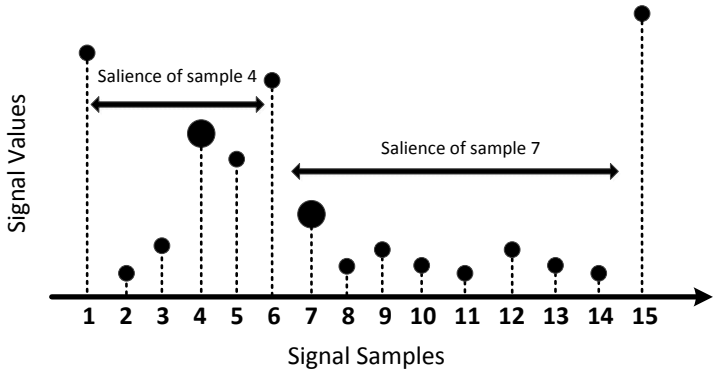

Figure 36. Salience of an example signal.

We have implemented all three schemes found in [Mertens] for computing the salience vector of a signal. These schemes include: 1- basic salience computation, 2- partial salience allocation, and 3- sliding window analysis. We found the sliding window approach to be the most suitable one for the purpose of step detection, as it offers faster execution time and it addresses the issues pertaining to the signal's origin. Implementation details for each of the schemes are explained in the Appendix C.

Our step detection algorithm is as follows:

1- As depicted in Figure 38, the three axes are combined and the result will be the combined acceleration signal, denoted as r (see Section 5.7.1 for more details):

$$r = \sqrt{A_x^{\,2} + A_y^{\,2} + A_z^{\,2}}\,. \tag{72}$$

2- The salience of each acceleration sample point in the input signal r is computed. The key property of the salience vector utilized for our step detection algorithm is that the starting point of each step (stride) has a large salience. Hence, steps can be found by locating these prominent points.

3- Compute the vector u, defined as $u = (r \;.\; s)/\max(s)$, where dot (.) represents an element-wise multiplication. The idea behind deriving u is to make peaks of r more pronounced and to diminish the rest of the samples.

4- Extract all the elements of u exceeding a certain threshold (e.g., $2 \times \max(u) / 3$) as potential cycle indices. Compute the difference vector, d, between adjacent extracted indices and remove the elements whose corresponding difference vector values are less than two from the potential cycle indices. This elimination phase helps to increase the accuracy of our step detection method by counting two close peaks only once. Based on the original assumption about the input signal, mean(d) will approximately be the average duration of each step, which can be used in estimating the walking speed.

5- Normalize d around its mean and extract all indices of points that fall within this threshold, i.e., $|d - \text{mean}(d)| < \text{mean}(d)$. The number of such points is indicative of the number of steps taken and in fact, these points are the start/end points of each step. Return a list of indices that these points correspond to.

Figure 38 illustrates the result of application of the proposed step detection algorithm to a given gait signal in Figure 37. Extracted gait cycles are specified by red bars in the top figure. It is noteworthy to mention that each gait cycle corresponds to two consecutive steps of the individual.

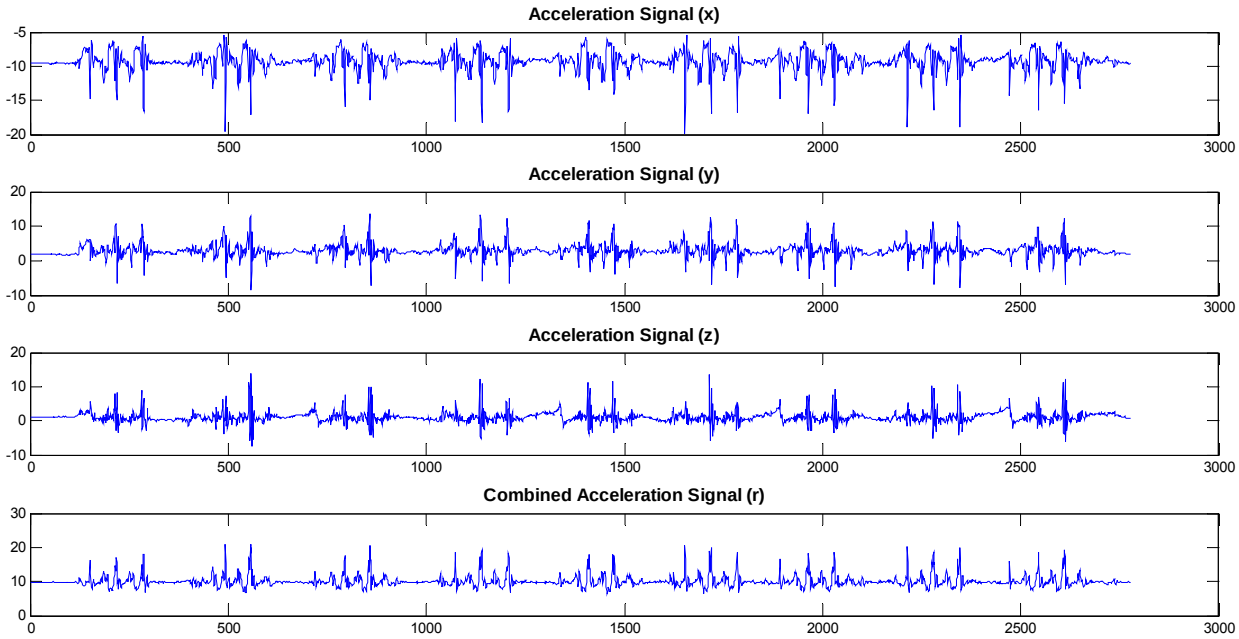

Figure 37. Gait acceleration signal, x,y, and z axes, as well as the combined signal *r*.

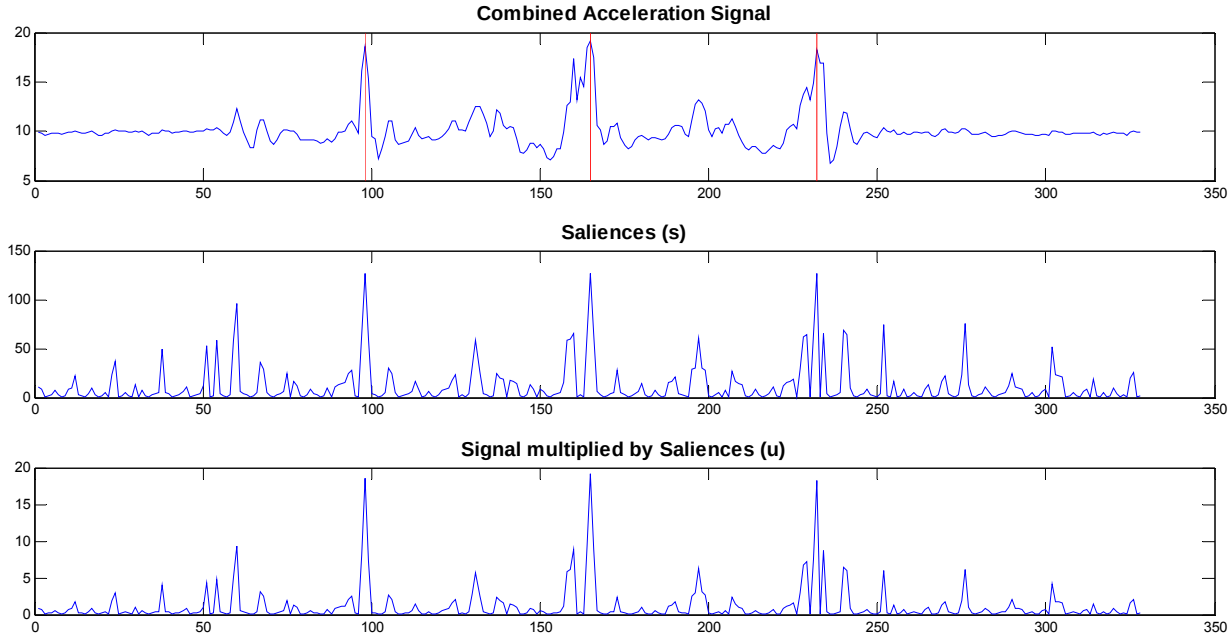

Figure 38. Original signal (top), the signal's salience vector (middle), and the salience vector after normalization (bottom). The normalization process amplifies the peaks.

5.7.4 Heading and Turn Detection

If the wearer of the smart insoles, or any other WBAN with off-body communications, moves towards the receiver, most probably the wireless channel will improve. On the other hand, if he/she moves away from the receiver (possibly after making a 180° turn after moving towards the receiver), the wireless channel is expected to deteriorate due to the growing distance between the WBAN and the receiver. Hence, user's heading and the occurrence of turns can both be valuable information for wireless protocols and more specifically, for TPC schemes to adjust the transmission power in a more informed manner.

Heading can be obtained from magnetometers (digital compasses) available in the smart insoles, smart phones, and many other devices. Magnetometers measure the response of the device to the Earth's magnetic north pole. In the smart insoles, the orientation of the magnetometer can be considered fixed; thus, the heading of the user can be easily specified. In a general WBAN, where the heading of the node may be different from the user's heading, a gyroscope sensor, albeit energy consuming, can be used along with an accelerometer to find the orientation of the node. With magnetometer data, the main issue is that the orientation reported becomes noisy when metallic objects are nearby.

In outdoor environments, in addition to magnetometer, GPS receivers help to infer a heading when a user is moving from one place to another. For example, the signal from the yaw output of the gyroscope sensor can be used to detect 180° turns. In the smart insoles, the yaw output provides the relative rotation of the user around an axis parallel to gravity. When a user wearing the smart insoles makes a 180° turn, a significant, persistent, and steep change in the yaw output can be substantiated. In [Salarian], a turning analysis algorithm is proposes by Salarian et al., which not merely detects 180° turns, but estimates the duration and direction of turns and provides other useful metrics.

5.7.5 Speed and Context Detection

The current implementation of our sensor-assisted TPC is tuned for normal walking speeds and for outdoor environments. More energy savings will be obtained in the sensor-assisted TPC by fine-tuning its

parameters (the smoothing factor as well as the thresholds) for different speeds and environments.

Clearly the speed of the user matters since it determines to what extent the transmission power level of the previous successful data transfer should contribute to the derivation of the transmission power level of the current transmission. The movement speed in smart insoles and generally in nodes in a typical WBAN is relatively low comparing to their data generation and communication rate. This implies that the transmission power level at which the previous successful data transfer was performed should be a reasonable estimate for the transmission power level of the current data packet. Obviously, the application's data rate and the speed of WLAN's mobile node greatly affect the transmission power level.

It should be emphasized once again that having a zero speed does not necessarily indicate that the WBAN is stationary. There are at least three approaches to find the speed: 1- Employing a GPS receiver in outdoor environments; 2- integrating the accelerometer readings; and 3- estimating the speed using the step time and length (Refer to the step detection algorithm in in Section 5.7.3).

Apart from the mobility state in which the user is, our characterization results in Section 5.3 suggest that in most indoor scenarios link quality metrics and hence, PRR values, undergo more variations. Such variations need to be accounted for, when adjusting the transmission power and the update periods. To understand whether the user is indoors or outdoors, one should take advantage of the fact that when the user is indoors, the GPS signal levels are not sufficient to calculate a position fix. Hence, GPS receivers could serve WBANs and TPC protocols as a context identifier. It is widely known that GPS receivers are energy consuming and costly, as they waste significant resources such as battery energy and CPU cycles before a time-out value is reached.

We leave tuning the sensor-assisted TPC for walking/running speed as well as automatic tuning for context (indoors and outdoors) as our future work.

5.8 Experimental Results

In this section, we first present the accuracy of the mobility state detection schemes. Then we demonstrate energy saving benefits as a result of utilizing the proposed sensor-assisted TPC in the smart insoles. Our

experiments include: 1- a fabricated scenario in which a subject spends equal amount of time in stationary and mobile states; 2- a real gait test, conducted as part of a routine evaluation for assessing a person's mobility, which requires both static and dynamic balance.

5.8.1 Mobility State Detection Outcomes

By keeping track of the standard deviation of the acceleration signal over a recent window of samples, we are able to perfectly detect all movements within 250 ms using the smart insoles and any other WBAN node attached to the legs or feet. A window of one second is used for the walking state detection scheme. Smaller window sizes cause the accuracy to suffer due to frequent and consistent activity primitives not having enough time to form; larger window sizes introduce noise, as multiple mobility states could exist. Furthermore, a larger window was not chosen so that the detection scheme will be able to work immediately. As for the step detection scheme, the window size for salience analysis takes 96 acceleration samples into account.

We examined the performance of our unsupervised walking state discovery method (refer to Section 5.7.2) through a pilot study involving 25 subjects (20 males and 5 females between the ages of 18-35); each subject attached two acceleration logging devices to the top of his/her shoes and had it on for 30 minutes, during which he/she was asked to perform a sample set of his/her own daily activities in the university environment. We set the sampling rate of the acceleration logger from Gulf Coast Data Concepts [Gulf] to 50 Hz. The device is suitable for long intervals of data collection because it has 1 GB of memory. In addition, the size of the device is relatively small (1 in. × 3.5 in. × .75 in.) and hence, it does not interfere with the normal activities of the subjects. We required the users to include a number of walking intervals in their activities. The collected time series data was divided into 3-minute subsequences. As such, a total of 500 time series samples were collected.

For each sample, the walking intervals were discovered via the unsupervised technique for the most frequent activity detection. 96% of the time series samples were detected to include walking periods. This rate is high due to the fact that subjects were asked to include walking periods in their activity. The

walking discovery algorithm had a consistent accuracy in detecting walking occurrences in the time series. On average 95% of all walking strides were discovered correctly (versus 84% reported by Kunze et al. [Kunze]). On average, a 2% false positive rate was observed, which denotes the number of non-walking activity occurrences that were labeled as walking (compared to a 4% rate reported by Kunze et al. [Kunze]). Since we are interested in finding relatively longer walking time intervals to adjust the transmission power, the effect of false positives is not prohibitive as they were sparsely distributed in the time series data. Additional sensors such as pressure sensors help to improve the accuracy of the detection at the expense of more energy consumption.

We have run the proposed step detection algorithm (refer to Section 5.7.3) on two sets of data, each containing a total of five test subjects. Each experiment required the test subject to walk about four meters, stop, turn around, and repeat this process for 60 seconds. Accelerometers were attached to each subject's foot. All subjects (age 18-40) were asked to walk at their normal speed. The step detection accuracy for all experiments was 90%.

5.8.2 First Experiment: Alternating Walking/Running and Standing

For the first set of experiment, we asked a male subject of height 175 cm to wear the smart insoles of size 10 in the middle of UCLA Intramural grass field. The subject was asked to walk/run along a predefined trajectory around the receiver (height = 0.5 m) at a constant speed; we also asked the subject to stay static at predefined locations for a certain amount of time as well as to run in the middle of the trial.

Shortly speaking, each trial includes a number of tasks (mobility states) in the following order: standing (5 s), walking (10 s), standing (10 s), running (10 s), standing (10 s), and walking (10 s); such mobility states comprise basic tasks needed for a person to be independently mobile.

We carried out a total of five trials and each trial took about 55 seconds to complete and had roughly the same amount of static and mobile (walking and running) periods. As a reminder, the packet rate of the smart insoles is 50 packets per second; the sampling rate of the accelerometer (and other sensors) is 50

Hz; the packet size is set to 54 bytes; and there are five available transmission power levels, which can be increased to ten.

Note that it is important to detect when the subject has just started walking/running from standing still, and vice versa; therefore, the movement detection and walking detection mechanisms, presented respectively in Sections 5.7.1 and 5.7.2, are utilized in real time so as to recognize the most updated mobility state.

Figure 39 presents the power levels utilized for a subsequence of the trial by the smart insole based on the proposed sensor-assisted TPC. The subsequence involves the following mobility states: 1- standing still; 2- walking; 3- running; and 4- standing still. Also shown, are the mobility states, combined acceleration signal, and the RSSI values at the receiver during the subsequence. The smoothing factor and the upper and lower thresholds for mobile states are set to $\alpha_m = 0.8$, $T_{mL} = -85$ dBm, and $T_{mH} = -80$ dBm. For stationary states, they are set as $\alpha_s = 0.2$, $T_{sL} = -90$ dBm and $T_{sH} = -85$ dBm to achieve the most appropriate energy-reliability trade-off.

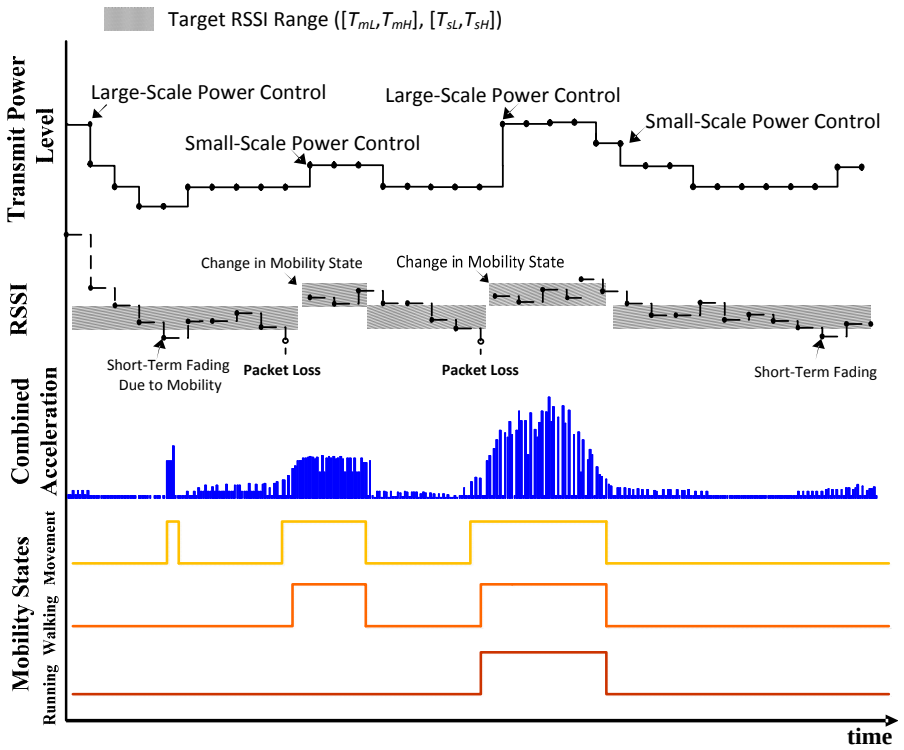

Figure 39. The operation of sensor-assisted TPC for different mobility states.

In the beginning of this subsequence, the average RSSI surpasses the upper threshold, T_{sH}; accordingly, the transmit power is gradually reduced to the point where the resulting RSSI resides in the target RSSI range. A few seconds later, a transient bad channel is experienced, when the subject is standing still, which can be attributed to a temporary fading of the channel as a result of the person moving his feet with no ambulation. Since there is no ambulation and also there is no packet loss, sensor-assisted TPC does not aggressively increase the transmission power and instead, it increases the transmit power by only one level, hence, saving energy. If there was a packet loss, the sensor-assisted scheme would have quickly reacted by increasing the transmission power in a multiplicative manner. The RSSI values are relatively stable during the rest interval, for which the transmission power is kept fixed at 12 mW. The rest interval is followed by a 10-second period of running; upon detecting a change in the mobility state, the sensor-assisted scheme immediately reacts by employing a larger smoothing factor ($\alpha_m = 0.8$ in comparison with $\alpha_s = 0.2$), thus, increasing the transmit power to 18 dBm from 12 mW in an aggressive fashion. A slower transition to the transmission power of 18 mW may seem to be more energy-efficient; nevertheless, such transition leads to a dramatic packet loss, which in turn works against the energy-efficiency of the smart insoles. In the last rest interval, RSSI values show a stable behavior, except for a short-term fading period, which is dealt with by a slight increase in the transmission power to save energy. If the same short-term fading had happened in a walking or running mobility state, the reaction would have been in the form of a more steep increase in the transmission power.

Based on a perceived mobility state of the system, sensor-assisted TPC automatically adapts the link quality thresholds used by the transmitter to select the proper transmit power. Such thresholds must be robust with respect to variations in the transmission and receive electronics. Sensor-assisted TPC refrains from reacting aggressively to the short-term attenuations due to inevitable small scale fading, as an example. The sensor-assisted scheme aggressively increases the transmission power upon detecting a packet failure (see Figure 39) and frequently tries to utilize lower transmission power levels when the channel conditions are not changing.

Similar to the approach taken by researchers in [Anastasi] and [Torres], we calculate the average current draw by dividing the total current draw by the total number of packet transmissions. The current draw is computed by recording both the number of transmission attempts and the transmission power levels used for each attempt. The current draw associated with each transmission power level is provided by Table 8; current draws of 100 mA, 132 mA, 185 mA, 224 mA, and 270 mA correspond with transmission power outputs of 10 dBm (PL-0), 12 dBm (PL-1), 14 dBm (PL-2), 16 dBm (PL-3) and, 18 dBm (PL-4), respectively.

Since all packets have equal size and the supply voltage is approximately constant, taking an average over current draw values provides a reasonable estimate of the energy consumption of the communication subsystem of the smart insoles. The energy consumption per one packet is related to the current draw based on the following equation:

$$E_{sender} = I \times V \times T_{DATA}, \tag{73}$$

where T_{DATA} is the duration of each data packet. Investigators in [JKim] have analyzed the energy consumption of the communication subsystem of a sender node and a receiver node in a WBAN with TPC capabilities as follows:

$$\begin{aligned} E_{sender} &= P_{Tx} \times T_{DATA} + P_{Rx} \times (T_{MAC} + T_{ACK}) \\ E_{receiver} &= P_{Tx} \times T_{ACK} + P_{Rx} \times (T_{MAC} + T_{DATA}) \\ T_{\mathrm{MAC}} &= T_{LIFS} + T_{BO} + T_{SIFS}, \end{aligned} \tag{74}$$

where T_{DATA}, T_{ACK}, T_{LIFS}, T_{SIFS}, and T_{BO} represent the time durations of the data packet, the acknowledge packet, the long inter-frame space, the short inter-frame space, and the average back-off time, respectively [IEEESTD, JKim]. Although we have not incorporated the energy consumption due to idle listening to the channel in (74), our measurements already take them into account. It is noteworthy to mention that the power dissipation due to idle listening to the channel greatly contributes to the total energy consumption in applications, where the data rate is not close the maximum RF data rate. In such applications, both transmitter and the receiver spend a remarkable amount of time listening to the channel.

Owing to the fact that XBee Pro transmitters are meant for long range transmissions, the transmission

power level on these transmitters is the dominant factor contributing to their current draw. It should be remembered that P_{Tx} significantly varies for different power levels; while, P_{Rx} is constant. The duration of data processing at the receiver can be longer than that for transmitter.

We compared our sensor-assisted scheme against a frame-based TPC approach and also against a simple 18 dBm transmission policy (named MAX hereafter). MAX always utilizes the maximum transmission power level in order to maximize the PDR, while the frame-based TPC is based upon either consecutive successes or failures of frames (packets); if more than a specified number of consecutive packets (e.g., four packets) succeed at the currently utilized power level, the transmission power is decreased by one level. If a transmission is not acknowledged at power level p, the transmitter retransmits the packet using power level $p + 1$, until the maximum power level is reached. We also analyze the energy cost of employing the minimum power level, i.e., 10 dBm, at all times to deduce an upper boundary for energy savings.

Table 11. Performance summary of different TPC schemes in comparison with maximum power transmission in experiment 1.

TPC Scheme	MAX	Frame-Based TPC	Sensor-Assisted TPC	Min
Average current draw for wireless communications	270 mA	216 mA	157 mA	100 mA
Average PRR	98%	85%	96%	<30%
Average energy per packet	4.516 mJ/pkt	3.612 mJ/pkt	2.625 mJ/pkt	1.672 mJ/pkt
Energy savings in communications	0	20%	42%	63%
Total current draw of each insole (only accelerometer on)	276 mA	222 mA	163 mA	105 mA
Total current draw of each insole (all sensors on)	414 mA	360 mA	301 mA	244 mA
Total energy saving	0%	13%	27%	39%
Expected battery lifetime (only accelerometer on)	4 h	5 h	6.75 h	10.5 h
Expected battery lifetime (all sensors on)	2.7 h	3 h	3.7 h	4.5 h

Table 11 summarizes current draw values, PRR values, average energy per bit, and energy savings pertaining to off-body wireless communications. Furthermore, the table lists total current draw and energy savings for different setups in order to find how much the battery lifetime will benefit from our proposed

TPC scheme. In one setup only the accelerometer sensor (the sensor we mainly use in our sensor-assisted TPC method) is kept on. In another setup, all of the sensors operate to provide comprehensive plantar pressure and gait data.

In comparison with a simple 18 dBm transmission policy, our sensor-assisted TPC scheme on average saved 42% energy pertaining to wireless communications from the smart insoles to the receiver. Utilizing the frame-based scheme results in less energy savings (20%), since it reacts the same to short-term fading and long-term fading situations. Furthermore, since the link quality is not taken into account, transmission power adjustments are less frequent; whereas, our sensor-based scheme provides higher granularity for adjusting the transmission power.

With regards to packet error rate, our scheme performs quite well, yielding an average PDR of 96% over the five trials. Most of the packet losses have occurred during short-term fading periods, in which our scheme slowly increases the transmit power in order to conserve energy. The frame-based TPC scheme was not able to meet our PDR needs, in that 15% of the transmissions fail, exceeding the maximum tolerable packet loss rate of 10%. Most of the packet transmission failures take place during ambulation; in each gait cycle after a few successful communications, the transmission power is decreased by the TPC scheme and it is abruptly followed by a number of consecutive packet losses (perhaps when the corresponding foot hits the ground) before the algorithm's slow response remedy the situation.

Also listed in the table is the average energy consumed for communicating one packet from the smart insole to the receiver. In finding so, we computed T_{DATA} in (74) according to the data rate of the smart insoles and by taking the overhead of each packet into account. The receive cost related to acknowledgement packets was considered part of the overhead cost. Given that the supply voltage is known, one can derive the energy cost of each packet.

Due to the existence of numerous sensors in the smart insole, the energy savings in the communication subsystem do not directly translate into longer battery lifetime. Nevertheless, the battery lifetime will be extended to 3.7 h (27% longer comparing to an insole with maximum transmission power) when all the

sensors need to operate at the same time. If only the accelerometer sensor is kept on, the insole's battery lifetime can be increased from 4 h to 6.75 h, i.e., an improvement of 59%.

5.8.3 Second Experiment: TUG Test

Our second experiment involves the Timed Up and Go test (TUG), an easy-to-administer and widely-used test conducted to assess a person's mobility, which necessitates both dynamic and static balance. As shown in Figure 40, TUG includes the time that an individual takes to stand up from a chair (1-3 s), walk three meters (3-10 s) , turn around (1-3 s), walk back to the chair (3-10 s), and turn and sit down (1-3 s). During the test, the individuals are expected to wear their regular footwear; hence, TUG is an excellent use case for the smart insoles; the body-fixed accelerometers embedded inside the smart insoles enhance the ability of TUG to assess fall risk in older adults an inconspicuous manner.

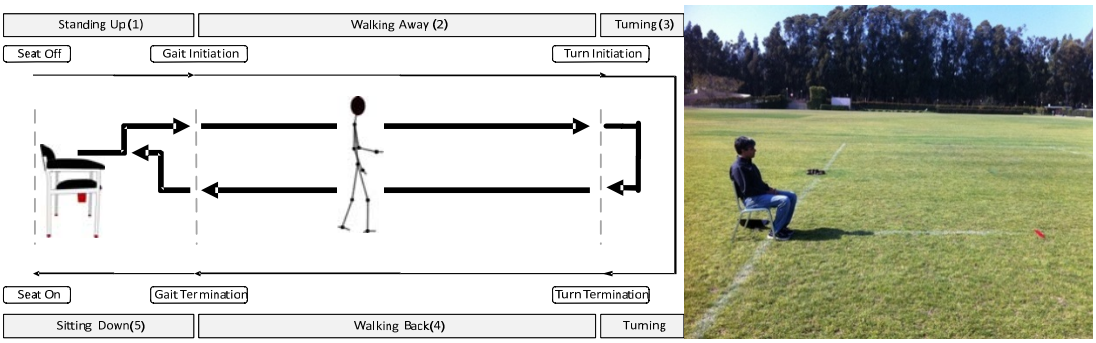

Figure 40. TUG test's chain of events.

We asked five male subjects of height 165-175 cm to perform a set of five TUG tests in the same outdoor setting as that of the first experiment. After passing a horizontal line, marked with a piece of red tape, the subjects are supposed to make a 180° turn and walk back to the chair. As with the previous experiment, TUG test involves both stationary and non-stationary mobility states, however, in TUG the duration of non-stationary mobility states dominate stationary ones. Each trial includes a number of tasks (mobility states) in the following order: sit to stand (1-2 s), walking (4-6 s), turning (1-2 s), walking back (4-6 s), turning, and sitting (1-2 s).

Each trial took on average twelve seconds, 70% of which was spent in non-stationary states. Similar to experiment, the smoothing factor and the upper and lower thresholds for mobile states are set to $\alpha_m = 0.8$, $T_{mL} = -85$ dBm, and $T_{mH} = -80$ dBm. For stationary states, they are set as $\alpha_s = 0.2$, $T_{sL} = -90$ dBm and $T_{sH} = -85$ dBm. The receiver node is attached to the chair at height of 0.5 from the ground. The packet rate of the smart insoles is 50 packets per second; the sampling rate of the accelerometer (and other sensors) is 50 Hz; the packet size is set to 54 bytes; and there are five available transmission power levels, which can be increased to ten. As with the previous experiment, detection methods presented in Sections 5.7.1 and 5.7.2, are utilized in real time to recognize the most updated mobility state.

Since most of the time is spent in non-stationary states, a higher frequency of power level adjustments is needed. Accordingly, it is expected that more energy savings will be obtained by using our sensor-assisted channel quality based TPC scheme as opposed to using the frame-based TPC scheme. In addition, unlike the previous experiment, the distance between the transmitter nodes (smart insoles) and the receiver node changes as the test is being performed; hence, the overall channel quality deteriorates in the first episode of walking and it improves in the second episode as the user becomes closer to the receiver. It should be noted that the 180° turn will result in a sudden change in antenna orientation. According to our characterization results, the highest quality wireless channel is obtained when the user wearing the insoles is facing towards the receiver.

Table 12 summarizes energy savings, PRR values, and expected battery lifetime for smart insoles used in the TUG test. In one setup only the accelerometer sensor (the sensor we mainly use in our sensor-assisted TPC method) is kept on. In another setup, all of the sensors are in use.

With regards to PRR and reliability of communications, of the fifty packets transmitted in each second, the maximum power, frame-based, sensor-assisted, and minimum power approaches deliver on average 49.5, 45.5, 47.5, and 32.5 packets, respectively. After experiencing a bad channel, the frame-based scheme is slower in increasing the transmission power, hence, a greater number of transmission attempts will be sacrificed comparing to the sensor-assisted approach.

Table 12. Performance summary of different TPC schemes in comparison with maximum power transmission in experiment 2.

TPC Scheme	MAX	Frame-Based TPC	Sensor-Assisted TPC	Min
Average current draw for wireless communications	270 mA	199 mA	136 mA	100 mA
Average PRR	99%	91%	95%	65%
Average energy per packet	4.516 mJ/pkt	3.323 mJ/pkt	2.271 mJ/pkt	1.672 mJ/pkt
Energy savings in communications	0%	27%	52%	63%
Total current draw of each insole (only accelerometer on)	276 mA	205 mA	142 mA	106 mA
Total current draw of each insole (all sensors on)	414 mA	343 mA	280 mA	244 mA
Total energy saving	0	17%	33%	39%
Battery lifetime (only accelerometer on)	4 h	5.4 h	7.8 h	10.5 h
Battery lifetime (all sensors on)	2.7 h	3.2 h	3.6 h	4.5 h

Based on Table 12, in the second experiment, less energy is consumed comparing to the first experiment. This can be attributed to the fact that the average distance between the smart insoles and the receiver node is less than that of the first experiment. For the same reason, the number of packet transmission failures in the second experiment is smaller. Furthermore, the second experiment (i.e., the tug test) does not include running episodes, which tend to associate with transmission failures.

In addition to outperforming the frame-based TPC scheme in terms of PRR, applying our sensor-assisted scheme saves twice as much energy as employing the frame-based TPC. It should be noted that the overall acknowledgement failure rate in this experiment is less than 1%.

Our final objective is to extend the battery life of wireless insoles in a low-cost way while meeting all the constraints as far as the packet loss, packet size, and data rate are concerned. Our sensor-assisted TPC method conserves a noticeable amount of energy compared to the frame-based and maximum transmission power schemes. The current battery lifetime with no TPC applied for the first and second setups is equal to 4 hours and 2.7 hours, respectively. Assuming that the smart insoles are continually used in TUG tests, our sensor-assisted TPC scheme will extend the battery lifetime of the first and second setups to 7.8 hours and 3.6 hours by adjusting the transmission power in a fine-grained and activity-aware

manner.

5.9 Discussion and Future Directions

Most of the time in a TUG test is spent in non-stationary mobility states. Frame-based TPC responds slowly to channel variations in non-stationary states and hence, it cannot keep up with the sensor-assisted TPC, which has fine-grained tools for adjusting the transmission power. By utilizing the sensor-assisted TPC scheme, the communication subsystem of the smart insoles consumes 25% and 22% less energy in the first and second experiments, respectively. Such energy savings are significant for the smart insole as a severely energy-constrained device.

For both frame-based and link quality based power control methods, there is a trade-off between having multiple packet failures at lower transmission power levels and temporarily increasing the power level beyond the minimum level necessary [Ko]. The second design parameter governs the strategy used to decrease the transmission power. The frame-based scheme performs well in motionless periods, in that it is able to decrease the transmit power at the same pace as the sensor-assisted scheme does. In non-stationary states, however, the performance of the frame-based TPC deteriorates in comparison with our sensor-assisted approach. The reason is that the transmission power of the sensor-assisted scheme can be quickly adjusted over time, whereas, the transmission power of the frame-based approach is slowly adjusted, as the frame-based scheme only keeps track of acknowledged/unacknowledged packets. In our sensor-assisted scheme, the mobility state of the system enables a WBAN node to know whether to expect transient link quality changes or not. Accordingly, a more informed strategy will be used to increase the transmission power.

Nevertheless, per our preliminary indoor experiments, the sensor-assisted scheme still performs better than the frame-based scheme as it is able to recognize the mobility state in which the transmitting node is. Our mobility state detection techniques are accurate and they do not require any training and perform well across a variety of conditions. Regardless of the environment/context and as long as the accelerometer sensor is attached to a subject's foot, the accuracy of our movement detection, walking/running detection,

and step detection methods are 100%, 95%, and 90%, respectively. In indoor environments, there are situations that can help or hurt each wireless transmission. For example, human activity in the surrounding environment (especially in the area between the transmitting and receiving nodes) worsens the quality of a wireless channel in indoor settings. On the other hand, in some cases due to the well-known corridor waveguide effect, wireless signals are reflected by wall surfaces at various angles, which results in a better propagation than expected.

In order to discover a range for our energy savings, we reported the energy consumption numbers for scenarios where the transmit power is fixed at the maximum transmit power (+18 dBm) and minimum transmit power (+10 dBm). Although the energy saving numbers for every TPC scheme reside in this range, it is not practical to benchmark an optimal power setting corresponding with an optimal TPC scheme; channel quality metrics cannot be measured for all power levels for every single packet transmission, thus, we are not able to find how much energy saving the optimal TPC scheme would bring about even for a specific experiment (e.g., TUG test). We can always find the energy savings of an optimal scheme offline by finding packets for which the link quality metric values were high and yet, the power level was not reduced. It also should be noted that the feedback mechanism is not perfect. As such, there are situations where the acknowledgment packet is lost and hence, we inevitably use a higher transmission power level than the necessary level. Our sensor-assisted TPC scheme saves a considerable amount of energy for WBAN nodes whose radio utilizes duty-cycling mechanisms. Since idle listening consumes substantial energy in low power radios, nodes that constantly keep their radios on will benefit less from out sensor-assisted TPC. Even with such nodes, controlling transmission power is beneficial, as it reduces interference range.

Smart insoles and, nodes in a typical WBAN in general, move at a relatively low speed comparing to their data generation and communication rate. This implies that the transmission power level at which the previous successful data transfer was performed should be a reasonable estimate for the transmission power level of the current data packet. Clearly, the application's data rate and the speed of WLAN's mobile node greatly affect the transmission power level. The characterization results in Section 5.3

showed that the high variability of RSSI measurements make the inference of transmission power levels from such measurements infeasible; accordingly, an averaging method is used as part of our TPC scheme. The configurations associated with our sensor-assisted TPC are tuned for outdoor settings and for walking speeds. Therefore, we can adapt the sensitivity of the TPC scheme based on context and mobility state. An interesting question concerns the optimization of the parameters (smoothing factors and thresholds) for a given operating scenario. Such optimization targets the inherent trade-off between reliability (packet loss margin) and energy (maximum battery lifetime) and hence, it governs how rapidly/slowly the TPC scheme should react to a degrading/improving channel. Even though the optimal settings obtained here do not directly apply to other scenarios, they provide insight which could conceivably be used by a system to adjust the parameters at run-time based on application requirements and operating conditions.

The goal of a transmission power control scheme is to reliably deliver packets with minimal energy consumption and interference [Ko]. In accomplishing this goal, our sensor-assisted scheme adheres to the following specifications: (1) it rapidly adapts to link quality variations as a result of mobility or changes in the operating environment; (2) it wisely uses the knowledge of past link conditions; (3) and each node independently calculates its power level. Nevertheless, there are still avenues to improve our scheme and there exist considerations that need to be addressed in a typical WBAN setup.

Memory and processing energy overheads: The AVR Atmega168 chip, which serves as the microcontroller in the smart insoles (Section 5.1), possesses 16 KB of flash memory to store programs. There are 1024 B of SRAM, in which, the TPC scheme creates and manipulates variables (e.g., running averages of link quality metrics) during execution. Further, ATmega160 has 512 B of EEPROM memory, which can also be used to store data for programs. The additional memory usage estimate for the frame-based TPC is 1 KB of program space, 20 B of SRAM, and 172 B of EEPROM. However, employing the sensor-assisted scheme incurs 2 KB of program space, 46 B of SRAM, and 396 B of EEPROM, mainly on account of running the mobility state detection methods. As the goal is to detect more mobility states and accomplish power control in a more fine-grained manner, one solution would be to perform mobility state detection on the receiver side, where the memory size is not a matter of concern. Moreover, the

memory size can always be augmented with interfacing external memory units to Arduino Pro Mini. It should be remembered that the excess processing energy for detecting mobility states is considered negligible as compared to the energy dissipated for the wireless communications.

Retransmissions and hidden terminal problem: Both power level and the number of transmission attempts affect the energy consumption. Generally, it is more energy-efficient to send a packet once at the maximum transmit power and succeed, as opposed to retransmitting the packet multiple times at lower transmit power levels. A concern that arises from utilizing a transmission power control scheme is the increasing rate of the hidden terminal problem. When a mobile node decreases its transmit power to the minimum level necessary to reach the intended receiver, carrier sensing mechanisms at other nodes are more likely to fail. Nevertheless, both the sensor-assisted scheme and the frame-based scheme address the hidden terminal problem by immediately increasing the transmission power upon noticing an unacknowledged packet, which re-enables carrier sensing for the other sources [Ko].

Acknowledgement loss issue: We also note that since acknowledgment frames play an essential role in any feedback-based TPC scheme, they are transmitted using maximum power levels at all times to assure reliable delivery with a single transmission attempt. The issue of high acknowledgement loss rate, perhaps arising from asymmetric links, is worthy of further studies, as this issue can have a negative impact on the efficacy of any feedback-based TPC scheme, i.e., link quality-based or frame-based.

Interference and TPC: The higher the transmit power, the higher the probability of wireless signals arriving at unintended receivers, which is known as interference. We aim at observing how the sensor-assisted power control scheme reduces the interference in contrast with the maximum transmit power scheme by placing few receivers at different locations with respect to the intended receiver.

Routing tables and sensor assisted TPC: From the routing layer perspective, routing tables may also need to be updated regularly according to mobility states, as the optimal next hop may depend on the speed and direction of movement.

More sensors and more mobility states: In our experimental results, we used a bimodal mobility indicating whether the WBAN node is stationary or mobile. Given that even such a simple mobility state

yielded significant energy savings, an obvious future direction is to generalize our scheme to use further and more fine-grained mobility states with different attributes pertaining to, for instance, environment (indoor/outdoor), speed, and heading. Deriving such fine-grained mobility states is feasible through utilizing additional sensors such as gyroscopes, GPS receivers, compasses, and pressure sensors.

Sensor assisted cellular communications: We can elevate our sensor-assisted approach one level higher; our mobility state detection methods process raw sensor data to extract useful information pertaining to the mobility state. For instance, our walking detection method expects relaxed requirements on how the device should be worn. As such, it can be used not only in the smart insoles, but on a variety of commodity smartphones and tablet devices. Commodity smartphones and tablet devices are integrated with a variety of sensors, including GPS, accelerometers, magnetic compasses, and gyroscopes, which can provide insights about the device's mobility state and its operating environment. Furthermore, sensors such as accelerometers on smartphones are kept on by default; thus, extracting mobility states from them consumes no extra energy.

Sensor assisted wireless protocols: the idea of making a connection between the sensing subsystem and communications subsystem can make wireless communications more efficient on many levels than just transmission power control. The whole wireless protocol stack can thus benefit from the information given by the sensing subsystem. Accordingly, the ideas of sensor-assisted rate adaptation, sensor-assisted packet size adaptation, sensor-assisted access point association, sensor-assisted topology maintenance, and sensor-assisted application-level tools are worthy of attention [Ravindranath]. In addition to using information from local sensors, a communication protocol can also adapt according to the information communicated from other nodes.

Correctness/compliance: Besides energy savings, our mobility state detection methods can be simultaneously exploited to verify the correctness of different sporting activities and to assess/improve compliance with medical advice without the person/patient noticing; this will significantly elevate the quality of medical data, productivity of self-directed exercises, and efficiency of fitness tests and therapy sessions via information from local sensors. In long-term, a more positive physician-patient or trainer-

trainee relationship is obtained in an inconspicuous way.

Other sensor-assisted approaches: A new sensor-assisted TPC scheme can be developed, which is inspired by a probe-based bit-rate selection algorithm for WLAN networks named SampleRate: After a certain number of packets have been transmitted, a packet is sent to probe one or two lower power levels; this way, we quickly determine whether or not it is safe to switch to a lower power level. The frequency of probe packets is specified by the mobility state of the system extracted from local sensors' data. One simple idea would be to probe regularly and frequently when a WBAN node is moving, and to probe less often when the WBAN node is immobile. Success intervals can also be incorporated in the adjustment of transmit power levels (Appendix D). For example, after successful transmissions at a particular power level for more than a specified time, the transmitter switches to a lower power level that has not failed in the last few milliseconds [Ravindranath]. Our sensor-assisted TPC scheme relies on transmission statistics over a sliding window period. Another approach is to change the periods at which the feedbacks (acknowledgements) are sent (Appendix E). In this manner, we can save more energy by not sending feedback packets for each individual packet. Such feedback packets increase the channel load and idle listening intervals at WBAN nodes, which are at odds with energy-efficiency objectives.

CHAPTER 6

Concluding Remarks

The idea of transmission power control (TPC) is to automatically reduce the utilized transmission output power when the transmission power is more than required. Reduced power translates to reduced interference problems and more energy savings. TPC techniques have been used in abundance in cellular networks and wireless LANs. In this dissertation, we have investigated the potential benefits and limitations of TPC as a means to extend the battery lifetime in wireless body area networks (WBANs) at the first three abstraction levels. The tuning of the transmission power results in cross-layer consequences; physical and MAC layers approach to TPC perform a local optimization, whereas network layer's TPC is capable of a global optimization. At the network layer, we analytically solved an optimization problem whose solution determines an important parameter, namely, energy-efficient cluster size for a class of routing/MAC protocols in WBANS. Assuming that the routes are established in an energy-efficient manner, we then experimentally profiled the 2.4 GHz on/off-body radio channel under several scenarios regarding mobility states and environments, and we showed that fixed transmission power either wastes energy or hinders reliability. Finally, we devoted our attention to a specific medical monitoring WBAN system, which is tied up with different characteristics in terms of user's mobility and 'unforgivingness' of the wireless channel. Our target WBAN system is our smart insoles for which we developed a sensor-assisted TPC schemes to improve the battery lifetime without significantly compromising the reliability of communications.

Current TPC schemes work for slowly varying channels and simple configurations, or they only compensate for mobility and hence, they are not optimal for static settings. We proposed and

implemented a sensor-assisted TPC scheme that switches strategies based on user's mobility state and the history of channel quality. We leverage available sensor information to detect different mobility states based on which the TPC scheme switches strategies. Our empirical evaluation includes extensive in-field trials, which involve both stationary and non-stationary mobility states. The results show that our sensor-assisted TPC scheme is able to adjust the transmission power in a fine-grained and activity-aware manner. Accordingly, it can almost double the battery lifetime of the smart insoles (from 4 h to 7.8 h) by reducing the average energy consumed for communication of one packet from 4.51 mJ/pkt to 2.27 mJ/pkt. Furthermore, the sensor-assisted scheme outperforms an existing TPC scheme in terms of packet reception ratio.

Although designed for the smart insoles as a severely energy-constrained device, the sensor-assisted TPC technique is readily deployable on many of today's commodity devices to make a connection between the sensing subsystem and the communication subsystem of such devices. In addition, the underlying mobility state detection schemes place relaxed the requirements on how the device should be worn (orientation and position) and hence, they can be used for a variety of purposes, such as to improve the compliance with medical advice.

Appendix A.

Optimal Cluster Size for Multi-Hop WBANs

A number of cluster-based communication protocols take chain-based approaches to convey cluster heads' data to the base station. As an example, HIT [Moh] pursues multi-hop routing from cluster heads to a base station to conserve energy.

For such multi-hop schemes, we perform the analysis to find the optimal number of clusters. We assume that N sensor nodes are uniformly deployed within a circular field of radius R. The base station is located at the center of the sensing field. We also hypothetically partition the circular field into m separate concentric segments (also known as corona, annulus, or ring in the literature) considering $m + 1$ concentric circles whose center is the BS. The radius of concentric circles is represented by r_0, r_1, r_2, …, $r_m = R$. In each round of the network operation, the network is divided into k_{opt} clusters and the cluster heads forward their aggregated data to the BS in a hop by hop fashion via cluster heads from closer segments. We denote segment i by S_i and we interpret S_0 as the BS. Hence, data traffic is forwarded hop by hop from S_i to S_{i-1} and so on until it reaches the BS.

Each non-cluster head node transmits its data to the cluster head once per round. Accordingly, the energy dissipation for non-cluster head nodes can be written as:

$$E_{non-CH} = lE_{elec}^{Tx} + l\varepsilon_{amp}d_{toCH}^{n}. \tag{75}$$

The expected value of the nth power of distance between cluster members and cluster heads is as follows:

$$E[d_{toCH}^{n}] = \frac{2}{n+2}\left(\frac{R}{\sqrt{k_{opt}}}\right)^{n}. \tag{76}$$

By substituting (64) into (65), the energy used in each non-cluster head node per round is given by:

$$E_{non-CH} = lE_{elec}^{Tx} + l\varepsilon_{amp}\frac{2}{n+2}(\frac{R}{\sqrt{k_{opt}}})^n. \quad (77)$$

Each cluster head dissipates energy receiving signals from the nodes, aggregating the signals, forwarding the incoming data to the inner segment, and transmitting the aggregated data to the inner segment. Hence, in each round, the energy dissipated in a cluster head node located in the *i*th segment becomes:

$$E_{CH}(S_i) = (\frac{N}{k_{opt}} - 1)lE_{elec}^{Rx} + \frac{N}{k_{opt}}lE_{DA} + l\frac{\sum_{j=i+1}^{m} S_j}{S_i}E_{elec}^{Rx} + l\frac{\sum_{j=i}^{m} S_j}{S_i}E_{elec}^{Tx} + l\frac{\sum_{j=i}^{m} S_j}{S_i}\varepsilon_{amp}d_{toS_{i-1}}^n, \quad (78)$$

where i resides in the interval [1, m], i.e., $1 \le i \le m$. In case i = 1, the energy consumption of a cluster head located in S_1, which is the potential hot spot due to the fact that it carries the most relay traffic across the sensing field, can be calculated as:

$$E_{CH}(S_1) = (\frac{N}{k_{opt}} - 1)lE_{elec}^{Rx} + \frac{N}{k_{opt}}lE_{DA} + l\frac{R^2 - r_1^2}{r_1^2 - r_0^2}E_{elec}^{Rx} + l\frac{R^2 - r_0^2}{r_1^2 - r_0^2}E_{elec}^{Tx} + l\frac{R^2 - r_0^2}{r_1^2 - r_0^2}\varepsilon_{amp}r_1^n. \quad (79)$$

If we assume that the energy being dissipated to run the transmitter's circuitry is equal to the one consumed by the receiver's circuitry, i.e., $E_{elec}^{Tx} = E_{elec}^{Rx} = E_{elec}$, (68) can be further simplified:

$$E_{CH}(S_1) = (\frac{N}{k_{opt}} - 1)lE_{elec} + \frac{N}{k_{opt}}lE_{DA} + l\frac{2R^2 - r_1^2 - r_0^2}{r_1^2 - r_0^2}E_{elec} + l\frac{R^2 - r_0^2}{r_1^2 - r_0^2}\varepsilon_{amp}r_1^n. \quad (80)$$

It is obvious that the network lifetime (E_{total}/E_{round}) is dominated by the lifetime of S_1. For simplicity, we use $p_i = \frac{S_i}{\pi(R^2 - r_0^2)}$ $(1 \le i \le m)$ to denote the area percentage. Hence, in each data gathering round, the energy consumed in S_1 is given as follows:

$$E(S_1) = k_{opt}p_1(E_{CH}(S_1) + (\frac{N}{k_{opt}} - 1)E_{non-CH}). \quad (81)$$

Thus, the lifetime of area S_1 can be estimated as:

$$T = p_1 NE_0 / E(S_1), \quad (82)$$

where E_0 denotes the initial energy of each sensor node. The above equation is governed by two factors: the optimal number of clusters (k_{opt}) and the radii of C_1, i.e., r_1. Hence, in order to maximize T, one should minimize the function $f(r_1,k_{opt})$:

$$f(r_1, k_{opt}) = 2E_{elec}\frac{R^2}{r_1^2}k_{opt} - E_{elec}k_{opt} + \varepsilon_{amp}R^2 r_1^{n-2}k_{opt} + \frac{2}{n+2}\varepsilon_{amp}N\frac{R^n}{k_{opt}^{n/2}}. \tag{83}$$

Taking the partial derivatives yields:

$$\begin{cases} \dfrac{\partial f(r_1, k_{opt})}{\partial r_1} = -4E_{elec}R^2 r_1^{-3}k_{opt} + (n-4)\varepsilon_{amp}R^2 r_1^2 k_{opt} \\ \dfrac{\partial f(r_1, k_{opt})}{\partial k_{opt}} = E_{elec}\dfrac{2R^2 - r_1^2}{r_1^2} + \varepsilon_{amp}R^2 r_1^{n-2} - \dfrac{n}{n+2}\varepsilon_{amp}NR^n k_{opt}^{-\frac{n+2}{2}}. \end{cases} \tag{84}$$

It is worth noting that for a given E_{elec}, n, and ε_{amp}, we can determine r_1 and k_{opt} in such a way that $f(r_1,k_{opt})$ becomes minimized, in other words T is maximized. Examining the function $\partial f(r_1, k_{opt}) / \partial f(r_1)$, we can find the value of r_1 for which the function becomes zero for $n > 2$. The fact that the function is decreasing for n = 2 shows that the optimal value of r_1 is:

$$r_{1\_opt} = \begin{cases} \sqrt[n]{\dfrac{4E_{elec}}{(n-2)\varepsilon_{amp}}} & 2 < \mathrm{n} \le 6 \\ \text{transmssion radius} & \mathrm{n} = 2. \end{cases} \tag{85}$$

Finally, we can obtain the optimal value of k_{opt} by finding r_{1_opt} and nulling the function $\partial f(r_1, k_{opt}) / \partial f(k_{opt})$. With the optimal value of k_{opt} and properly choosing the size of r_1, we can achieve the optimized lifetime of S_1, hence, maximize the lifetime of the whole network.

Appendix B.

Transitional Region Model for 2.4GHz O-QPSK Communications

Traditional simulation models for wireless communications only consider connected and disconnected regions. However, several works have reported the existence of a third "transitional region" in which the Packet Reception Rate (PRR) is quite erratic.

The existence of this region is important as upper layer protocols may disregard it when for example, they make routing decisions. Zuniga et al. [Zuniga] determine the underlying causes of this region using analytical techniques from communications theory along with practical results. These experiments were performed using a radio architecture that employs NRZ (Non-return-to-zero) encoding and non-coherent FSK (Frequency-shift keying). However, their analytical model does not apply to IEEE 802.15.4 communications, which use O-QPSK (Offset Quadrature Phase Shift Keying) modulation; they observed a significant extent of transition region although no specific values were provided. Hence, a new model to cover such schemes is required.

Zuniga et al. analyze the transition region model for radios using NRZ encoding and a non-coherent FSK modulation scheme. They also claim that it can be extended to other types of radio architecture. According to their study, there are three components affecting the width of the transition region: the wireless channel, radio transmission characteristics, and the noise floor. However, this model was only confirmed using a radio architecture that employs NRZ and non-coherent FSK and it may be difficult to directly apply with systems employing more complex modulation schemes, such as O-QPSK. This is because the probability of bit error can be easily expressed in function of E_b/N_0 (the energy per bit to noise power spectral density ratio) for non-coherent FSK modulation.

The radio model is based on the work of Dhananjay et al. [Dhananjay], where the probability p of successfully receiving a packet is given by

$$p = (1-P_e)^{8l}(1-P_e)^{8(f-l)} = (1-P_e)^{8f} = PRR$$
or
$$P_e = 1 - PRR^{1/8f}, \tag{86}$$

where P_e is the probability of bit error (BER), f is the frame size, and l is the preamble length (both expressed in bytes). This equation is not directly applicable to O-QPSK with DSSS schemes. However, it provides a close approximation of the true PRR expression used also by other researchers [Jiu-Qiang], [fedor].

For O-QPSK modulation in the IEEE 802.15.4 standard, P_e is determined as follows [IEEESTD]:

$$P_e = \frac{8}{15} \times \frac{1}{16} \times \sum_{k=2}^{16} -1^k \binom{16}{k} e^{20 \times SINR \times (\frac{1}{k} - 1)}, \tag{87}$$

where *SINR* is Signal to Interference plus Noise Ratio that is calculated as $SINR = P / (I + N)$ where P is signal power, I is interference power and N is noise power. Using (86) and (87), we can derive the proper SINR target, which fulfills the receiver sensitivity requirement of IEEE 802.15.4 (PRR of 99%) for packets of length 20 bytes:

$$SINR_{target} \approx 0.402 \text{ dbm}. \tag{88}$$

[O'Rourke] et al. have used the following equation in order to make a connection between SINR and RSSI:

$$SINR = 10 \log \frac{10^{RSSI/10} - 10^{P_N/10}}{10^{P_I/10}}, \tag{89}$$

where P_N is the noise floor at the receiver side in dBm, which depends on both the radio architecture and the environment. For the case when the receiver and antenna have the same ambient temperature the noise floor can be derived analytically using the equation [Rappaport]:

$$P_N = FkT_0B, \tag{90}$$

where F is the noise figure of the radio, T0 is the ambient temperature, and B is the noise equivalent bandwidth [Fedor]. The value of F can be assumed to be 11-12 dB, however, finding the value of B is not straightforward. As an approximation, we use the bandwidth of each 802.15.4 channel (i.e., 3 MHz) instead. Accordingly, the approximate value for the noise floor is:

$$P_N(\text{dB}) = 12 - 198.6 + 10\log(300) + 10\log(3\times10^6) \approx -97 \text{ dBm}. \tag{91}$$

If we assume that there is no external interference, i.e., $P_I = P_N$, we can find the analytical $RSSI_{target}$ (corresponding to $SINR_{target}$) as follows:

$$RSSI_{target} = P_N + 10\log(10^{\frac{\text{SINR}_{\text{target}}}{10}} + 1). \tag{92}$$

Using (91) and (92), one can derive:

$$RSSI_{target} \approx P_N + 3.21. \tag{93}$$

If the receiver's noise floor is known and there is no interference present, the proper RSSI target can be found via (93) without performing a complex calculation. A number of studies, e.g., [JKim], have reported up to 2 dB discrepancy between the target RSSI based on (93) comparing to empirical measurements.

It should be remembered that (93) is only an estimation as it ignores interference from other sources that may deteriorate the measured RSSI value. Among the sixteen available channels offered by IEEE 802.15.4, channels 25 and 26 experience no interference from 802.11 b/g communications (see Figure 41). However, these channels are not available in XBee Pro platforms. For XBee Pro modules, channels 15 and 20 undergo less 802.11 b/g interference comparing to other channels.

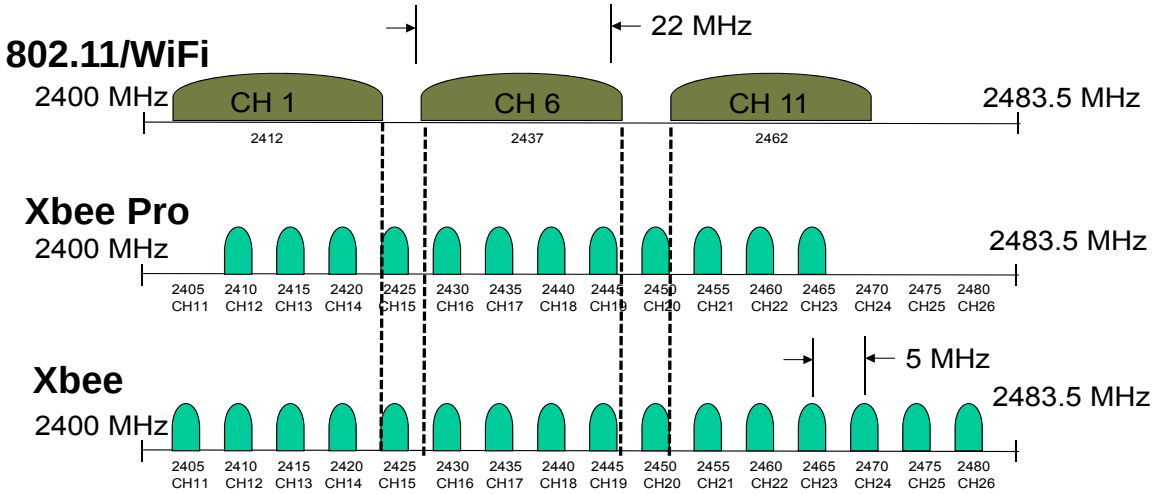

Figure 41. Channel overlap between 802.11 and 802.15.4. Note that XBee Pro modules do not offer the last three channels.

Appendix C.

Signal Salience Derivation

The goal is to calculate the salience vector for a given input signal.

Basic scheme: The calculation of salience involves taking into account all possible analysis intervals within the given signal of size N and recording the length of the longest interval for which a sample is a maximum. The calculation of the salience vector requires the following steps:

1- Initialization: Since each sample is a maximum with respect to itself, all salience values are set equal to 1. Thus, the length of the analysis interval (n) is set as $n = 2$.

2- Subdivide the input signal of length N into analysis intervals of length n. The length of the last interval will be between 1 and n.

3- Find the maximum point within each interval and assign a salience of n to the corresponding sample.

4- Increase the size of analysis interval by one and go back to step 2.

When n becomes equal to the length of the input signal the algorithm stops. At this point, all samples are assigned at least one and up to N salience values. The last calculated salience will be reported as the salience for a given sample. As an example, Figure 42 demonstrates different steps of the basic salience computation algorithm for an input signal of size 16.

In Figure 42, the second sample's salience is 1. However, if we had taken the second sample as the starting point of the signal, the salience would have been equal to 4. Since there is no information available about the samples outside the signal being processed, there is a chance that false salience values will be assigned to the samples close to the boundary. Boundary effects may be addressed by rotating the samples of the input signals for N times, so that each sample takes the left and right boundary positions once. Final saliences will be the average saliences, which may be considered to be independent of their

positions with respect to the boundaries. When rotating, samples that are far from each other may be put in contact, which may cause bias of saliences. Furthermore, rotation increases processing time.

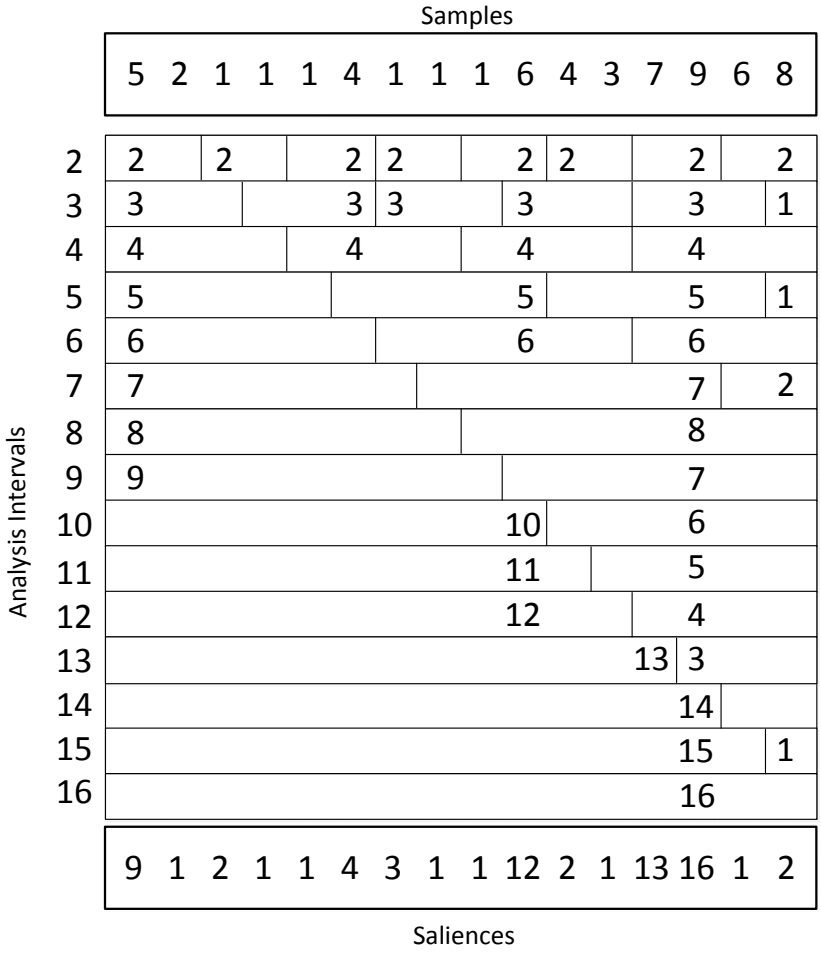

Figure 42. An example input signal and step by step derivation of its salience vector using the basic scheme.

Partial Salience Allocation: As an alternative to the basic scheme, partial salience allocation is used in applications where computationally expensive functions cannot be tolerated. Partial salience allocation utilizes takes advantage of the tabular representation of samples (see Figure 43). Instead of finding maxima over analysis intervals with increasing length 2, 3, 4, …, one can determine the maximum over frames of decreasing lengths. Let *j* be the position of the global maximum of the input signal. Obviously this sample is a maximum for the previous *j*-1 first samples. Accordingly, assuming that *j* is known, one

can compute the maximum over j-1 first samples only and assign it a salience of j-1 and so on, until a salience has been assigned to the first sample. For samples with assigned salience values, the left and right saliences are also stored. Figure 43 depicts the application of partial salience scheme to the same input signal as Figure 42.

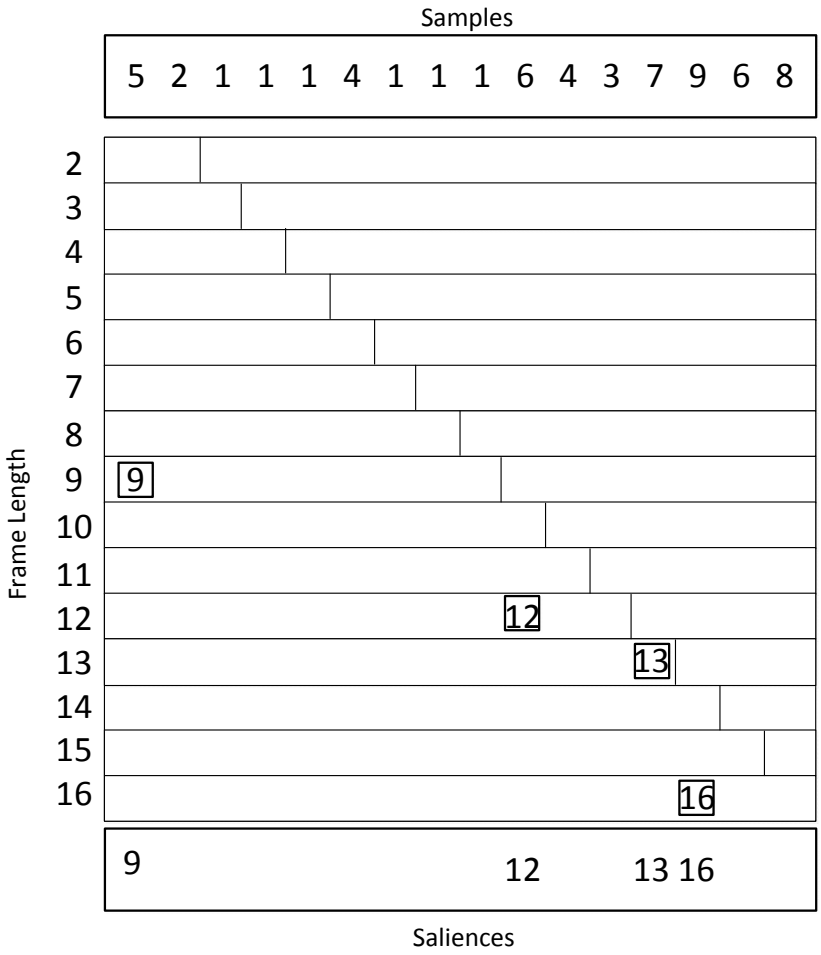

Figure 43. An example input signal and derivation of its partial salience.

Sliding window salience computation scheme: Partial salience method cannot find salience values for all the samples in the input signal. Furthermore, the problems related to samples near the boundaries are not addresses in this scheme. The intuition behind the sliding window scheme is to apply a window to the input signal and move the window sample by sample in order to address the boundary problem. In this method, a sliding window $w_M(i)$, of length M ($M < N$) and origin i, is placed at the beginning of the signal

and is shifted sample by sample towards the end point of the signal. Saliences $s(k,i)$, $s_l(k,i)$, $s_r(k,i)$ are then computed with regard to the sliding window. If the proper window size is chosen, the running saliences obtained will suffice for most applications. From now on, we define local saliences with reference to the position of a given window. Moreover, running saliences $s^*(k)$, $s_l^*(k)$, $s_r^*(k)$, are defined as the maximum of the local saliences of sample k for all window positions (previous and current). Thus, running saliences are non-decreasing. Here we outline the sliding window analysis scheme:

1- Initialization: all saliences s^* are set equal to 1 and all saliences s_l^* and s_r^* are set equal to zero.

2- Apply the partial salience allocation scheme to the samples within the sliding window with origin i and compute the local $s(k,i)$, $s_l(k,i)$, and $s_r(k,i)$ saliences, where $k = i, i + 1, \ldots, i + M - 1$.

3- Update running saliences as follows: for each sample k, $s^* = s(k,i)$, $s_l^*(k,i) = s_l(k,i)$, $s_r^*(k) = s_r(k,i)$ if their values will be increased, otherwise, skip this step.

4- Shift the sliding window to the right by one sample, i.e., $(i \rightarrow i + 1)$ and go back to step 2.

Once the sliding window reaches the right boundary of the input signal, the final salience vector, $s_f(k)$ is given by:

$$s_f(k) = s_r^*(k) + s_l^*(k) + 1 \quad k = 1,2...M \tag{94}$$

Since the sliding window was shifted sample by sample, at this point, each sample has been assigned a salience value. It should be remembered that the left-most sample within each window is always assigned a salience value in the partial salience allocation scheme (see Figure 43). One should discard the $M - 1$ first and the $M - 1$ last elements of the derived salience vector. Such elements suffer from the negative effect of the boundaries. It is straightforward to show that the basic scheme and the sliding window scheme achieve identical salience vectors. In case, one of the left or right running saliences is greater than the window size M, the sample salience will be truncated to a value smaller than M. In this case the result of the sliding window scheme will be different than that of the basic scheme. When both running saliences are greater than N, the sample salience will be equal to $2N - 1$.

The length of the sliding window must be chosen in a way that the loss of information due to the signal boundaries will be minimized. Also, window size must maximize the relevance of the salience values with respect the goal of the analysis. It should be noted that the salience analysis via the sliding window scheme can be further speeded up by performing additional tests on the salience values computed at previous positions of the sliding window.

Appendix D.

Frame-Based Sensor-Assisted Transmission Power Control Based on Success Intervals

MobilityAdaptiveTPC(gotACK,X,mobile, P_{TX}^{latest})

Require: P_{TX}^{latest} {The latest transmit power used}

Require: mobility state

► Modifies transmission power (P_{TX}) considering mobility state

1: **if** (!gotACK) **then**
2: **failedTime[** P_{TX}^{latest} **]** ← **currTime**()
3: **if** (sample) **then**
4: $P_{TX} \leftarrow oldP_{TX}$
5: **else**
6: $P_{TX} \leftarrow \min\{P_{TX}^{\max}, P_{TX}^{latest} + 1\}$
7: sample ← 0
8: **else**
9: sample ← 0
10: if (**currTime() –** pickedTime[P_{TX}^{latest}] > $\delta_{success}$) **then**
11: $P_{TX} \leftarrow \max\{i \mid \forall j \le i$: **currTime**() **–** failedTime[j] > $\delta_{fail}\}$
12: sample ← 1
13: $oldP_{TX} \leftarrow P_{TX}$
14: else $P_{TX} \leftarrow P_{TX}^{latest}$
15: **if** $P_{TX} \neq P_{TX}^{latest}$
16: pickedTime[P_{TX}] ← **currTime**()
17: return P_{TX}

Figure 44. Frame-based TPC adapts depending on transmission success intervals for each power level. Mobility state information updates the success and fail thresholds.

Appendix E.

Frame-Based Sensor-Assisted Transmission Power Control with Adaptive Feedbacks

AdaptiveTransmissionPowerControl
Require: X {Link quality metric from the most recent packet}
Require: $\overline{X}$ {Running average of X}
► Modifies transmission power and update periods
1: if $\overline{X} > T_H$
2: **then** decrease transmit power
3: reduce update period
4: **else if** $\overline{X} < T_L$
5: **then** increase transmit power
6: reduce update period
7: **else** increase update period

CalcXValues
1: if $X < X_{lowest}$
2: **then** $X_{lowest} \leftarrow X$
3: $\overline{X} \leftarrow (1-\alpha)X_{lowest} + \alpha X$

Figure 45. Transmission power control with adaptive feedbacks/updates. Mobility state information determines the frequency of feedbacks.

REFERENCES

[Ullah] Sana Ullah, Henry Higgins, Bart Braem, Benoit Latre, Chris Blondia, Ingrid Moerman, Shahnaz Saleem, Ziaur Rahman and Kyung Sup Kwak, A Comprehensive Survey of Wireless Body Area Networks: On PHY, MAC, and Network Layers Solutions, Journal of Medical Systems, IN PRESS, pp. 1-30.

[Latre1] Benoît Latré, Bart Braem, Ingrid Moerman, Chris Blondia and Piet Demeester, A survey on Wireless Body Area Networks, Wireless Networks Journal, Vol. 17, Issue 1, January 2011, pp. 1-18.

[Correia] Luiz Henrique Andrade Correia, Daniel Fernandes Macedo, Aldri Luiz dos Santos and José Marcos Silva Nogueira, Transmission Power Control Techniques in Ad Hoc Networks, Computer Communications and Networks, 2009, pp. 469-489.

[Lin1] Xiao-Hui Lin, Yu-Kwong Kwok, and Hui Wang, Energy-Efficient Resource Management Techniques in Wireless Sensor Networks, Computer Communications and Networks, 2009, pp. 439-468.

[Kleisouris] K. Kleisouris, B. Firner, R. Howard, Y. Zhang, and R. P. Martin. Detecting intraroom mobility with signal strength descriptors. In MobiHoc'10, pages 71–80, 2010.

[Amini1] N. Amini, W. Xu, Zhinan Li, Ming-Chun Huang M. Sarrafzadeh, "Experimental Analysis of RF Transmission Characteristics for On/Off body communications," to appear in Proc. of the IEEE International Symposium on Personal, Indoor and Mobile Radio Communications (PIMRC), Sept 2011, Toronto, Canada.

[Wiki1] http://en.wikipedia.org/wiki/Power_control

[Hanson] Hanson, M.A.; Powell, H.C., Jr.; Barth, A.T.; Lach, J. Enabling Data-centric Energy-fidelity Scalability in Wireless Body Area Sensor Networks. In Proceedings of the 4th International Conference on Body Area Networks, Los Angeles, CA, USA, April 2009.

[Quwaider] Quwaider, M., J. Rao, and S. Biswas. 2010a. Transmission power assignment with postural position inference for on-body wireless communication links. ACM Trans. Embedded Computer System s 10(1): Article 14.

[Gomez] J. Gomez and A.T. Campbell, "A Case for Variable-Range Transmission Power Control in Wireless Multihop Networks," Proc. IEEE INFOCOM, 2004.

[Oh] Oh, S.J., Wasserman, K.M., Optimality of greedy power control and variable spreading gain in multi-class cdma mobile networks. In: MobiCom '99: Proceedings of the 5th Annual ACM/IEEE International Conference on Mobile computing and networking, pp. 102–112. ACM Press, New York (1999)

[Rashid-Farrokhi] Rashid-Farrokhi, F., Liu, K., Tassiulas, L.: Downlink power control and base station assignment. IEEE Communications Letters 1(4), 102–104 (1997).

[Qiao] Qiao, D., Choi, S., Jain, A., Shin, K.G.: Miser: An optimal low-energy transmission strategy for ieee 802.11a/h. In: MobiCom '03: Proceedings of the 9th Annual International Conference on Mobile Computing and Networking, pp. 161–175. ACM Press, New York (2003).

[Kubisch] Kubisch, M., Karl, H., Wolisz, A., Zhong, L.C., Rabaey, J.: Distributed algorithms for transmission power control in wireless sensor networks. In: Proc. IEEE Wireless Communications and Networking Conference (WCNC'03), vol. 1, pp. 558–563 (2003).

[Moh] Moh, M., Culpepper, B. J., Dung, L., Moh, T. S., Hamada, T., and Su, C., On data gathering protocols for in-body biomedical sensor networks. in the Proc. of IEEE Conference on Global Telecommunications (GLOBECOM 2005), Vol. 5, 2005.

[Shankar] V. Shankar, A. Natarajan, S. K. S. Gupta, and L. Schwiebert, "Energy efficient protocols for wireless communication in biosensor networks," in Proc. of 12th IEEE Int Symp. Personal, Indoor and Mobile Radio Communication, San Diego, CA, Sep. 2001, pp. D-114–D-118.

[Li] Jingyuan Li, Tejaswi Tamminedi, Guy Yosiphon, Anurag Ganguli, Lei Zhang, Jacob Yadegar, John Stankovic 2010. Remote Physiological Monitoring of First Responders with Intermittent Network Connectivity, accepted by Wireless Health 2010.

[Sivaraman] V. Sivaraman, S. Grover, A. Kurusingal, A. Dhamdhere, and A. Burdett, "Experimental study of mobility in the soccer field with application to real-time athlete monitoring," in Proceedings of IEEE WiMob, Niagara Falls, Canada, Oct. 2010.

[Noshadi1] H. Noshadi, S. Ahmadian, H. Hagopian, J. Woodbridge, F. Dabiri, N. Amini, M. Sarrafzadeh, N. Terrafranca, "HERMES - Mobile Balance and Instability Assessment System," Proc. of the International Conference on Bio-inspired Systems and Signal Processing (BIOSIGNALS 2010), Valencia, Spain, Jan. 2010, pp. 264-270.

[Amini2] N. Amini, J. Matthews, F. Dabiri, A. Vahdatpour, H. Noshadi, M. Sarrafzadeh, "A Wireless Embedded Device for Personalized Ultraviolet Monitoring," Proc. of the International Conference on Biomedical Electronics and Devices (BIODEVICES 2009), Porto, Portugal, Jan. 2009, pp. 200-205.

[Monton] E. Monton, J. F. Hernandez, J. M. Blasco, T. Herve, J. Micallef, I. Grech, A. Brincat, and V. Traver, "Body area network for wireless patient monitoring," Telemed. E-Health Commun. Syst., vol. 2, pp. 215–222, 2008.

[IEEE] http://en.wikipedia.org/wiki/IEEE_802.15.4

[Nike+] www.apple.com/ipod/nike/

[VShoe] http://www.myvitali.com/en/projects/vitalishoe/

[Jagosa] Harald Jagosa, Johannes Oberzauchera, Martin Reichelb, Wolfgang L. Zaglerc and Walter Hlauscheka, A multimodal approach for insole motion measurement and analysis, Proc. of the 8th Conference of the International Sports Engineering Association (ISEA), Volume 2, Issue 2, June 2010, Pages 3103-3108.

[Aiden] www.i-shoe.net/

[Noshadi2] Hyduke Noshadi, Foad Dabiri, Navid Amini and Majid Sarrafzadeh, "HERMES: Mobile System for Instability Analysis and Balance Assessment", to appear in ACM Transaction on Embedded Computing Systems.

[Noshadi3] H. Noshadi, N. Amini, J. Woodbridge, W. Xu, M. Lan, H. Hagopian, N. Terrafranca and M. Sarrafzadeh, "Lightweight Context-Aware Smart Insole for Gait Analysis, Research and Rehabilitation," Parkinsonism & Related Disorders, Vol. 16, Supp. 1, Feb. 2010, pp. S29.

[Fresnel] http://en.wikipedia.org/wiki/Fresnel_zone

[Kawadia] Kawadia, V., Kumar, P.R.: Principles and protocols for power control in wireless ad hoc networks. IEEE Journal on Selected Areas in Communications 23(1), 76–88 (2005).

[Correia] Luiz Henrique Andrade Correia, Daniel Fernandes Macedo, Aldri Luiz dos Santos and José Marcos Silva Nogueira, Transmission Power Control Techniques in Ad Hoc Networks, Computer Communications and Networks, 2009, pp. 469-489.

[Monks] Monks, J.P.: Transmission Power Control for Enhancing the Performance of Wireless Packet Data Networks. Phd. Thesis, University of Illinois at Urbana-Champaign, Urbana, IL (2001).

[Gomez] Gomez, J., Campbell, A.T.: A case for variable-range transmission power control in wireless multihop networks. In: Proceedings of the IEEE Infocom, vol. 2, pp. 1425–1436 (2004)

[Gupta] Gupta, P., Kumar, P.: Capacity of wireless networks. IEEE Transactions of Information Theory 46(2), 388–404 (2000).

[TI1] Texas Instruments 2009 Texas Instruments ez430-rf2500 Development Tool User's Guide (online). Available at www.ti.com/lit/pdf/slau227 (retrieved June 2011).

[TI2] Instruments ez430-rf2500 Development Tool User's Guide (online). Available at www.ti.com/lit/pdf/slau227 (retrieved June 2011).

[TI3] T. Instruments, CC2500 datasheet, 2005. [Online]. Available: http: //focus.ti.com/lit/ds/symlink/ cc2500.pdf

[Ren] Ren, H., & Meng, M. Q. H. (2006). Rate control to reduce bioeffects in wireless biomedical sensor networks. In 3rd Annual international conference on mobile and ubiquitous systems— Workshops, San Jose, CA, pp. 1–7.

[Tang] Tang, Q., Tummala, N., Gupta, S. K. S., and Schwiebert, L. (2005) Communication scheduling to minimize thermal effects of implanted biosensor networks in homogeneous tissue. IEEE Transactions on Biomedical Engineering, 52(7), 1285–1294.

[Bag] Bag, A., & Bassiouni, M. A. (2006). Energy efficient thermal aware routing algorithms for embedded biomedical sensor networks. In 2006 IEEE international conference on mobile adhoc and sensor systems (MASS), Vancouver, BC, pp. 604–609.

[Takahashi] Takahashi, D., Xiao, Y., Hu, F., Chen, J., & Sun, Y. (2008). Temperature-aware routing for telemedicine applications in embedded biomedical sensor networks. EURASIP Journal on Wireless Communications and Networking, Vol. 2008, no. Article ID 572636, 2008, 11 p.

[Watteyne] Watteyne, T., Auge´-Blum, S., Dohler, M., & Barthel, D. (2007). Anybody: A self-organization protocol for body area networks. In Second international conference on body area networks (BodyNets), Florence, Italy, June 11–13, 2007.

[Heinzelman] W. B. Heinzelman, A. P. Chandrakasan, H. Balakrishnan, "An Application-Specific Protocol Architecture for Wireless Microsensor Networks," IEEE Transactions on Wireless Communications 2002; Vol 1, No. 4, pp. 660–670.

[Moh] Moh, M., Culpepper, B. J., Dung, L., Moh, T.-S., Hamada, T., & Su, C.-F. (2005). On data gathering protocols for in-body biomedical sensor networks. In Global telecommunications conference. GLobecom 2005.

[Madan] Madan, R., Cui, S., Lall, S., & Goldsmith, N. A. (2006). Cross layer design for lifetime maximization in interference-limited wireless sensor networks. IEEE Transactions on Wireless Communications, 5(11), 3142–3152.

[Melodia] Melodia, T., Vuran, M., & Pompil, D. (2005). The state of the art in cross-layer design for wireless sensor networks. In Euro- NGI workshop on wireless and mobility, ser. LNCS 3883, pp. 78–92.

[Ruzzelli] Ruzzelli, A. G., Jurdak, R., OHare, G.M., and Stok, P. V. D., Energy-efficient multi-hop medical sensor networking. in the Proc. of 1st ACM SIGMOBILE international workshop on Systems and networking support for healthcare and assisted living environments, pp. 37–42. ACM: New York, NY, USA, 2007.

[Zasowski] Zasowski, T. (2007). A system concept for ultra wideband (UWB) body area networks.PhD Thesis, ETH Zu¨rich, No. 17259.

[De Poorter] De Poorter, E., Latre´, B., Moerman, I., & Demeester, P. (2008). Sensor and ad-hoc networks: Theoretical and algorithmic aspects, ser. Lecture Notes Electrical Engineering. Springer, June 2008, Vol. 7, Chap. Universal Framework for Sensor Networks.

[Latre2] Latre, B., Braem, B., Moerman, I., Blondia, C., Reusens, E., Joseph, W., and Demeester, P., A low-delay protocol for multihop wireless body area networks. in the Proc. of 4th International Conference on Mobile and Ubiquitous Systems: Networking and Services, pp. 479–486. Philadelphia, PA, USA, 2007.

[Latre3] Latre, B., De Poorter, E., Moerman, I., & Demeester, P. (2007). Mofban: A lightweight framework for body area networks. Lecture Notes in Computer Science, Proceedings of Embedded and Ubiquitous Computing (EUC 2007), 4808, 610–622.

[Joseph] Wout Joseph, Bart Braem, Elisabeth Reusens, Benoît Latré, Luc Martens & Chris Blondia Design of Energy Efficient Topologies for Wireless On-Body Channel 17th European Wireless Conference, Vienna, Austria, pp. 82-88, IEEE Computer Society, 2011.

[Braem] B. Braem, B. Latre, I. Moerman, C. Blondia, E. Reusens, W. Joseph, L. Martens, and P. Demeester, "The Need for Cooperation and Relaying in Short-Range High Path Loss Sensor Networks," in Proc. 2007 Int. Conf. Sensor Technol. Appl. (SENSORCOMM 2007), pp. 566–571.

[Reusens] E. Reusens, W. Joseph, B. Latre, B. Braem, G. Vermeeren, E. Tanghe, L. Martens, I. Moerman, and C. Blondia, "Characterization of on-body communication channel and energy efficient topology design for wireless body area networks," IEEE Trans. Inf. Technol. Biomed., vol. 13, no. 6, pp. 933–945, Nov. 2009.

[Sayrafian-Pour] K. Sayrafian-Pour, W.-B. Yang, J. Hagedorn, J. Terrill, and K. Y. Yazdandoost, "A statistical path loss model for medical implant communication channels," in Proc. IEEE Int. Symp. Pers., Indoor Mobile Radio Commun. (PIMRC), Tokyo, Japan, Sep. 2009, pp. 2995–2999.

[Abouei] Jamshid Abouei, J. David Brown, Konstantinos N. Plataniotis, Subbarayan Pasupathy: Energy Efficiency and Reliability in Wireless Biomedical Implant Systems. IEEE Transactions on Information Technology in Biomedicine 15(3): 456-466 (2011).

[Domingo] Mari Carmen Domingo Packet Size Optimization for Improving the Energy Efficiency in Body Sensor Networks, ETRI Journal, vol.33, no.3, June 2011, pp.299-309.

[Yazdandoost] K.Y. Yazdandoost and K. Sayrafian-Pour, "Channel Model for Body Area Network," Report to the IEEE P802.15, ID: IEEE 802.15-08-0780-02-0006, Apr. 2009.

[Fort] A. Fort, J. Ryckaert, C. Desset, P. De Doncker, P. Wambacq, and L. Van Biesen, "Ultra-wideband channel model for communication around the human body," IEEE J. Sel. Areas Commun., vol. 24, no. 4, pp. 927–933, Apr. 2006.

[Receveur] R. A. M. Receveur, F. W. Lindemans, and N. F. D. Rooij, "Microsystem technologies for implantable applications," J. Micromech. Microeng., vol. 17, no. 5, pp. R50–R80, May 2007.

[Au] L. K. Au, W. H. Wu, M. A. Batalin, D. H. McIntire, and W. J. Kaiser, "Microleap: Energy-aware wireless sensor platform for biomedical sensing applications," BioCas 2007, pp. 158–162.

[Shu] T. Shu, M. Krunz, S. Vrudhula, "Power Balanced Coverage-Time Optimization for Clustered Wireless Sensor Networks," In Proc. of the MobiHoc 2005, pp. 111–120.

[NKim] N. Kim, S. Han, W. H. Kwon, "Optimizing the Number of Clusters in Multi-Hop Wireless Sensor Networks," IEICE Transactions on Communications, Vol. E91-B, No. 1, pp. 318-321.

[Paschalidis] I. C. Paschalidis, W. Lai, and D. Starobinski, "Asymptotically optimal transmission policies for large-scale low-power wireless sensor networks," IEEE/ACM Trans. Networking 2007, Vol. 15, No. 1, pp. 105–118.

[Madan] R. Madan, N. B. Mehta, A. F. Molisch, and J. Zhang, "Energy-Efficient decentralized cooperative routing in wireless networks," IEEE Transactions on Automatic Control 2009, Vol. 54, No. 3, pp. 512–527.

[Hwang] Q. H. Wang, B. H. Zhao, "Protocol for the Application of Cooperative MIMO Based on Clustering in Sparse Wireless Sensor Networks," Journal of China Universities of Posts and Telecommunications, 2007, Vol. 14, No. 2, pp. 51-57.

[Kumar] D. Kumar, C. A. Trilok, R. B. Patel, "EEHC: Energy Efficient Heterogeneous Clustered Scheme for Wireless Sensor Networks," Computer Communication (Elsevier), Vol. 32, No. 4, 2009, pp. 662-667.

[Chan] T. J. Chan, C. M. Chen and T. R. Chen, "Optimal Cluster Number Selection in Ad-hoc Wireless Sensor Networks", WSEAS Transactions on Communications: Issue 8, Volume 7, August 2008, pp. 837-846.

[HKim] H. Kim, S. W. Kim, S. Lee, and B. Son, "Estimation of the Optimal Number of Cluster-Heads in Sensor Network," LNAI 2005, pp. 87-94.

[Wu] X. Wu, G. Chen, and S. Das, "Avoiding Energy Holes in Wireless Sensor Networks with Nonuniform Node Distribution," IEEE Tran. on Parallel and Distributed Systems, vol. 19, no. 5, pp. 710–720, May 2008.

[Chang] J. Chang and L. Tassiulas, "Maximum lifetime routing in wireless sensor networks," IEEE/ACM Trans. Networking, vol. 12, no. 4, pp. 609-619, Aug. 2004.

[Bhardwaj] M. Bhardwaj and A. Chandrakasan, "Coding under Observation Constraints," in Pro.s of the Allerton Conference on Communication, Control, and Computing, Monticello, IL, Sep. 2007, pp. 1082-1088.

[Crossbow] Crossbow MICA2 datasheet: http://www.xbow.com.

[ANT] ANT AT3 RF Transceiver Module datasheet: http://www.thisisant.com.

[GPSports] GPSports Systems, "SPI Pro." [Online]. Available: http://gpsports.com

[VXSport] Visuallex Sport International Ltd, "VXSport: Performance You Can See." [Online]. Available: http://www.vxsport.com/

[Kurusingal] A. Kurusingal, A. Dhamdhere, and V. Sivaraman, "Modeling signal strength of body-worn devices," in Proceedings of IEEE Int'l. Conf. on Local Computer Networks (LCN), Denver, Colorado, Oct. 2010.

[Srinivasan1] Kannan Srinivasan, Prabal Dutta, Arsalan Tavakoli, and Philip Levis. Understanding the Causes of Packet Delivery Success and Failure in Dense Wireless Sensor Networks. Technical Report SING-06-00, Stanford University, Department of Electrical Engineering, 2006.

[Kara] A. Kara and H.L. Bertoni. Blockage/shadowing and polarization measurements at 2.45 GHz for interference evaluation between Bluetooth and IEEE 802.11 WLAN. Antennas and Propagation Society International Symposium, 3:376 - 379, 2001.

[Obayashi] S. Obayashi and J. Zander. A body-shadowing model for indoor radio communication environments. IEEE Transactions on Antennas and Propagation, 46:920-927, 1998.

[Ruiz] J.A. Ruiz, J. Xu, and S. Shimamoto. Propagation characteristics of intra-body communications for body area networks. In Consumer Communications and Networking Conference, CCNC 2006. 3rd IEEE, volume 1, pages 509 513, 2006.

[Shah1] R.C. Shah and M. Yarvis. Characteristics of On-body 802.15.4 Networks. 2nd IEEE Workshop on Wireless Mesh Networks, pages 138{139, 25-28 Sept.2006.

[Jea] D. Jea and M.B. Srivastava. Channels Characteristics for On-Body Mica2Dot Wireless Sensor Networks. IEEE International Conference on Mobile and Ubiquitous Systems (MobiQuitous), 2005.

[Natarajan] A. Natarajan, M. Motani, B. Silva, K.-K. Yap, and K.C. Chua. Investigating network architectures for body sensor networks. In Proceedings of the 1st ACM SIGMOBILE international workshop on Systems and networking support for healthcare and assisted living environments, pages 19 { 24, 2007.

[Ren] H. Ren, M.-H Meng, and C. Cheung. Experimental Evaluation of On Body Transmission Characteristics for Wireless Biosensors. In Proceedings of 2007, IEEE International Conference on Integration Technology, ICIT, March 2007.

[Shah2] R.C Shah, L. Nachman, and C. Wan. On the performance of bluetooth and IEEE 802.15.4 radios in a body area network. In Proceedings of the ICST 3rd international conference on Body area networks, 2008.

[Arduino] Arduino, [Online]. Available: http://www.arduino.cc/

[Hackmann] G. Hackmann, O. Chipara, , and C. Lu. Robust topology control for indoor wireless sensor networks. In ACM Conference on Embedded Network Sensor Systems, pages 57–70, 2008.

[Kleisouris] K. Kleisouris, B. Firner, R. Howard, Y. Zhang, and R. P. Martin. Detecting intra-room mobility with signal strength descriptors. In MobiHoc'10, pages 71–80, 2010.

[Wang_1] L. Wang, A. Chen, and S. Huang, “A Cross-Layer Investigation for the Throughput Performance of CSMA/CA-Based WLANs with Directional Antennas and Capture Effect, IEEE Transactions on Vehicular Technology, Vol. 56, No. 5, pp. 2756-2766.

[Tsai] Y. R. Tsai, “Coverage-Preserving Routing Protocols for Randomly Distributed Wireless Sensor Networks,” IEEE Transactions on Wireless Communications 2007, Vol. 6, No. 4, pp. 1240–1245.

[Amini2] N. Amini, A. Vahdatpour, F. Dabiri, H. Noshadi, M. Sarrafzadeh, “Joint Consideration of Energy-Efficiency and Coverage-Preservation in Microsensor Networks,” Wireless Communications and Mobile Computing, http://dx.doi.org/10.1002/wcm.852, 2009.

[Watteyne] T. Watteyne, I. Aug´e-Blum, M. Dohler, and D. Barthel, “Anybody: a self-organization protocol for body area networks,” in Proceedings of the ICST 2nd international conference on Body area networks, ser. BodyNets ’07. ICST, Brussels, Belgium, Belgium: Institute for Computer Sciences, Social-Informatics and Telecommunications Engineering, 2007, pp. 6:1–6:7.

[Alippi] C. Alippi, R. Camplani, M. Roveri, “An Adaptive LLC-Based and Hierarchical Power-Aware Routing Algorithm,” IEEE Transactions on Instrumentation and Measurement 2009, Vol. 58, No. 9, pp. 3347–3357.

[XBEE] XBee modules, [Online]. Available: http://www.digi.com/products/

[Levendovszky] Janos Levendovszky, Andras Olah, Gergely Treplan and Long Tran-Thanh Reliability-Based Routing Algorithms for Energy-Aware Communication in Wireless Sensor Networks, Performance Models And Risk Management In Communications Systems, Springer Optimization and Its Applications, 2011, Volume 46, pp. 93-126.

[Tang] Q. Tang, N. Tummala, E. K. S. Gupta, L. Schwiebert, S. Member, and S. Member, “Communication scheduling to minimize thermal effects of implanted biosensor networks in homogeneous tissue,” IEEE Tran. Biomedical Eng, vol. 52, pp. 1285–1294, 2005.

[Bag] A. Bag andM. Bassiouni, “Energy efficient thermal aware routing algorithms for embedded biomedical sensor networks,” IEEE International Conference on Mobile Adhoc and Sensor Systems Conference, vol. 0, pp. 604–609, 2006.

[Honeine] Paul Honeine, Farah Mourad, Maya Kallas, Hichem Snoussi, Hassan Amoud and Clovis Francis, Wireless Sensor Networks In Biomedical: Body Area Networks, Proc. of the 7th International Workshop on Systems, Signal Processing and their Applications (WOSSPA), Tipaza, Algeria, May 2011, pp. 388-391.

[Culpepper] B. J. Culpepper, L. Dung, and M. Moh, “Design and analysis of hybrid indirect transmissions (hit) for data gathering in wireless micro sensornetworks,” SIGMOBILE Mob. Comput. Commun. Rev., vol. 8, pp. 61– 83, January 2004.

[Moh] M. Moh, B. Culpepper, L. Dung, T.-S. Moh, T. Hamada, and C.-F. Su, “On data gathering protocols for in-body biomedical sensor networks,” in IEEE Global Telecommunications Conference (GLOBECOM’05), St. Louis, MO, USA, Dec. 2005.

[Tang] Q. Tang, N. Tummala, E. K. S. Gupta, L. Schwiebert, S. Member, and S. Member, “Communication scheduling to minimize thermal effects of implanted biosensor networks in homogeneous tissue,” IEEE Tran. Biomedical Eng, vol. 52, pp. 1285–1294, 2005.

[Bag] A. Bag andM. Bassiouni, “Energy efficient thermal aware routing algorithms for embedded biomedical sensor networks,” IEEE International Conference on Mobile Adhoc and Sensor Systems Conference, vol. 0, pp. 604–609, 2006.

[Takahashi] D. Takahashi, Y. Xiao, F. Hu, J. Chen, and Y. Sun, “Temperature-aware routing for telemedicine applications in embedded biomedical sensor networks,” EURASIP J. Wirel. Commun. Netw., vol. 2008, pp. 26:1–26:26, January 2008.

[NCRP] “A practical guide to the determination of human exposure to radiofrequency fields,” NCRP, Tech. Rep. 119, 1993.

[Zhen] B. Zhen, K. Takizawa, T. Aoyagi, and R. Kohno, “A body surface coordinator for implanted biosensor networks,” in Proceedings of the 2009 IEEE international conference on Communications, ser. ICC’09. Piscataway, NJ, USA: IEEE Press, 2009, pp. 475–479.

[Schwiebert] L. Schwiebert, S. Gupta, and J. Weinmann. Research challenges in wireless networks of biomedical sensors. In Proceedings of the 7th Annual International Conference on Mobile Computing and Networking, pages 151– 165, ACM Press, 2001.

[Zhao] F. Zhao, J. Liu, J. Liu, L. Guibas, and J. Reich, “Collaborative Signal and Information Processing: An Information-Directed Approach,” Proc. IEEE, Aug. 2003, Vol. 91, No. 8, pp. 1199-1209.

[Dardari] D. Dardari, A. Conti, C. Buratti, and R. Verdone, “Mathematical Evaluation of Environmental Monitoring Estimation Error through Energy-Efficient Wireless Sensor Networks,” IEEE Transactions on Mobile Computing, Vol. 6, Issue 7, Jul. 2007, pp. 790–802.

[Amini2] N. Amini, A. Vahdatpour, W. Xu, M. Sarrafzadeh, “Cluster Size Optimization in Sensor Networks with Decentralized Cluster-Based Protocols,” Under second review, Computer Communications Journal - Elsevier.

[Landsiedel] O. Landsiedel, K. Wehrle, and S. Gotz, “Accurate prediction of power consumption in sensor networks,” The Second Workshop on Embedded Networked Sensors (EmNetS-II). IEEE, 2005, pp. 37-44.

[Arduino] Arduino CC. Arduino Pro Mini. http://arduino.cc.

[Misal Chaitanya S. Misal, “Analysis of Power Consumption of an End Device in a ZigBee Mesh Network,” University of North Carolina, Raleigh-Durham, NC, 2007, http://coe.uncc.edu/~jmconrad/GradStudents/Thesis_Misal.pdf.

[Wang_2] X. Wang, J. Yin, D.P. Agrawal, Effects of Contention Window and Packet Size on the Energy Efficiency of Wireless Local Area Network, Proceedings of IEEE WCNC, vol. 1, 2005, pp. 94–99.

[Lin2] S. Lin, J. Zhang, G. Zhou, L. Gu, T. He and J.A. Stankovic, “ATPC: Adaptive Transmission Power Control for Wireless Sensor Networks,” ACM SenSys, Oct 2006, Boulder, CO, USA.

[Zuniga] M. Zuniga and B. Krishnamachari, “Analyzing the transitional region in low power wireless links,” in Proc. IEEE Sensor Ad Hoc Commun. Networks Conf., 2004, pp. 517-526.

[Srinivasan2] K. Srinivasan, P. Dutta, A. Tavakoli, and P. Levis, “An Empirical Study of Low-Power Wireless,” ACM Transactions on Sensor Networks, vol. 6, pp. 1-49, 2010.

[Cotton] S. L. Cotton, A. McKernan, A. J. Ali & W. G. Scanlon, “An experimental study on the impact of human body shadowing in offbody communications channels at 2.45 GHz,” 5th European Conf. Antennas and Prop. (EUCAP), pp. 3288–3292, Rome, Italy, Apr. 2011.

[XBee2] XBee & XBee-PRO OEM RF Module Antenna Considerations, http://www.digi.com.

[Wiki2] http://en.wikipedia.org/wiki/Radiation_pattern.

[Vahdatpour1] A. Vahdatpour, N. Amini, M. Sarrafzadeh, “Toward Unsupervised Activity Discovery Using Multi Dimensional Motif Detection in Time Series,” Proc. of the Twenty-first International Joint Conference on Artificial Intelligence (IJCAI) 2009, Pasadena, California, pp. 1261-1266.

[Amini5] N. Amini, M. Sarrafzadeh, A. Vahdatpour, W. Xu, "Accelerometer-based on-body sensor localization for health and medical monitoring applications," Pervasive and Mobile Computing Journal – Elsevier, Vol. 7, Issue 6, December 2011, pp. 746-760.

[Chiu] B. Chiu, E. Keogh, S. Lonardi, Probabilistic discovery of time series motifs, in: KDD ’03, 2003, pp. 493–498.

[Vahdatpour2] A. Vahdatpour, M. Sarrafzadeh, Unsupervised discovery of abnormal activity occurrences in multi-dimensional time series, with applications in wearable systems, in: SDM '10: Siam Conference on Data Mining, 2010.

[Aslam] J. Aslam, K. Pelekhov, D. Rus, A practical clustering algorithm for static and dynamic information organization, in: SODA '99: Proceedings of the Tenth Annual ACM-SIAM Symposium on Discrete Algorithms, Society for Industrial and Applied Mathematics. Philadelphia, PA, USA, 1999, pp. 51–60.

[Kunze] K. Kunze, P. Lukowicz, Using acceleration signatures from everyday activities for on-body device location, in: ISWC '07: Proceedings of the 2007 11th IEEE International Symposium on Wearable Computers, IEEE Computer Society, Washington, DC, USA, 2007, pp. 1–2.

[Gulf] Gulf coast data concepts, http://gcdataconcepts.com/x6-2.html/ retrieved on June 2011.

[Jiu-Qiang] X. Jiu-Qiang, S. Pei-Gang, Z. Hai, Z. Xi-Yuan, Z. Jian, and C. Dawei, An analytical model for link evaluation of wireless sensor networks, Network and Parallel Computing Workshops, 2007. NPC Workshops. IFIP International Conference on, (18-21 Sept. 2007), pp. 386–391.

[Fedor] S. Fedor, "Cross-Layer Energy Optimization Of Routing Protocols In Wireless Sensor Networks" Phd thesis, Dublin City University, April 2008.

[IEEESTD] Wirelessmedium access control (mac) and physical layer (phy) specifications for low rate wireless personal area networks (lr-wpans), IEEE std. 802.15.4-2006 (Revision of IEEE Std 802.15.4-2003), (2006).

[O'Rourke] D. O'Rourke, S. Fedor, C. Brennan, and M. Collier, Reception region characterisation using a 2.4 GHz direct sequence spread spectrum radio," Proc. EmNets, Cork, Ireland, pp.68-72, Jun. 2007.

[Rappaport] T. Rappaport, Wireless Communications: Principles and Practice, Prentice Hall PTR, Upper Saddle River, NJ, USA, 2001.

[Dhananjay] L. Dhananjay, A. Manjeshwar, F. Herrmann, E. Uysal-Biyikoglu, and A. Keshavarzian, Measurement and characterization of link quality metrics in energy constrained wireless sensor networks, Global Telecommunications Conference, 2003. GLOBECOM '03. IEEE, 1 (1-5 Dec. 2003), pp. 446–452.

[JKim] J. Kim and Y. Kwon, "Interference-aware Transmission Power Control for Wireless Sensor Networks," IEICE Trans. Commun., 2008, E90-B, (11), pp.3434-3441.

[Janek] John F. Janek, Jeffrey J. Evans, "Predicting Ground Effects of Omnidirectional Antennas in Wireless Sensor Networks", International Journal of Sensor Network 2(12): 879-890 (2010).

[Raynor] A.J. Raynor, C.J. Yi, B. Abernathey, Q.J. Jong, "Are transitions in human gait determined by mechanical, kinetic or energetic factors?" Human Movement Science. 21:785-805(2002).

[Locomotion_Wiki] http://en.wikipedia.org/wiki/Transition_from_walking_to_running

[Salarian] A. Salarian, C. Zampieri, F. B. Horak, P. Carlson-Kuhta, J. G. Nutt, K. Aminian, "Analyzing 180° Turns Using an Inertial System Reveals Early Signs of Progression of Parkinson's Disease," Proc. 31st Annual International Conference of the IEEE Engineering in Medicine and Biology Society, pp. 224-227. 2009.

[Wang_3] F. Wang, M. Skubic, C. Abbott, and J. Keller, "Quantitative Analysis of 180 Degree Turns for Fall Risk Assessment Using Video Sensors," Proceedings, IEEE Engineering in Medicine and Biology Conference, Boston, MA, August 30-September 3, 2011, pp 7606-7609.

[Xiao] S. Xiao, A. Dhamdhere, V. Sivaraman, and A. Burdett. Transmission Power Control in Body Area Sensor Networks for Healthcare Monitoring. In IEEE Journal on Selected Areas in Communications, volume 27, pages 37–48, January 2009.

[Ravindranath] L. Ravindranath, C. Newport, H. Balakrishnan, and S. Madden. Improving wireless network performance using sensor hints. Proceedings of the 8th USENIX conference on Networked systems design and implementation, pp. 21-35.

[Chen] B. Chen, B. Lee, S. Chen, "Adaptive Power Control of Cellular CDMA Systems via the Optimal Predictive Model," IEEE Transactions on Wireless Communications, vol. 4, no. 4, Jul 2005.

[Wiki3] http://en.wikipedia.org/wiki/Exponential_smoothing

[Gait1] Critical Biomechanical Principles, http://www.golfmed.net/orthotics/gait/bio_princ.html

[Mertens] C. Mertens, F. Grenez, and J. Schoentgen, "Speech sample salience analysis for speech cycle detection," Proc. of the 10th Annual Conference of the International Speech Communication Association INTERSPEECH, Brighton, 2009, pp. 939- 942.

[Torres] M. G. Torres. Energy Consumption in Wireless Sensor Networks Usig GSP. Master's thesis, Universidad Pontificia Bolivariana, Medellín, University of Pittsburgh, 2006.

[Anastasi] G. Anastasi , A. Falchi , A. Passarella , M. Conti , E. Gregori, "Performance measurements of motes sensor networks," Proceedings of the 7th ACM international symposium on Modeling, analysis and simulation of wireless and mobile systems, October 04-06, 2004, Venice, Italy .

[Shnayder] V. Shnayder, M. Hempstead, B.-r. Chen, G. Werner-Allen, and M. Welsh. Simulating the power consumption of large-scale sensor network applications. In Proc. of the 2nd Int'l Conf. on Embedded Networked Sensor Systems, pp. 188–200, 2004.

[Ko] J. Ko and A. Terzis. Power Control for Mobile Sensor Networks: An Experimental Approach. In Proc. of the IEEE Sensor, Mesh and Ad Hoc Comm. and Networks (SECON 2010), June 2010, pp. 1-9.

[Wiki4] http://en.wikipedia.org/wiki/Compliance_(medicine)

[WHO] World Health Organization (WHO), Adherence to Long-Term Therapies: Evidence for Action, Geneva: WHO, 2003, p. 7.

[Bicket] J. Bicket. Bit-rate Selection in Wireless Networks. Master's thesis, Massachusetts Institute of Technology, February 2005.